Aus dem Institut für Klinische Neuroimmunologie

Klinikum der Ludwig-Maximilians-Universität München

Vorstand: Prof. Dr. Martin Kerschensteiner

T:B cell communication in
ectopic lymphoid follicles in CNS autoimmunity

Dissertation
zum Erwerb des Doktorgrades der Naturwissenschaften
an der Medizinischen Fakultät der
Ludwig-Maximilians-Universität zu München

vorgelegt von

Anna Kolz

aus

Püttlingen

2022

Mit Genehmigung der Medizinischen Fakultät

der Universität München

Betreuerin: Dr. Anneli Peters

Zweitgutachter: Prof. Dr. Ludger Klein

Dekan: Prof. Dr. med. Thomas Gudermann

Tag der mündlichen Prüfung: 27.09.2022

Für meine Familie

Real change, enduring change, happens one step at a time.

Ruth Bader Ginsburg (1933-2020)

<u>Contents</u>

List of Figures

List of Tables

List of Supplementary Tables

List of Abbreviations

AA	Amino acid
AID	Activation-induced cytidine deaminase
AF	Alexa Fluor
APC	Antigen-presenting cell
Av-HRP	Avidin-horseradish peroxidase
BCR	B cell receptor
BSA	Bovine serum albumin
BV	Brilliant Violet
CD	Cluster of differentiation
cDNA	Complementary DNA
CDR3	Complementarity determining region 3
CFA	Complete Freund`s adjuvant
CFP	Cyan fluorescent protein
CIA	Collagen-induced arthritis
cLN	Cervical lymph node
CNS	Central nervous system
CRAC	Calcium release-activated calcium
CSF	Cerebrospinal fluid
CSR	Class switch recombination
CTLA4	Cytotoxic T-lymphocyte antigen 4
Cy	Cyanine
DAMPs	Damage-associated molecular patterns
DAPI	4′,6-diamidino-2-phenylindole
DC	Dendritic cell
DMEM	Dulbecco's Modified Eagle's Medium
DNA	Deoxyribonucleic acid
EAE	Experimental autoimmune encephalomyelitis
EDTA	Ethylendiamintetraacetat
eLFs	Ectopic lymphoid follicles
ELISA	Enzyme-linked immunosorbent assay
ER	Endoplasmic reticulum
FACS	Fluorescence-activated cell sorting
FBS	Fetal bovine serum

FDC	Follicular dendritic cell
FITC	Fluorescein isothiocyanate
FoxP3	Forkhead-Box-Protein P3
FRC	Fibroblastic reticular cell
FRET	Fluorescence resonance energy transfer
FR3	Framework region 3
GC	Germinal center
GEM	Gel beads in emulsion
GFP	Green fluorescent protein
GM-CSF	Granulocyte macrophage-colony stimulating factor
HC	Heavy chain
HEPES	(4-(2-Hydroxyethyl)-1-piperazineethanesulfonic acid
HEV	High endothelial venules
HTO	Hashtag oligonucleotide
IFN	Interferon
Ig	Immunoglobulin
iGB cell	Induced germinal center B cell
IHC	Immunohistochemistry
IL	Interleukin
ILC	Innate lymphoid cell
IP_3	Inositol-1,4,5-trisphosphate
i.p.	Intraperitoneally
i.v.	Intravenously
KO	Knockout
LC	Light chain
LN	Lymph node
LT	Lymphotoxin
LTi cell	Lymphoid tissue inducer cell
MBP	Myelin basic protein
MHC	Major histocompatibility complex
min	Minutes
MOG	Myelin oligodendrocyte glycoprotein
MOGtet	MOG tetramer
mRNA	Messenger ribonucleic acid
MS	Multiple sclerosis

MSCV	Murine stem cell virus
MZ	Marginal zone
NFAT	Nuclear factor of activated T cells
NF-κB	Nuclear factor kappa B
NK	Natural killer cell
OCBs	Oligoclonal bands
OD	Optical density
OSE	Opticospinal EAE
OVA	Ovalbumin
PAMPs	Pathogen-associated molecular patterns
PBS	Phosphate-buffered saline
PD-1	Programmed cell death 1
PD-L1	Programmed cell death 1 ligand 1
PE	Phycoerythrin
PerCP	Peridinin chlorophyll protein
PFA	Paraformaldehyde
PKC	Proteinkinase C
PLP	Proteolipid protein
PMA	Phorbol 12-myristate 13-acetate
PNA	Peanut agglutinin
PPMS	Primary progressive MS
PRRs	Pattern-recognition receptors
RA	Rheumatoid arthritis
Rag	Recombination activating gene
ROI	Region of interest
RORγt	RAR-related orphan receptor γt
RRMS	Relapsing-remitting MS
RT	Room temperature
scBCR-seq	Single-cell BCR sequencing
scRNA-seq	Single-cell RNA sequencing
SHM	Somatic hypermutation
SLE	Systemic lupus erythematosus
SLOs	Secondary lymphoid organs
SPMS	Secondary progressive MS
SS	Sjögren`s syndrome

STIM	Stromal interaction molecule
TCR	T cell receptor
Tfh	T follicular helper cell
TGF	Transforming growth factor
Th cell	T helper cell
TLOs	Tertiary lymphoid organs
TLR	Toll-like receptor
TnC	Troponin C
TNF	Tumor necrosis factor
Treg cell	Regulatory T cell
Tr1 cell	Type 1 regulatory T cell
UMAP	Uniform Manifold Approximation and Projection
WT	Wildtype
YFP	Yellow fluorescent protein

<u>Summary</u>

Multiple sclerosis (MS) is a life lasting disease of the central nervous system (CNS) characterized by chronic autoimmune inflammation and massive demyelination, resulting in neuronal damage and progressive paralysis. MS research traditionally focused on autoreactive T cells, which have long been accepted to be important drivers of CNS inflammation. To our current knowledge, autoreactive T helper cells become activated in the periphery before they invade the CNS and attack the myelin sheath. Both Th1 and Th17 cells contribute to pathogenesis in MS and its animal model experimental autoimmune encephalomyelitis (EAE). In the past decade, B cells have received increasing attention since compelling evidence also suggests a pivotal role of B cells in CNS autoimmunity. However, it is poorly understood how T and B cells cooperate to induce and propagate disease. In MS, meningeal ectopic lymphoid follicle-like structures (eLFs) have been hypothesized to fuel chronic inflammation directly in the CNS. To differentiate between Th1- and Th17-driven aspects of disease, we established adoptive transfer EAE with *in vitro* differentiated myelin oligodendrocyte glycoprotein (MOG)-specific Th1 or Th17 cells. Both Th1 and Th17 cells induced EAE with similar severity, and maintained their original cytokine profile also in the inflamed CNS. Confirming previous reports, large lymphocytic aggregates were found in association with meninges of brain and spinal cord primarily in Th17 recipients. The aim of this thesis was to investigate the unique relationship of Th17 cells and B cells in EAE development, and, in particular, to assess the nature of their interaction in eLFs.

Employing our Th17 adoptive transfer EAE model, it was demonstrated that eLFs contain clusters of proliferating T and B cells, show expression of germinal center markers, and are reminiscent of follicle-like structures in MS patients. Transcriptomic analysis showed that clusters of activated B cells and Marginal Zone-like B cells are overrepresented in the CNS and provides evidence for enhanced antigen presenting-function as well as ongoing B cell maturation. B cell receptor (BCR) repertoire analysis revealed expanded clones in the CNS, supporting our hypothesis that these may differentiate/expand in eLFs. In addition, transferred Th17 cells recruited and expanded autoreactive B cells with the same antigen specificity from the endogenous pool, a process which may take place inside eLFs. To determine whether and how Th17 cells and B cells communicate in eLFs, Th17 cells were labeled with a genetically-encoded

protein activation sensor, allowing us to study their interactions with tdTomato-labeled B cells in real-time using intravital two-photon microscopy of the CNS. Thereby, it was demonstrated for the first time that there is extensive communication and long-lasting contacts between T and B cells in eLFs, and that B cells are able to reactivate T cells. Consistent with these findings, it was shown that T cells depend on B cells to maintain a highly pro-inflammatory cytokine profile in the CNS.

Taken together, the data presented in this thesis provide evidence that interaction of T and B cells in meningeal eLFs not only promotes activation, differentiation, and clonal expansion of B cells, but also leads to reactivation of CNS T cells and thereby supports smoldering inflammatory processes within the CNS. Thus, our results may provide a direction for future research into the function of eLFs in MS.

Zusammenfassung

Multiple Sklerose (MS) ist eine lebenslange Erkrankung des zentralen Nervensystems (ZNS), bei der chronische autoimmune Entzündungsprozesse und Demyelinisierung zur Schädigung von Nervenzellen sowie fortschreitender Lähmung führen. Traditionell fokussierte sich die MS Forschung auf autoreaktive T-Zellen, die seit langem als wichtiger krankheitsverursachender Zelltyp angesehen werden. Nach aktuellem Kenntnisstand werden autoreaktive T-Helferzellen in der Peripherie aktiviert, bevor sie in das ZNS einwandern und die Myelinscheiden von Nervenzellen angreifen. Dabei tragen sowohl Th1- als auch Th17-Zellen zur Pathogenese der MS und ihrem Tiermodell, der experimentellen autoimmunen Enzephalomyelitis (EAE), bei. In der letzten Dekade erhielten die B-Zellen zunehmende Aufmerksamkeit, da sich die Hinweise verdichteten, dass auch sie eine wichtige Rolle bei der ZNS-Autoimmunität innehaben. Jedoch ist noch nicht verstanden, wie T-Zellen und B-Zellen miteinander kooperieren, um den Entzündungsprozess auszulösen und aufrechtzuerhalten. Es wird vermutet, dass ektopische Lymphfollikel, die sich in den Hirnhäuten von MS Patienten befinden, die Entzündung direkt im ZNS vorantreiben können. Um zwischen Th1- und Th17-verursachten Krankheitsaspekten unterscheiden zu können, haben wir die adoptive Transfer-EAE mittels *in vitro*-differenzierten Myelin-Oligodendrozyten-Glycoprotein (MOG)-spezifischen Th1- oder Th17-Zellen etabliert. Dabei verursachten Th1- und Th17-Zellen EAE mit ähnlichem Schweregrad und behielten ihr ursprüngliches Zytokinprofil auch im entzündeten ZNS bei. Wie bereits zuvor beschrieben, wurden große Lymphozyten-Aggregate hauptsächlich in den Hirnhäuten von Mäusen gefunden, denen Th17-Zellen injiziert wurden. Das Ziel dieser Dissertation bestand darin, die einzigartige Wechselwirkung von Th17-Zellen und B-Zellen in der Entwicklung der EAE zu entschlüsseln und ihre Interaktionen in ektopischen Lymphfollikeln zu untersuchen.

Mit Hilfe unseres Th17-induzierten EAE Modells konnte gezeigt werden, dass ektopische Lymphfollikel Aggregate aus proliferierenden T-Zellen und B-Zellen enthalten, Marker von Keimzentren exprimieren und Ähnlichkeit zu Follikel-Strukturen in MS Patienten aufweisen. Unsere Transkriptomanalyse belegt, dass aktivierte B-Zellen und B-Zellen, die den Marginalzonen B-Zellen ähnlich sind, im ZNS überrepräsentiert sind, und liefert Hinweise auf eine verstärkte Funktion als Antigen-

präsentierende Zellen sowie auf fortlaufende B-Zell Reifung. Durch die Analyse des B-Zell-Rezeptor (BZR) Repertoires wurden expandierte Klone im ZNS nachgewiesen, wodurch unsere Hypothese untermauert wird, dass B-Zellen in ektopischen Lymphfollikeln differenzieren und/oder expandieren können. Des Weiteren konnte gezeigt werden, dass die transferierten T-Zellen autoreaktive B-Zellen mit der gleichen Antigen-Spezifität aus dem endogenen Repertoire rekrutieren, wobei dieser Prozess in ektopischen Lymphfollikeln stattfinden könnte. Um herauszufinden, ob und wie Th17-Zellen und B-Zellen in ektopischen Lymphfollikeln miteinander kommunizieren, wurden Th17-Zellen mit einem genetisch kodierten Aktivierungssensorprotein markiert. Dadurch wurde es möglich, ihre Interaktionen mit tdTomato-markierten B-Zellen in Echtzeit mit Hilfe der intravitalen Zwei-Photonen-Mikroskopie des ZNS zu untersuchen. Es konnte zum ersten Mal nachgewiesen werden, dass intensive Kommunikation und langanhaltende Kontakte zwischen T-Zellen und B-Zellen in den ektopischen Lymphfollikeln stattfinden, und dass B-Zellen dabei T-Zellen reaktivieren können. Mit diesen Ergebnissen übereinstimmend konnte gezeigt werden, dass T-Zellen auf B-Zellen angewiesen sind, um ihr stark pro-inflammatorisches Zytokinprofil im ZNS aufrechtzuerhalten.

Zusammenfassend deuten die Ergebnisse dieser Dissertation darauf hin, dass die Interaktion von T und B-Zellen in meningealen ektopischen Lymphfollikeln nicht nur die Aktivierung, Differenzierung und klonale Expansion von B-Zellen unterstützt, sondern auch zur Reaktivierung von T-Zellen beiträgt und somit schwelende Entzündungsprozesse im ZNS fördert. Aus diesem Grund könnte unsere Studie eine neue Richtung vorgeben für die zukünftige Erforschung der Funktion von ektopischen Lymphfollikeln in der MS.

1. Introduction

1.1 The immune system

Our body`s ability to protect itself from a universe of constantly evolving pathogens has been key to our evolutionary success. The immune system employs enormous resources to continuously surveil all parts of our body and mount responses to invading microbes, toxins or allergens. Two branches of immunity act in concert to eliminate these pathogenic threats. As first line of defense, the innate immune system formulates a rapid response within minutes to hours upon recognition of a pathogen. Innate immune cells contain infection and, in addition, activate the adaptive immune system, which is equipped with lymphocytes providing a highly specific protection against a particular pathogen. Adaptive immune cells can form a long-lasting memory protecting the host from reinfection, sometimes for the entire lifespan. Tight regulation and optimal performance of the immune system are inevitable for successfully fighting infections, while preserving the integrity of our body`s tissues.

1.1.1 Innate immune system

At the site of an invading pathogen, innate immune cells, including dendritic cells (DCs), macrophages and neutrophils, induce rapid inflammatory responses to locally combat the infection. These cells rely on germline-encoded receptors called pattern-recognition receptors (PRRs), e.g. toll-like receptors (TLRs), to detect microbes via highly conserved structures, referred to as pathogen-associated molecular patterns (PAMPs) [1, 2]. In addition, stressed, damaged or dying cells can be sensed via damage-associated molecular patterns (DAMPs) [3]. Innate immunity is armed with a diverse set of both myeloid and lymphoid cell types, each fulfilling distinct tasks. Uptake and subsequent destruction of pathogens via phagocytosis is a crucial defense mechanism deployed by a number of myeloid innate immune cells. Macrophages and DCs further orchestrate subsequent immune responses by acting as antigen-presenting cells (APCs). Further defense strategies include release of toxic factors, secretion of cytokines and chemokines, and activation of the complement cascade. More recently, the contribution of innate lymphoid cells (ILCs) was discovered. These cells lack a somatically recombined antigen receptor and are classified depending on

their transcriptional programs and cytokine expression associated with T helper (Th) or cytotoxic T cells [4]. One of these subgroups, the natural killer (NK) cells, is specialized in killing virus-infected and tumor cells by secreting pro-inflammatory cytokines and cytotoxic substances [5]. Traditionally, the ability to form memory was thought to be restricted to adaptive immunity. The description of memory responses of NK cells and other ILCs, termed "trained immunity", has challenged this dogma during the past decade [6]. In addition to this broad range of defense functions, innate immune cells stimulate adaptive immunity to induce a strong systemic response targeting specifically the invading pathogen [7].

1.1.2 Adaptive immune system

Adaptive immunity is primarily orchestrated by T and B cells, which mount cell-mediated and humoral immune responses, respectively, to clear pathogens which have escaped innate immunity. Hallmark of these adaptive immune cells is their specific antigen receptor. In contrast to innate immune cells, the specificity of the T cell receptor (TCR) and B cell receptor (BCR) is determined by somatic rearrangement of several hundred genomic elements [8]. The resulting myriad of possible combinations equips T and B cells with an extraordinarily broad spectrum of receptors, which allows recognition of every potentially harmful antigen. This unique ability of adaptive immune cells is key to keep pace with the continuous evolution of pathogens. The competence of our immune system to properly select and clonally expand T and B cells of required specificity enables us to fight infections during our entire lifespan.

T and B cells differ substantially in their mechanisms of antigen recognition. B cells can bind antigens directly with their surface immunoglobulin, i.e. the BCR, whereas T cells depend on APCs to process antigens and present peptide fragments on class I and class II major histocompatibility complex (MHC) molecules [8]. The TCR is a heterodimer consisting of TCR α and β chains. To become activated, T cells form a stable TCR:peptide:MHC complex. The TCR α and β chains are associated with CD3 proteins which are responsible for intracellular transmission of the TCR signal upon antigen recognition. For proper T cell activation, the MHC molecule needs to be bound additionally by the CD4 or CD8 co-receptor [9]. $CD4^+$ and $CD8^+$ T cells perform different roles in adaptive immunity.

The main task of CD8$^+$ T cells is the identification and destruction of infected cells. CD8$^+$ T cells recognize antigens that are bound to MHC class I molecules, which are expressed on the surface of almost all cells of the body. Since they present peptides derived from proteins synthesized within the cell, they inform CD8$^+$ T cells about intracellular pathogens like viruses and bacteria. Upon activation, CD8$^+$ T cells unleash their cytotoxic potential by inducing a diverse set of effector pathways resulting in elimination of infected cells and/or recruitment of other immune cells [8, 10].

CD4$^+$ T cells are also called T helper (Th) cells because they regulate both the T cell and B cell-mediated branch of adaptive immunity, as well as innate immune cells. They require antigen presentation on MHC class II molecules, which are only expressed by APCs including DCs, macrophages and B cells. The presented peptides are derived from exogenous antigens, which have been internalized and proteolytically processed before being loaded onto MHC-II. Depending on the cytokine microenvironment, naïve CD4$^+$ T cells differentiate into various different subsets. Each lineage expresses a distinct set of cytokines, thereby modulating the immune response in a specific direction (described in detail in section 1.4.1) [11, 12].

B cells constitute the humoral branch of the adaptive immune system. In addition to production of high-affinity immunoglobulins (Ig), they modulate immune responses by secreting cytokines and presenting antigens. Mature naïve B cells can generally be divided into three subsets: B-1 B cells, marginal zone (MZ) B cells and follicular B cells. These cell types differ regarding location, ability to migrate and mode of activation [13]. B-1 cells are enriched in body cavities, such as pleura and peritoneum, where they react promptly to newly arriving pathogens. They can undergo T cell-independent responses and generate antibodies with broad reactivity, thereby conferring early protection [14]. MZ B cells are also thought to be innate-like cells that can develop into short-lived plasma cells without BCR stimulation. They are primarily localized in the MZ of the spleen, where they are well positioned to respond to blood-borne pathogens [13]. They can also capture these antigens and transport them to splenic follicles, thereby contributing to T cell-dependent immune responses [15, 16]. Due to their high expression of MHC-II, CD80 and CD86, MZ B cells are potent antigen presenters and activators of CD4$^+$ T cells [17, 18]. In addition, they can present lipid antigens on CD1d to NKT cells [19]. Follicular B cells represent the majority of naïve B cells. They

recirculate freely through the lymph and blood, and shuttle to the bone marrow, where they are localized around sinusoids and mount T cell-independent responses to blood-borne microbes by secreting IgM [20, 21]. In addition, they home to B cell areas of spleen, lymph nodes and Peyer`s patches [13]. Here, the B cell follicles are situated adjacent to T cell zones. This close vicinity allows intense interactions between B cells and Th cells, educating these follicular B cells in responses to antigens that require help from Th cells [22]. Initially, B cell zones contain $IgM^+ IgD^+$ naïve B cells. When they encounter antigen, they start proliferating and move towards the interfollicular region to interact with cognate $CD4^+$ T cells that have adopted a T follicular helper (Tfh) cell phenotype upon priming by DCs [23-25]. Being activated, some of these B cells migrate to extrafollicular foci, where they differentiate into short-lived plasmablasts secreting low-affinity antibodies. The remaining B cells migrate back to the B cell follicle and form germinal centers (GCs), where effector cells with high affinity for the antigen are being produced. After interaction with cognate B cells, Tfh cells differentiate into GC Tfh cells and participate in GC reactions. Within GCs, B cells proliferate massively and undergo somatic hypermutation (SHM) to modify the affinity of their antigen receptor. Follicular dendritic cells (FDCs) express CXCL13 to recruit B cells into follicles via the receptor CXCR5 [26] and additionally, they present the antigen to GC B cells, which then capture and internalize it via their BCR and present the processed peptide loaded on MHC-II to Tfh cells [27]. B cells with higher affinity can capture higher amounts of antigen and form more intense contacts with Tfh cells [28, 29]. Hence, they receive more help from Tfh cells via CD40 ligation and interleukin (IL)-21, and are selected to continue the maturation process. B cells with lower affinity are deleted through apoptosis [30, 31]. This process of SHM and subsequent clonal selection, also called affinity maturation, is repeated several times, allowing only high affinity B cells to survive. Besides, class switch recombination (CSR) leads to production of isotype-switched antibodies. The choice of isotype - IgG, IgE or IgA - depends on the pathogenic stimulus and the cytokines provided by the resulting Tfh help. Eventually, positively selected B cells either develop into long-lived plasma cells that home to the bone marrow or memory B cells. Both cell types are crucial for long-lasting antibody responses and immunological memory [27]. An overview of the follicular B cell response is depicted in Figure 1.
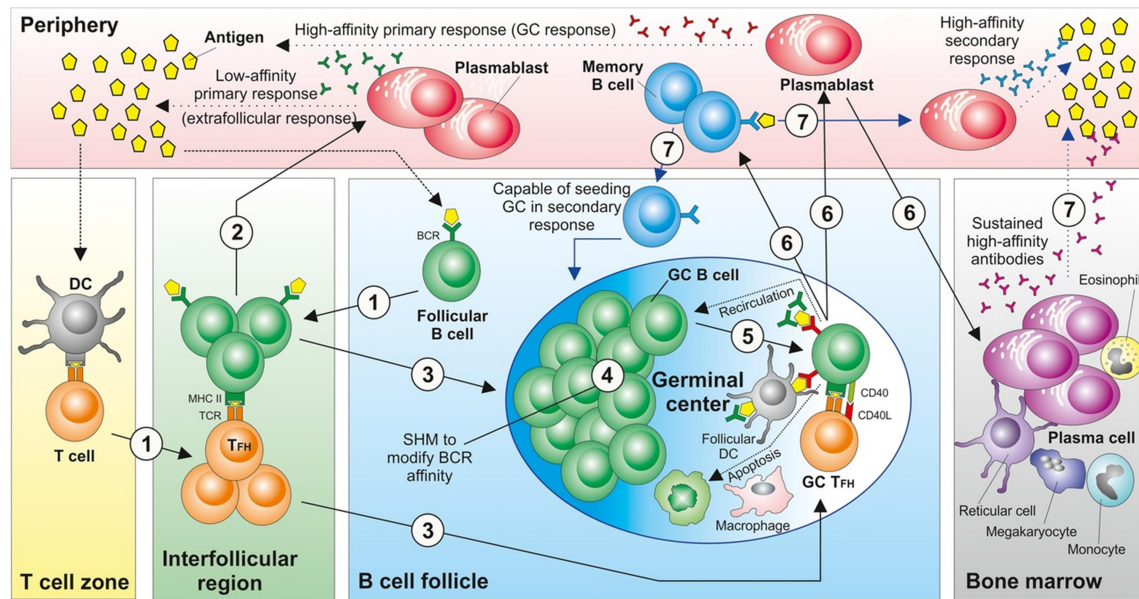
Figure 1. Summary of all steps involved in the follicular B cell response. Upon antigen encounter, follicular T helper (TFH) cells and follicular B cells engage in a germinal center (GC) reaction. B cells undergo somatic hypermutation (SHM) and clonal selection, eventually giving rise to high affinity plasma cells or memory B cells. Adapted by permission from [27].

1.1.3 Mechanisms of T and B cell tolerance

Our immune system is well equipped to mount rapid and strong responses against invading pathogens. At the same time, it must avoid targeting its own tissues. Therefore, a strong sense of what is "self" and what is "foreign" is indispensable. The immune system has developed several mechanisms to educate its cells and ensure tolerance against self-structures.

During T cell development in the thymus, the TCR, generated through random rearrangement of genomic elements, is tested for its functionality by mechanisms of central tolerance. Thymic epithelial cells and dendritic cells present self-peptides, whereupon T cells which express a TCR that can bind the peptide-MHC complex and recognize the self-antigen with low affinity are positively selected. In contrast, T cells that bind self-peptide with high affinity are either deleted by apoptosis or differentiate into a regulatory T cell (Treg). Central tolerance, however, does not eliminate every self-reactive T cell, partly because not all autoantigens are efficiently presented in the thymus. Therefore, mechanisms of peripheral tolerance come into play to induce tolerance of T cells which encounter their cognate self-peptide in the periphery [32, 33]. If the antigen is sequestered in an immune privileged site or its concentration is very low, the autoreactive T cells never come in contact or do not get sufficiently stimulated,

respectively. On the contrary, self-reactive T cells, which constantly encounter their antigen, undergo apoptosis, mediated by engagement of the death receptor Fas, IL-2 signaling and induction of the mitochondrial death pathway. TCR ligation might also lead to functional inactivation, called anergy, if CTLA4 (cytotoxic T-lymphocyte antigen 4) and PD-1 (programmed cell death 1) signaling is induced in T cells by co-inhibitory signals from tolerogenic APCs. Alternatively, a fully activated self-reactive T cell can still be harmless if it develops a non-pathogenic phenotype in terms of cytokine and chemokine receptor expression [34, 35]. In addition, there are also T cell-extrinsic mechanisms for dampening immune responses against self-structures. Tolerogenic DCs secrete immunomodulatory cytokines, such as IL-10 and transforming growth factor β (TGFβ), to inhibit T cell effector functions and induce Treg differentiation [36]. Tregs are very important in controlling autoreactive T cells by suppressing proliferation, activation and effector functions via cell-cell contact (CTLA4, PD-1), as well as via anti-inflammatory cytokines (IL-10, IL-35, TGFβ) [37]. Besides, type 1 regulatory T cells (Tr1 cells) develop from chronically stimulated $CD4^+$ T cells [38] and perform suppressive functions similar to Tregs [39].

Similar to T cells, B cells are also subjected to several tolerance mechanisms - both central and peripheral - to prevent potentially destructive immune responses to self-tissues. During central tolerance in the bone marrow, immature B cells, which recognize self-antigen, undergo receptor editing, followed by clonal selection. Receptor editing describes the process by which B cells reprogram the specificity of their antigen receptor. Upon BCR ligation, autoreactive B cells undergo secondary rearrangements of Ig genes, leading to replacement of the light chain and, thus, altered BCR specificity. If the B cell still strongly interacts with self-antigen, it is deleted through apoptosis. In contrast, if the BCR has been swapped for a non-autoreactive one, the cell becomes positively selected and can continue developmental maturation. In case the autoantigen is present in small amounts or the BCR has a low affinity for the self-ligand, the B cell can become anergic, showing reduced responsiveness to BCR stimulation. Peripheral tolerance mechanisms occur at later stages of B cell development and negatively regulate the survival and functionality of autoreactive B cells [40, 41]. In secondary lymphoid organs, anergy is an important measure to promote tolerance. Repetitive BCR ligation renders the B cell anergic, unless the antigen is also sensed by a T helper cell, which then stimulates the B cell [42]. Thus,

mechanisms of T cell tolerance also contribute to controlling autoreactive B cells. Compared to non-autoreactive B cells, these anergic B cells have a reduced lifespan and are gradually displaced [43]. Besides, self-reactive B cells show decreased expression of CD86 and CXCR5 in response to continuous BCR stimulation, preventing them from migrating into lymphoid follicles and causing their death in the interfollicular zone [44-46].

The immune system employs great efforts to maintain tolerance and yet, sometimes these protective mechanisms fail which can cause tissue damage and development of autoimmunity. If the autoantigen is systemically present, self-reactive lymphocytes can induce tissue inflammation in multiple organs. In contrast, restricted expression of the autoantigen leads to development of organ-specific autoimmune diseases such as type 1 diabetes, rheumatoid arthritis or multiple sclerosis.

1.2 Multiple sclerosis

Multiple sclerosis (MS) is a life lasting disease of the central nervous system (CNS) characterized by chronic autoimmune inflammation and massive demyelination, resulting in neuronal damage and progressive paralysis. MS is the most common neuro-inflammatory disease with around 2.5 million patients being affected worldwide, and numbers are on the rise. First symptoms usually appear at the age of 20 to 40 years, with a higher prevalence in women compared to men [47]. The disease is very heterogeneous and presents with a wide range of clinical symptoms, including deficits in sensible, sensory, motor and cognitive function. Depending on the clinical course, three different forms of MS have been described. The majority of patients develop the relapsing-remitting form of MS (RRMS), characterized by sequential attacks of neurological disability followed by partial or full recovery. In many of these patients, the disease turns into a progressive form (secondary progressive MS) after 10 to 20 years, resulting in increasing and irreversible disability. Around 15 % of patients develop a progressive form from the beginning of neurological symptoms, called primary progressive MS (PPMS) [48].

The features of MS were first described by the French neurologist Jean-Martin Charcot in 1868 and yet, the disease pathogenesis is not well understood. Both environmental

and genetic risk factors have been identified. Environmental factors include vitamin D deficiency, cigarette smoking, diet and obesity, and are known to contribute to the risk of MS development [49]. Also microbial infections can increase the risk, as was shown for infection with Epstein-Barr virus in young adulthood [50]. More recently, the intestinal microbiota emerged as a potential triggering factor for autoimmune activation [51]. On the other hand, relatives of MS patients show an increased risk for developing the disease. The concordance rate of 5 % in dizygotic twins is raised to about 30 % in monozygotic twins, pointing towards a prominent impact of genetics on MS susceptibility [51, 52]. Genome wide association studies have led to discovery of over 200 risk-increasing gene variants, many of them being associated with regulation or activation of Th cells [53]. The HLA-DRB1*1501 allele confers the highest susceptibility to MS [54]. Taken together, the combination of genetic susceptibility and environmental trigger is considered to be causative for disease development.

Inflammatory plaques are the histopathological hallmark of MS and can affect various areas of the CNS - brain, spinal cord and/or optic nerve - during different stages of the disease. These lesions are characterized by infiltration of immune cells, glial reaction and demyelination in the white matter. Some lesions also contain deposition of complement and antibodies. After the acute phase, the remaining axons can either be remyelinated or the inflammation resolves without repairing the myelin sheath or, in the worst case, the inflammation and degeneration persists. These smoldering lesions are prominent in progressive phases of the disease. In younger patients, repair of lesions appears to be more effective [48]. When the disease reaches the progressive stage (SPMS and PPMS), also the cortex is severely damaged. Cortical demyelination was found in the forebrain as well as in the cerebellum [55]. Interestingly, these subpial cortical lesions are often associated with lymphoid follicle-like structures in the leptomeninges. These aggregates were shown to contain T cells, proliferating B cells, plasma cells and follicular dendritic cells (FDCs), suggestive of germinal center formation. Their role in disease pathogenesis is still being investigated [56].

1.3 Experimental autoimmune encephalomyelitis

To investigate the molecular and cellular components as well as their functional interplay in MS, the animal model experimental autoimmune encephalomyelitis (EAE)

was developed in the 1930s [57]. Disease induction in EAE is based on an autoimmune response, orchestrated by activated CNS-reactive T cells, which cross the blood-brain barrier, recruit other immune cells and coordinate the attack of the myelin sheath. The resulting inflammation, demyelination and axonal damage lead to progressive paralysis. The EAE model was instrumental in deciphering pathogenic mechanisms of CNS autoimmunity and, further, was indispensable for development of several disease-modifying therapies for MS [58].

The myelin sheath is formed by oligodendrocytes and is mainly composed of lipids and myelin proteins (Figure 2). Several myelin antigens have been identified which can be used for EAE induction, including myelin oligodendrocyte glycoprotein (MOG), myelin basic protein (MBP), or proteolipid protein (PLP). Although MOG is present only in low amounts, its localization on the outermost surface of the myelin sheath together with its extracellular Ig-domain renders it well accessible to antibodies or immune cells and, therefore, very immunogenic [59]. Several methods of EAE induction have been established with mice being the most commonly used animal model.
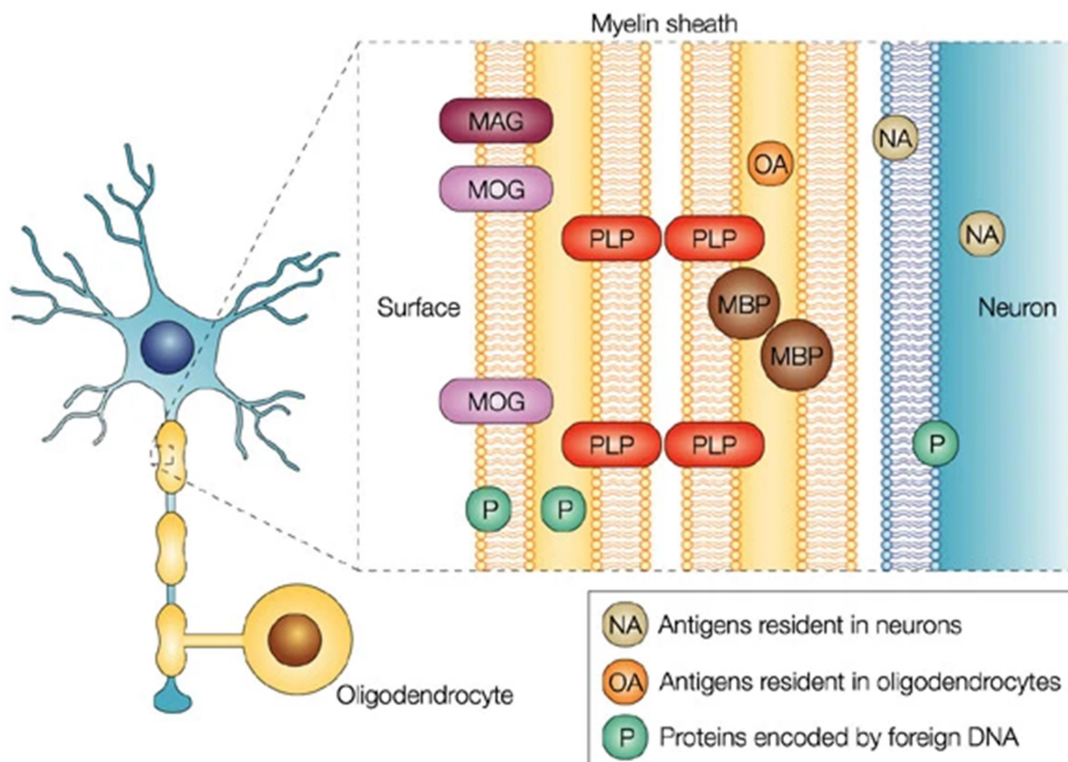
Figure 2. **Architecture of the myelin sheath around axons in the CNS.** Myelin-associated glycoprotein (MAG); myelin basic protein (MBP); myelin oligodendrocyte glycoprotein (MOG); proteolipid protein (PLP). Adapted by permission from [60].

A widely-used model is active EAE, which is induced by immunizing mice with a myelin protein or peptide emulsified in complete Freund`s adjuvant (CFA). The choice of myelin antigen and the genetic background of the animal determine the lesion distribution and the clinical phenotype. For example, $PLP_{139-151}$-induced EAE in SJL mice leads to lesion formation predominantly in the spinal cord and development of a relapsing-remitting disease course [61-63]. In contrast, C57BL/6 mice immunized with MOG_{35-55} peptide develop a monophasic disease course, characterized by ascending paralysis and followed by a recovery phase. In these mice, lesions are distributed throughout the CNS [64].

In addition, generation of several transgenic mouse lines provided models for spontaneous EAE development. 2D2 mice carry a transgenic TCR specific for the MOG_{35-55} peptide on the C57/BL6 background and show a very low incidence (4 %) [65]; however, when they are crossed to IgH^{MOG} (also referred to as Th) mice [66], 60 % of these double transgenic OSE (opticospinal EAE) mice develop EAE with a progressive disease course due to cooperation of MOG-specific T and B cells [67, 68]. Furthermore, in the TCR^{1640} (also referred to as RR) model on the SJL genetic background, transgenic MOG-specific T cells recruit MOG-specific B cells from the endogenous repertoire and the mice develop a relapsing-remitting disease course, closely resembling the most common MS variant [69]. Similar to traditional active EAE, pathogenic T cell responses in these transgenic models involve both Th1 and Th17 cells, which are T cell effector subsets important for organ-specific autoimmunity and are further explained in section 1.4.1.

The third option of inducing EAE is the adoptive transfer of encephalitogenic T cells. Here, myelin antigen-primed T cells can be isolated from immunized mice, followed by *in vitro* restimulation in Th1 or Th17-skewing conditions and subsequent transfer into recipient mice [70, 71]. On the other hand, naïve TCR transgenic T cells recognizing MOG_{35-55} can be obtained from 2D2 mice, differentiated *in vitro* into Th1 and Th17 cells for adoptive transfer, which represents a more rigorous protocol [72].

1.4 Adaptive immune cells and their role in CNS autoimmunity

1.4.1 T helper cells

MS research traditionally focused on autoreactive T cells which have long been accepted to be important drivers of CNS inflammation. To our current knowledge, autoreactive T helper cells become activated in the periphery before they invade the CNS and attack the myelin sheath. Depending on the cytokine microenvironment, T helper cells differentiate into different effector T helper cell subsets.

Based on their cytokine expression, Th cells were first classified into two subsets with very distinct effector functions, Th1 and Th2 cells [73]. Th1 cells predominantly produce interferon (IFN)γ, rendering them very effective in activating macrophages. Therefore, Th1 cells are crucial in protecting the host against intracellular pathogens. In contrast, the Th2 subset, along with its signature cytokines IL-4, IL-5 and IL-13, plays a critical role for immune responses directed against extracellular parasites. In addition, Th2 cells are also implicated in allergic and asthmatic diseases [74]. By secreting IL-4, Th2 cells provide help to B cells, by inducing them to switch their isotype [75]. While several studies have shown that Th2 cells are unable to induce EAE [72, 76, 77], Th1 cells were considered to be the sole disease-driving cell type for many years, as indicated by robust evidence from MS and EAE studies. In CNS and CSF of MS patients, the expression of IL-12, the cytokine important for Th1 differentiation, and IFNγ was correlated with increased disease activity [78]. In addition, administration of IFNγ caused exacerbation of MS symptoms [79]. In EAE, CNS-infiltrating T cells were found to secrete IFNγ, which could also be detected in inflammatory lesions in the CNS of mice [80, 81] and MS patients [82]. Mice deficient in STAT4 and T-bet (Th1 transcription factors) proved to be resistant to EAE [83, 84]. Furthermore, adoptively transferred Th1 cells are able to induce EAE [72, 76, 85], confirming the pathogenic potential of Th1 cells.

However, the paradigm of Th1 cells being the sole pathogenic effector cells was challenged when mice deficient in IFNγ or STAT1 were shown not to be resistant to EAE, but even exhibit exacerbated disease [84, 86]. In addition, the demonstration that IL-12p35 - knockout (KO) mice are susceptible to EAE, whereas IL-12p40-KO mice are protected from disease development [87], further raised questions regarding the contribution of Th1 cells to pathogenesis. IL-12 is composed of two subunits, p35 and

p40, the latter of which can also pair with another subunit, p19, forming the cytokine IL-23 [88]. The seminal finding that mice lacking IL-23 (p40 or p19 KO) do not develop EAE, while mice lacking only IL-12 (p35 KO) are still susceptible to disease [89], pointed towards IL-23, rather than IL-12, to be indispensable for development of CNS autoimmunity. The observation that these IL-23-deficient mice lack an IL-17 producing T cell population lead to the discovery of a new Th cell subset, the Th17 cells [70]. Naïve T cells differentiate into the Th17 lineage in the presence of IL-6 and TGFβ [90-92], which induce expression of the master transcription factor RAR-related orphan receptor γt (RORγt) [93]. In addition, IL-1β can synergize with IL-6 in Th17 cell induction [94]. Importantly, Th17 cells depend on IL-23 signaling for stabilizing their lineage and acquiring their full pathogenic potential [72, 91, 95, 96]. In the absence of IL-23, Th17 cells develop into a non-pathogenic phenotype, inducing only mild to no disease upon adoptive transfer [96, 97]. Th17 cells secrete a set of different cytokines – IL-17A, IL-17F, IL-21, and IL-22 – and play an important role in defending the host against infections with fungi and some bacteria [98]. In addition, non-pathogenic Th17 cells are crucial for the intestinal homeostasis [99, 100]. Th17 cells can also acquire production of the Th1 cytokine IFNγ, demonstrating the plasticity of this subset [72, 101, 102]. Since the receptors of their cytokines are broadly expressed, Th17 cells have the potential to induce massive tissue inflammation [103]. In addition, they are important players in organ-specific autoimmune diseases, including CNS autoimmunity. In MS, elevated amounts of IL-17 transcripts were found in chronic lesions compared to acute lesions or healthy controls [104]. Besides, a higher frequency of Th17 cells could be detected in blood and CSF of MS patients, especially during relapses [105]. In mice, IL-17A neutralizing antibodies cause amelioration of EAE [106], and IL-17A deficiency results in attenuated disease [107, 108].

Taken together, accumulating evidence suggests both Th1 and Th17 cells to be important players in CNS autoimmunity. Adoptive transfer experiments demonstrated the capacity of Th1 and Th17 cells to induce EAE independently of each other. Interestingly, each subset caused a distinct pattern of lesion formation and immune cell infiltration [72], with ectopic lymphoid follicle - like structures being found predominantly in Th17 recipients [109].

1.4.1.1 Visualizing T cell activation by intravital microscopy

Today, it is widely accepted that encephalitogenic T cells are activated in the periphery, before they migrate to the CNS. Here, they cross the BBB, become reactivated by local APCs, such as macrophages and DCs, presenting autoantigen and initiate the inflammatory response. By using genetically-encoded calcium indicators, this local reactivation can be visualized *in vivo* [110].

Intracellular calcium (Ca^{2+}) is one of the key signaling components involved in T cell activation. T cells possess several types of Ca^{2+} channels in the plasma membrane and organelles to allow tight regulation of spatial and temporal calcium microdomains required for proper T cell function [111]. In resting T cells, the cytosolic Ca^{2+} concentration ranges between 50 and 100 nM, and can be increased up to 1 µM in response to TCR ligation. The two main Ca^{2+} storages responsible for this massive Ca^{2+} influx into the cytosol are the endoplasmic reticulum (ER) and the extracellular space [112]. TCR engagement causes production of the second messenger inositol-1,4,5-trisphosphate (IP_3), which causes a transient release of Ca^{2+} from the ER upon binding to its receptor channels. The depletion of the ER Ca^{2+} store is sensed by stromal interaction molecule 1 (STIM1) and STIM2 [111]. These proteins, in turn, mediate activation of calcium release-activated calcium (CRAC) channels in the plasma membrane, leading to prolonged Ca^{2+} influx from the extracellular space into the cell [113]. Calcium signaling regulates multiple downstream targets depending on the signal length. As a rapid response, reorganization of the cytoskeleton as well as changes in motility stabilize contacts between APCs and T cells [112]. This stable APC-T cell junction is referred to as the immunological synapse and integrates the interaction of these two cell types via three receptors: MHC-II:antigen:TCR, costimulatory, and adhesion molecules [114]. While costimulatory receptors have only little signaling activity on their own, they increase signaling and adhesion in combination with stimulation via the TCR, and are therefore important for stable synapse formation [115-117]. Longer calcium signals - minutes to hours - result in translocation of transcription factors such as nuclear factor kappa B (NF-κB) or nuclear factor of activated T cells (NFAT) into the nucleus, thereby inducing transcription of activation-dependent gene expression. Prolonged calcium signaling is required for various functions, including proliferation, maturation and cytokine production [118, 119].

When signaling via the TCR is discontinued, the calcium ions are transported out of the cell or sequestered again in the ER [111]. Calcium signaling in T cells can exhibit a variety of different patterns, ranging from irregular spikes to plateaus and sustained oscillations, and leading to various cellular responses [112]. Calcium oscillations are considered to drive distinct gene expression patterns due to differential activation of NFAT and NF-κB [120, 121]. In addition, these oscillations have been implicated to sensitise T cells when the antigen is available only in low amounts or has a low affinity [120, 122].

The development of genetically-encoded calcium indicators provided a powerful tool to not only visualize cellular movement, but also monitor cellular function in living lymphocytes by two-photon microscopy. The fluorescence resonance energy transfer (FRET) - based ratiometric sensor Twitch-2B allows to study T cell activation in real-time by measuring the intracellular calcium concentration [110]. Twitch-2B was optimized for use in mouse T cells and represents an enhanced version of TN-XXL (Figure 3) [123]. Cyan fluorescent protein (CFP) and cpCitrine in TN-XXL were replaced by mCerulean3 and a codon-diversified cpVenus[CD], respectively. In addition, Twitch-2B contains a calcium-binding moiety with higher affinity compared to Troponin C (TnC). In case of low calcium levels, the sensor emits cyan fluorescence upon excitation of mCerulean3. When the calcium concentration increases, the binding of the
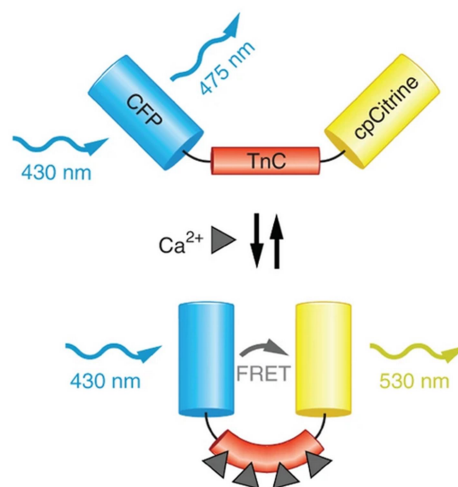
Figure 3. Schematic representation of the FRET-based calcium indicator TN-XXL. TN-XXL consists of cyan fluorescent protein (CFP) and cpCitrine, connected by the calcium-binding domain Troponin C (TnC). Adapted by permission from [123]

TnC domain by calcium ions causes a conformational change bringing the two fluorophores in close proximity. The resulting FRET from mCerulean3 to cpVenus leads to a drop in blue fluorescence and an increase in yellow fluorescence. Thereby, the ratio of yellow and blue fluorescence directly reflects the change in the intracellular calcium concentration in real-time [123, 124].

1.4.2 B cells

Although MS research traditionally focused on autoreactive T cells, B cells have received increasing attention in the past decade since accumulating evidence suggests a pivotal role of B cells in disease pathogenesis. B cells do not only produce antibodies, but also play important roles as APCs and cytokine producers. All three of these effector functions could contribute to MS pathogenesis.

In MS lesions, both B cells and antibody/complement depositions have been detected [125, 126]. Antibodies are also present in the cerebrospinal fluid (CSF) of patients and form oligoclonal bands (OCBs) – a long established biomarker for the diagnosis of MS [127]. Most OCBs were proven to be a product of local, CNS resident B cells [128]. Surprisingly, many of these antibodies are not specific for CNS antigens [129] and myelin oligodendrocyte glycoprotein (MOG)-specific antibodies can only be found in a subgroup of MS patients [130]. Whether these antibodies are pathogenic is discussed controversially, but some patients benefit from plasmapheresis [131], supporting the potential of antibodies to promote disease. The contribution of B cells as antibody producers was demonstrated in the murine TCR^{1640} model, which closely resembles the disease course of relapsing-remitting MS. Here, MOG-specific B cells are expanded from the endogenous (non-transgenic) repertoire by transgenic MOG-specific T cells and produce anti-MOG autoantibodies, which induce large demyelinating lesions and increased EAE severity upon transfer into immunized wildtype mice [69].

A breakthrough in MS therapy was the efficacy of B cell depleting anti-CD20 antibodies (Rituximab and Ocrelizumab), which substantially reduce relapse frequency and MRI lesions [132, 133]. Importantly, antibody-producing plasma cells do not express CD20 and are therefore not depleted by this treatment. This suggests a role for B cells as

cytokine-producing and/or antigen-presenting cells rather than antibody producers in disease pathogenesis. Being an important source of cytokines, B cells can shape T cell-mediated immune responses. In MS patients, B cells upregulate the expression of pro-inflammatory cytokines such as IL-6, lymphotoxin (LT) and tumor necrosis factor (TNF)α, while downregulating IL-10 production [134-136]. In EAE, IL-6 secretion by B cells is crucial for EAE development [137, 138]. In contrast to this pro-inflammatory phenotype, B cells can also have a regulatory function in CNS autoimmunity. Regulatory B cells suppress inflammation and promote EAE recovery by secretion of IL-10, IL-35 and TGFβ [139-143]. Additionally, B cells can propagate inflammation by presenting antigen on MHC-II to cognate CD4$^+$ T cells. Their important role as APCs in neuroinflammation was reported in mice immunized with human MOG protein (instead of MOG peptide) [144], where B cells are required to process and present the antigen to drive pathogenic T cell responses [138, 145]. Furthermore, studies in OSE mice indicate that MOG-specific B cells present antigen very efficiently to cognate T cells and are superior to other APCs [67, 68].

In addition, histopathological analysis revealed ectopic lymphoid follicle-like structures (eLFs) in the leptomeninges of certain MS patients. These aggregates contain various immune cells, most importantly T and B cells, and have been hypothesized to fuel chronic inflammation directly in the CNS. A detailed description is given in the next section.

1.4.3 Ectopic lymphoid follicles

Secondary lymphoid organs (SLOs) like spleen and lymph nodes represent important platforms for the generation of adaptive immune responses. Their architecture allows collecting antigen and APCs from peripheral tissues and subsequent presentation to T and B cells. SLOs are organized in different compartments that facilitate intense interactions between different cellular components. In the T cell zone, naïve T cells become activated upon antigen recognition, resulting in clonal expansion and differentiation into effector or memory T cells. The differentiation and maturation of B cells in germinal centers of B cell follicles is explained in detail in section 1.1.2. However, in peripheral tissues affected by chronic inflammation, including autoimmunity, persistent infection and cancer, infiltrating immune cells can form ectopic

lymphoid follicle-like structures (eLFs), often also called tertiary lymphoid organs (TLOs) [146]. In contrast to SLOs, these aggregates are mostly transient structures without a capsule, which disintegrate when the antigen has been cleared [147].

In MS, eLFs were first described by Serafini et al. in 2004 and found in the leptomeninges of patients with a chronic progressive disease course [56, 148]. Later, similar aggregates were also described in early stages of RRMS [149]. Initially, they were thought to be restricted to brain meninges, where they are localized mainly in sulci, but they can also form in spinal cord meninges [150]. These aggregates show varying degrees of maturation, ranging from loose clusters of cells to highly organized follicle structures, which contain plasma cells, proliferating B cells, T cells and FDCs, and therefore are suggestive of germinal center formation (Figure 4). Clinical data show a correlation between the presence of eLFs and a more severe disease course – younger age at disease onset, irreversible disability, and death, as well as a more pronounced cortical pathology [56, 148, 151-153]. Thus, these follicles have been postulated to maintain or exacerbate chronic inflammation directly in the CNS.
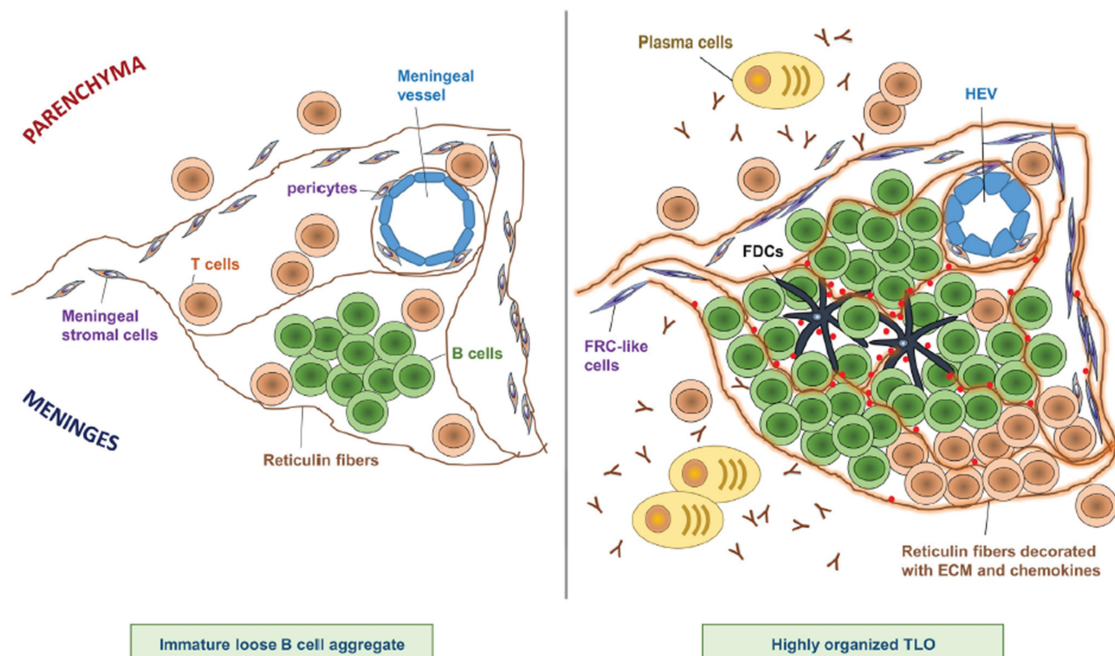
Figure 4. Composition of eLFs in the CNS. eLFs appear in different stages of organization, ranging from immature loose B cell aggregates (left) to highly organized tertiary lymphoid organs (TLOs) (right) containing T cells, B cells and sometimes FDCs, all being surrounded by reticulin fibers produced by FRC (fibroblastic reticular cell) - like cells. Plasma cells and antibodies are found in close vicinity. Additionally, high endothelial venules (HEV) have been observed in some eLFs. Adapted by permission from [147].

After eLFs had been described in the MS, they were also identified in several EAE models differing regarding genetic background, mode of EAE induction and auto-antigen [109, 154-157]. However, the clinical relevance of eLFs remains elusive. A correlation between eLF presence and a more severe disease course was only found in the spontaneous OSE model, carrying a MOG-specific T and B cell receptor [156]. Across all EAE models, eLFs are characterized by the presence of B cell zones, whereas T cells appear to be more scattered. In addition, meningeal eLFs were reported to be positive for germinal center markers [109, 155, 158, 159] and to recapitulate some features of SLOs [147]. However, a detailed characterization of the cellular components of meningeal eLFs on a transcriptional or protein-level is still lacking. Since eLFs provide a good microenvironment for the interaction of B and T cells, it can be hypothesized that they fuel inflammation in the CNS by supporting differentiation and maturation of CNS-specific effector B and T cells behind the blood-brain barrier. On the other hand, it is also possible that eLFs develop as a counterregulatory process to dampen ongoing inflammation in the CNS.

Importantly, in adoptive transfer EAE, histological analysis revealed that eLF-like structures were predominantly found in the leptomeninges of Th17 recipients, whereby a longer disease duration with a high clinical score leads to a more advanced developmental stage of eLFs [109]. Indeed, several lines of evidence speak in favor of a special relationship between Th17 cells and B cells. On the one hand, Th17 cells produce IL-21, which promotes B cell proliferation, maturation and isotype switching, and they are excellent B cell helpers in SLO GC reactions [160]. In addition, Th17 cells induce eLF formation also in other settings, for example in the intestine during infection with Citrobacter rodentium [161] or following infection or inflammation in the lung [162]. In the Th17 adoptive transfer EAE model, transferred T cells were shown to express markers of Tfh cells, as well as GC markers in the CNS [109], suggesting that they may provide help to the B cells on site. On the other hand, B cells are efficient APCs for the activation of T cells with the same antigen specificity [163]. They also produce IL-6 [137], an important cytokine for pathogenic Th17 cell differentiation in EAE [138]. Since B cells are well positioned in meningeal eLFs to interact with infiltrating T cells, they are a good candidate as APCs for the reactivation of T cells in the CNS, which is crucial for disease development and progression. However, whether B cells fulfill this function in eLFs, still needs to be investigated. Taken together, it can be hypothesized that Th17

cells are uniquely equipped to recruit B cells to the CNS and to interact with them in a GC-like reaction in eLFs.

2. Objectives

Pathogenic T cells have long been accepted to be important disease drivers in CNS autoimmunity. During the past decade, compelling evidence has also suggested a pivotal role of B cells. However, it is only poorly understood how T cells and B cells cooperate to induce disease. Meningeal ectopic lymphoid follicle-like structures (eLFs) in MS and EAE have been hypothesized to fuel chronic inflammation directly in the CNS by supporting differentiation and maturation of CNS-specific effector T and B cells. Using adoptive transfer EAE, Th17 cells, but not other Th cell subsets, were demonstrated to induce the formation of eLFs. The aim of this thesis was to investigate the unique relationship of Th17 cells and B cells in EAE development, and, in particular, to assess the nature of their interaction in eLFs.

First, adoptive transfer EAE was established to compare the ability of Th1 and Th17 cells to induce EAE and recruit B cells into the CNS. To investigate the localization, structural organization and cellular composition of eLFs, a detailed histological analysis of spinal cord and brain of Th17-EAE mice was performed. As eLFs have been reported to recapitulate some features of SLOs, they were examined for T and B cell proliferation and expression of germinal center markers (section 4.1). Second, it was investigated whether Th17 cells shape a pathogenic B cell response. In addition to antibody production and cytokine secretion, B cells could reactivate T cells in the CNS by upregulating their capacity to present antigen and provide costimulatory stimuli. To address this, the phenotype of CNS-infiltrating B cells was characterized by single-cell RNA sequencing and compared to peripheral B cells to clarify whether CNS B cells have a pro-inflammatory function contributing to disease pathogenesis. BCR repertoire analysis was performed to investigate whether infiltrating B cells undergo clonal expansion in the CNS. Further, it was tested whether transferred T cells recruit autoreactive B cells with the same antigen specificity from the endogenous pool (section 4.2). Third, the role of B cells in reactivating T cells in the CNS was investigated. Th17-mediated EAE was performed in B cell-deficient Mb1-KO mice to learn more about the contribution of B cells to disease development and T cell functions in the CNS. In addition, the interaction of T and B cells in eLFs was observed in real-time using intravital two-photon microscopy to shed light on the role of eLFs in supporting smoldering inflammation within the CNS (section 4.3).

3. Material and Methods

3.1 Mice

C57BL/6 mice were purchased from Janvier Labs. C57BL/6 mice with a transgenic TCR specific for the MOG_{35-55} peptide, here referred to as 2D2 mice, have been described previously [65] and were purchased from The Jackson Laboratory. IgH^{MOG} mice on a C57BL/6 background, here referred to as Th mice, carrying an Ig heavy chain knock-in of the rearranged VDJ gene from the MOG-specific monoclonal antibody 8.18C5, have been described previously [66] and were kindly provided by Prof. Hartmut Wekerle. Mb1-Cre mice on a C57BL/6 background carry a codon optimized Cre recombinase, replacing exon 2 and 3 of the *Cd79a* gene, which encodes the Ig-α subunit of the BCR and is exclusively expressed in B cells. This knock-in leads to abolishment of endogenous *Cd79a* gene function and expression of Cre recombinase under control of the *Cd79a* promoter [164]. Mb1-Cre mice were purchased from The Jackson Laboratory. Homozygous mice are B cell-deficient and hereafter referred to as Mb1-KO mice. Mb1-Cre mice were crossed to ROSA26 tdTomato mice to obtain mice that are heterozygous for both Mb1-Cre and ROSA26 tdTomato, thereby expressing tdTomato specifically in B cells for intravital microscopy experiments. ROSA26 tdTomato mice on a C57BL/6 background carry a *loxP*-flanked STOP cassette and *tdTomat*o gene, both inserted into the ROSA26 locus. Upon Cre-mediated recombination, tdTomato fluorescence is robustly expressed in these mice [165]. ROSA26 tdTomato mice were purchased from The Jackson Laboratory. OT-II mice, carrying a transgenic TCR specific for the $ovalbumin_{323-339}$ peptide on a C57BL/6 background [166], were purchased from The Jackson Laboratory.

All animals used in this study were housed and bred in specific pathogen-free conditions in the Core Facility Animal Models at the Biomedical Center of the Ludwig-Maximilians-Universität München. Animal experiments were designed and performed in accordance with regulations of the animal welfare acts and under approval by the animal ethics committee of the state of Bavaria (Regierung von Oberbayern) in accordance with European guidelines.

3.2 Isolation of cells from spleen and lymph nodes

Spleens were mashed and centrifuged at 300 g for 5 minutes (min) at 4 °C. To lyse erythrocytes, the cells were resuspended in ACK buffer (150 mM NH_4Cl (Merck), 10 mM $KHCO_3$ (Merck), 0.1 mM EDTA (Sigma)) and incubated for 1.5 min at RT. The reaction was stopped by adding 9 ml T cell medium (RPMI 1640 (Sigma) supplemented with 10 % heat-inactivated FBS, 1 % penicillin-streptomycin, 10 mM HEPES, 2 mM L-glutamine, 1 % non-essential amino acids, 1 mM sodium pyruvate and 50 µM β-mercaptoethanol), and the cell suspension was passed through a 70 µm cell strainer. After centrifugation, the cells were resuspended in T cell medium.

Lymph nodes (LNs) were cut into pieces, mashed and filtered through a 70 µm cell strainer. Then, the cells were centrifuged at 300 g for 5 min at 4 °C and resuspended in T cell medium.

3.3 *In vitro* differentiation of T effector cells

Naïve CD4$^+$ T cells were purified from spleen and lymph nodes of 6-15 week old 2D2 mice or OT-II mice using the naïve CD4$^+$ T cell isolation Kit (Miltenyi Biotec) according to the manufacturer`s instructions. After isolation of naïve CD4$^+$ T cells the rest of the cells (flow-through from T cell purification) was irradiated at 35 Gy and used as APCs for costimulation of differentiating T cells. Naïve T cells were cultured at a concentration of $1.5-2x10^6$ ml^{-1} in T cell medium in the presence of $7.5-10x10^6$ ml^{-1} irradiated APCs (ratio T cells : APCs is 1 : 5) and 2.5 µg/ml soluble anti-CD3 antibody (clone 145-2C11, BioXCell). Th1 cells were generated by addition of IL-12 at a concentration of 10 ng/ml and anti-IL-4 antibody (clone 11B11, BioXCell) at a concentration of 10 µg/ml into the culture. For the generation of Th17 cells, naïve T cells were cultured with IL-6 at a concentration of 30 ng/ml, TGFβ at a concentration of 3 ng/ml, IL-1β at a concentration of 20 ng/ml, and anti-IFNγ (clone XMG1.2, BioXCell) and anti-IL-4 antibody (clone 11B11, BioXCell) at a concentration of 10 µg/ml. After 48h, Th1 cells and Th17 cells were split with medium containing 10 ng/ml of IL-2 and medium containing 10 ng/ml of IL-23, respectively. All cytokines were purchased from Biolegend except IL-23 (Miltenyi Biotec). The different T cell subsets were analyzed for cytokine production after 4 days by intracellular cytokine staining and subsequent flow

cytometry. After 5-8 days of primary culture, T cells reached a resting state and were restimulated at a concentration of $2x10^6$ ml^{-1} for 48 h in the presence of plate-bound anti-CD3 (clone 145-2C11, BioXCell) and anti-CD28 (clone PV-1; BioXCell) antibodies both at 2 µg/ml in fresh medium without any cytokines.

3.4 Retrovirus production

The production of retroviral particles containing the calcium indicator Twitch-2B was performed using Phoenix cells [167], which were cultured in retroviral transduction medium (RTM; DMEM containing 10 % heat-inactivated FBS, 1 % penicillin-streptomycin, 2 mM L-glutamine, 360 mg/l asparagine, 1 % non-essential amino acids, 1 mM sodium pyruvate and 57.2 µM β-mercaptoethanol). Phoenix cells were split every 2-3 days to prevent the cells from reaching confluence, as this would reduce transfection efficiency. For splitting, cells were washed once with PBS and then detached with Trypsin-EDTA (Sigma) for 1-2 min. To stop the reaction, four volumes of RTM were added and cells were centrifuged at 300 g for 5 min at 4 °C. The cell pellet was resuspended in RTM and diluted 1:6 to 1:8 for further cultivation. Phoenix cells were plated at $1.5-2x10^6$ per 10 cm dish in 10 ml RTM and allowed to attach to the plate for 18-24 hours. At this subconfluent stage, transfection works best, producing the highest virus titers possible. First, chloroquine diphosphate (Sigma) was added at a concentration of 25 µM. Per dish, 12 µg pMSCV-Δneo-Twitch-2B plasmid (kindly provided by Dr. Naoto Kawakami) and 3.5 µg pCL-Eco packaging plasmid (kindly provided by Dr. Gurumoorthy Krishnamoorthy) were prepared in 438 µl H_2O. Subsequently, 62 µl 2 M $CaCl_2$ (Riedel de Haën) were added followed by dropwise addition of 500 µl 2X BES (50 mM N,N-bis(2hydroxyethyl)-2-aminoethanesulfonic acid (Sigma) + 280 mM NaCl (Sigma) + 1.5 mM Na_2HPO_4 (Roth) in H_2O) while vortexing. This mixture was incubated for 20 min at 37 °C and then added dropwise to the cells. On the next day, the medium was replaced with 8 ml fresh and warm RTM. Following another day of incubation, the cell culture supernatant, containing viral particles, was collected using a 10 ml syringe and filtered through a 0.45 µm filter and kept at 4 °C. To every dish, 4 ml fresh and warm RTM was added and the cells were incubated for another day. The supernatant was collected again, filtered through a 0.45 µm filter and pooled with the supernatant from the day before. Then, the supernatant was

concentrated by centrifugation at 1000 g at 4 °C through Amicon® Ultra 15 mL Centrifugal Filters (100 K; Merck). Finally, the concentrated supernatant was snap frozen using dry ice and stored at -80 °C.

3.5 Retroviral transduction of Th17 cells

Th17 cells can be transduced with the Twitch-2B calcium indicator either during the primary or secondary phase of the *in vitro* culture (section 3.3.).

Retroviral transduction during primary phase: After 48 h of primary culture, Th17 cells were split (usually 1:3) and transduced by adding 1:80-diluted retroviral supernatant (section 3.4) and 4 µg/ml polybrene (Sigma) in addition to 10 ng/ml IL-23 and 10 µg/ml anti-IFNγ antibody (all diluted in pre-warmed T cell medium and calculated for culture volume). Then, cells were spin-infected at 480 g for 90 min at 30 °C. On the next day, half of the medium was replaced with fresh and warm T cell medium containing 10 ng/ml IL-23 and 10 µg/ml anti-IFNγ antibody. 48 h after transduction, Twitch-2B expression was analyzed via GFP-signal by flow cytometry.

Retroviral transduction during secondary phase: 24 h after restimulation with anti-CD3/CD28 antibodies, half of the medium was taken up and Th17 cells were transduced by adding 1:80-diluted retroviral supernatant (section 3.4) and 4 µg/ml polybrene (Sigma) (all diluted in pre-warmed T cell medium and calculated for culture volume). Then, cells were spin-infected at 480 g for 90 min at 30 °C. On the next day, half of the medium was replaced with fresh and warm T cell medium. If cells were used for EAE experiments, cells were collected and washed for adoptive transfer, while an aliquot of cells, with half of the medium being replaced with fresh and warm T cell medium, was kept for determining the transduction efficacy. 48 h after transduction, Twitch-2B expression was analyzed via GFP-signal by flow cytometry.

3.6 EAE induction

In this study, EAE was induced by adoptive transfer of *in vitro* differentiated T cell subsets. Naïve MOG-specific CD4^{+} T cells, isolated from spleen and lymph nodes of 2D2 mice, were differentiated into Th1 or Th17 cells and restimulated with anti-CD3

and anti-CD28 antibodies as described in section 3.3. 48 h after restimulation, cells were collected and washed three times with PBS. In Th1-EAE, $1.7\text{-}3.2\times10^6$ IFNγ-producing cells were injected intraperitoneally (i.p.) into C57BL/6 recipients. In Th17-EAE, 4×10^6 IL-17A-producing cells were injected i.p. or intravenously (i.v.) into C57BL/6 or Mb1-KO or Mb1Cre x ROSA26 tdTomato recipients. In case of 2D2 and OT-II T cell co-transfer, 3×10^6 IL-17A-producing 2D2 cells and 2×10^6 IL-17A-producing OT-II cells were injected together i.p. into Mb1Cre x ROSA26 tdTomato recipients. Clinical disease developed 8-15 days post transfer.

3.7 EAE scoring

Mice were monitored daily for the development of clinical signs of EAE, including classical and atypical disease signs, according to the following criteria: 0, no disease; 0.5, decreased tail tonus; 1, limp tail or mild balance defects; 1.5, limp tail and ataxia; 2, hind limb weakness, or severe balance defects that cause spontaneous falling over; 2.5, partial hind limb paralysis; 3, complete hind limb paralysis or very severe balance defects that prevent walking; 3.5, complete hind limb paralysis and partial front limb paralysis; 4, complete front and hind limb paralysis or inability to move body weight into a different position; 5, moribund state. Animals with a minimum score of 2 were provided with food pellets and gel pads at the bottom of the cage.

3.8 Isolation of infiltrating mononuclear cells from the CNS

Recipient mice were sacrificed at indicated time points and perfused through the left cardiac ventricle with PBS. Brains were dissected by removing the skull using forceps and scissors, while spinal cords were flushed out from the bone column using a 21 gauge needle attached to a syringe filled with PBS. In addition, the vertebral column was opened to collect parts of meninges, which were still connected to the vertebrae. Then, brains and spinal cords were cut into pieces and digested for 30 min at 37 °C with DNase I (Sigma-Aldrich or Roche) at a concentration of 1 mg/ml and collagenase D (Roche) at a concentration of 3.75 mg/ml. Subsequently, the tissues were mashed and passed through a 70 µm cell strainer to prepare a single-cell suspension, followed by centrifugation at 350 g for 10 min at 4 °C. The cell pellet was resuspended in 5 ml

70 % Percoll (Cytiva), which was prepared by mixing 30 ml Percoll with 18 ml Percoll Mix Solution (mixture of 90 ml 10X PBS and 264 ml H_2O). Then, the cell suspension was slowly and carefully overlaid with 5 ml 37 % Percoll, which was prepared by diluting the 70 % Percoll solution with 1X PBS, followed by centrifugation at 650 g for 30 min at 21 °C. Then, mononuclear cells were collected from the interface between the 70 % and 37 % layer and washed twice with T cell medium to remove residual Percoll. Finally, cells were either stimulated for intracellular cytokine staining or stained directly for flowcytometric analysis.

3.9 Production of MOG tetramer

Mouse MOG_{1-125} protein (mMOG) was produced in human embryonic kidney cells expressing the Epstein-Barr virus nuclear antigen-1 (HEK-EBNA1) according to previously published protocols [168], a cell line designed for large-scale production of recombinant proteins [169]. Monomer production and tetramerization was performed as previously described [170]. Briefly, purified mMOG monomers were biotinylated using BirA ligase to enable multimerization. The biotin-binding protein streptavidin was used to form stable tetramer structures consisting of four biotinylated mMOG monomers. As the streptavidin was directly conjugated to AF 488, staining with MOG tetramer could be used to identify MOG-specific B cells by flow cytometry or confocal microscopy.

3.10 Flow cytometry

To analyze the cytokine expression of T cells by intracellular cytokine staining and flow cytometry, cultured or isolated cells were stimulated with 50 ng/ml phorbol 12-myristate 13-acetate (PMA; Sigma-Aldrich) and 500 ng/ml ionomycin (Sigma-Aldrich) in the presence of 0.7 µL/ml monensin (GolgiStop; BD Biosciences) for 4 h at 37 °C in 5 % CO_2. The phorbol ester PMA activates proteinkinase C (PKC) due to its structural similarity to the PKC activator diacylglycerol [171]. The calcium ionophore ionomycin induces an increase in intracellular Ca^{2+} levels, leading to Ca^{2+}-mediated signal transduction and further activation of PKC [172]. PKC stimulation through the combined action of PMA and ionomycin causes T cell activation and cytokine production. The

ionophore monensin inhibits protein transport within the Golgi apparatus [173], thereby preventing T cells from secreting intracellularly synthesized cytokines.

For surface stainings, the cells were washed with PBS. To exclude dead cells and debris, the samples were stained with the Zombie Violet[TM] or UV[TM] fixable viability kit (Biolegend) for 20 min at RT, whereby the viability dyes were diluted 1:600 in PBS. Then, cells were washed twice with FACS buffer (PBS containing 2 % FBS and 0.05 % sodium azide), and unspecific binding of antibodies to Fc receptors was blocked by incubating the cells with TruStain FcX[TM] (Biolegend) diluted 1:50 in FACS buffer for 15 min at 4 °C. The last step was omitted when *in vitro* differentiated T cells were analyzed. Afterwards, cells were stained with fluorophore-conjugated antibodies against surface markers diluted in FACS buffer for 20-30 min at 4 °C. If biotinylated antibodies were used, the samples were washed and subsequently stained with fluorophore-conjugated streptavidin (SA) diluted in FACS buffer for 20 min at 4 °C. After two washing steps, cells were resuspended in FACS buffer for analysis. For intracellular cytokine staining, cells were fixed for 30 min at 4°C with 0.4 % paraformaldehyde (PFA, Merck KGaA) and permeabilized by washing twice with permeabilization buffer (PBS containing 2 % FBS and 0.1 % saponin (Sigma-Aldrich)). Then, samples were incubated with antibodies against intracellular markers diluted in permeabilization buffer for 30 minutes at 4 °C, washed twice and resuspended in FACS buffer for analysis. Data were acquired on a BD LSRFortessa[TM] in the Core Facility Flow Cytometry at the Biomedical Center of the Ludwig-Maximilians-Universität München or BD FACSverse[TM] flow cytometer and analyzed using Flowjo software (version 10.6.2; TreeStar).

Table 1. Antibodies / reagents used for flow cytometry

Surface Markers					
Specificity	**Clone**	**Host**	**Conjugate**	**Company**	**Dilution**
anti-mouse CD19	1D3	Rat IgG2a, κ	PerCP-Cy5.5, PE-Cy7	BioLegend	1:200
anti-mouse CD19	6D5	Rat IgG2a, κ	BV 605	BioLegend	1:200
anti-mouse CD138	REA104	Recombinant human IgG1	APC	Miltenyi	1:50
anti-human/mouse GL7	GL7	Rat IgM, κ	eFluor 660	eBioscience, BD Pharmingen	1:200
anti-mouse CD1d	1B1	Rat IgG2b, κ	PerCP-Cy5.5	BioLegend	1:200

anti-mouse CD4	RM4-5	Rat IgG2a, κ	BV 605, PerCP-Cy5.5	BioLegend	1:200
anti-mouse CD45	30-F11	Rat IgG2b, κ	eFluor 450	eBioscience	1:200
anti-mouse IgD	11-26c.2a	Rat IgG2a, κ	FITC	BD Pharmingen	1:200
anti-mouse IgM	II/41	Rat IgG2a, κ	PE-Cy7	eBioscience	1:200
anti-mouse TCR Vα3.2 [b, c]	RR3-16	Rat IgG2b, κ	FITC, APC	BioLegend	1:50
anti-mouse TCR Vß5.1/5.2	MR9-4	Mouse IgG1, κ	APC	Invitrogen	1:50
anti-mouse/human B220	RA3-6B2	Rat IgG2a, κ	PerCP-Cy5.5	BioLegend	1:200
anti-mouse/human B220	RA3-6B2	Rat IgG2a, κ	PE	BioLegend	1:200
anti-mouse/human CD11b	M1/70	Rat IgG2b, κ	AF 700, APC, PE-Cy7	BioLegend	1:200
anti-mouse CD21/CD35	7E9	Rat IgG2a, κ	APC	BioLegend	1:200
anti-mouse CD8a	53-6.7	Rat IgG2a, κ	APC-Cy7	BioLegend	1:200
anti-mouse CD11c	N418	Armenian Hamster IgG	FITC	BioLegend	1:200
PNA			Biotin	Vector Laboratories	1:400
mMOGtet-SA488				housemade	1:50
Streptavidin			PE	eBioscience	1:100

Intracellular Markers					
Specificity	**Clone**	**Host**	**Conjugate**	**Company**	**Dilution**
anti-mouse IFNγ	XMG1.2	Rat IgG1, κ	PE-Cy7	BioLegend	1:100
anti-mouse IL-10	JES5-16E3	Rat IgG2b, κ	PE	BioLegend	1:100
anti-mouse/rat IL-17A	eBio17B7	Rat IgG2a, κ	APC	eBioscience	1:100
anti-mouse IL-17A	TC11-18H10.1	Rat IgG1, κ	PerCP-Cy5.5, PE	BioLegend	1:100

AF, Alexa Fluor; APC, Allophycocyanin; BV, Brilliant Violet™; Cy, Cyanine;
FITC, Fluorescein isothiocyanate; PE, Phycoerythrin; PerCP, Peridinin chlorophyll protein

3.11 Immunohistochemistry (IHC) on cryosections

To increase the chances for finding eLFs in the CNS, IHC was performed using Th17-EAE mice that had a high score for several days. The mice were perfused through the left cardiac ventricle with 10 ml PBS and 10 ml 4 % PFA. Then, the brain was dissected by carefully removing the skull using forceps and scissors. After removal of the outer muscle layer, the spinal cord was dissected by snapping each vertebra open with forceps to carefully remove it from the vertebral column in one piece leaving the leptomeninges as intact as possible. Thereby, peripheral nerves were cut off. Spleens and lymph nodes were also dissected as control tissue. After post-fixation in PBS containing 4 % PFA for 2 h at 4 °C, the organs were dehydrated in PBS containing 30 % sucrose for 24 h at 4 °C. Then, they were embedded in O.C.T. compound medium

(Sakura or VWR Chemicals), frozen using dry ice and stored at -80 °C. Subsequently, the brain was cut into 20 µm coronal sections on a Leica CM1850 cryostat. From spinal cord, spleen and lymph nodes, 10 µm sections (longitudinal for spinal cord and spleen) were prepared and placed on slides (Superfrost Plus™, Thermo Scientific) and frozen at -80 °C.

3.11.1 Giemsa staining

To screen for eLFs, every 15th section of brain and spinal cord was fixed in 10 % methanol for 10 min, air-dried for 20-30 min and stained with Giemsa-stain (AppliChem), diluted 1:20 in deionized water, for 45 min. After washing with deionized water, the sections were dried overnight and mounted using Eukitt mounting medium (Sigma-Aldrich). Sections were screened for immune cell infiltrates by light microscopy using a Leica DM2500 microscope with DMC2900 CMOS camera in the Core Facility Bioimaging of the Biomedical Center of the Ludwig-Maximilians-Universität München.

3.11.2 Immunofluorescence staining

Following identification of eLF-containing sections via Giemsa staining, neighboring sections were stained with fluorescently labeled antibodies. After thawing, sections were fixed in cold acetone for 10 min and air-dried for 20-30 min. Then, sections were outlined with a Pap-pen and O.C.T. medium was rinsed off twice with PBS. Afterwards, sections were blocked with PBS containing 1 % bovine serum albumin (BSA) and 1:300-diluted TruStain FcX™ (Biolegend) for 1 h at RT, and incubated with primary antibodies diluted in PBS containing 1 % BSA in a chamber humidified with PBS for 1 h at RT, followed by three washing steps with PBS containing 0.1 % Tween20 for 7 min. Then, sections were stained with secondary antibodies diluted in PBS containing 1 % BSA in a dark, humidified chamber for 1 h at RT. When intracellular markers, such as activation-induced cytidine deaminase (AID), were stained, the sections were incubated with antibodies diluted in PBS containing 1 % BSA and 0.1 % saponin to permeabilize the tissue. Following three washing steps with PBS containing 0.1 % Tween20 for 5 min, sections were mounted with VECTASHIELD Antifade Mounting Medium with DAPI (Vector Laboratories) and analyzed by confocal microscopy using a

Leica SP8X WLL microscope in the Core Facility Bioimaging of the Biomedical Center of the Ludwig-Maximilians-Universität München.

3.11.3 MOG tetramer staining

Sections were fixed in cold acetone for 5 min and O.C.T. medium was rinsed off three times with PBS for 5 min. Then, sections were outlined with a Pap-pen and blocked with PBS containing 4 % BSA, 4 % goat serum and 1:300-diluted TruStain FcX™ (Biolegend) for 1 h at RT in a humidified dark chamber. After washing three times with PBS for 5 min, sections were incubated with rat anti-mouse B220 (1:200, clone RA3-6B2, BD Pharmingen) and mMOGtet-SA488 (1:1000, housemade (see section 3.9)) diluted in PBS containing 4 % BSA and 1 % goat serum overnight at 4 °C. Subsequently, sections were washed three times with washing buffer (PBS containing 0.3 % Triton and 1 % goat serum) for 5 min and fixed in 4 % PFA for 30 min at RT. After three washing steps in washing buffer, sections were incubated with rabbit anti-SA488 (1:10000, Life technologies) for 3 h and goat anti-rat AF 633 (1:200, Life technologies) for 1 h diluted in PBS containing 4 % BSA and 1 % goat serum at RT in a humidified dark chamber. After three washing steps in washing buffer, sections were incubated with goat anti-rabbit Cy3 (1:1000, Life technologies) diluted in PBS containing 4 % BSA and 1 % goat serum for 3 h at RT in a humidified dark chamber, followed by three washing steps in washing buffer. Then, sections were mounted with VECTASHIELD Antifade Mounting Medium with DAPI (Vector Laboratories) and analyzed by confocal microscopy using a Leica SP8X WLL microscope in the Core Facility Bioimaging of the Biomedical Center of the Ludwig-Maximilians-Universität München.

Table 2. Antibodies / reagents used for immunohistochemistry

Primary / directly labeled antibodies			
Specificity	Clone	Dilution	Company
Syrian hamster anti-mouse CD3e	500A2	1:400	BD Pharmingen
Rat anti-mouse B220	RA3-6B2	1:200	BD Pharmingen
Rat anti-mouse B220 (biotinylated)	RA3-6B2	1:400	BD Pharmingen
Rat anti-mouse B220 AF 488	RA3-6B2	1:400	BD Pharmingen

Rabbit anti-mouse/human laminin	-	1:200	Abcam
Rat anti-mouse/human CD11b AF 647	M1/70	1:100	BioLegend
Mouse anti-mouse/human Ki67 647	B56	1:100	BD Pharmingen
Rat anti-mouse/human AID	mAID-2	1:25	eBioscience
Rat anti-mouse CD1d (biotinylated)	1B1	1:200	BioLegend

Secondary antibodies / reagents			
Specificity	**Clone**	**Dilution**	**Company**
Goat anti-hamster AF 568	-	1:400	Invitrogen
Goat anti-hamster AF 647	-	1:400	Invitrogen
Goat anti-rabbit AF 568	-	1:400	Life technologies
Goat anti-rabbit AF 647	-	1:400	Life technologies
Goat anti-rabbit Cy3	-	1:1000	Life technologies
Goat anti-rat AF 633	-	1:200	Life technologies
Rabbit anti-SA488	-	1:10000	Life technologies
Peanut agglutinin (PNA) (biotinylated)	-	1:50	Vector Laboratories
mMOGtet-SA488	-	1:1000	housemade
Streptavidin AF 488	-	1:300 - 1:400	Life technologies

3.12 Enzyme-linked immunosorbent assay (ELISA)

Anti-MOG IgG1 antibodies were measured in the serum of Th17- and Th1-EAE mice by ELISA. At indicated time points, blood was collected and, after 2-5 h at RT, centrifuged at 10.000 rpm for 10 min at 4 °C. The supernatant was carefully taken up and the centrifugation step was repeated. After removal of the supernatant, the serum was frozen and stored at -20 °C. For ELISA, 96 well high affinity, protein-binding plates (Nunc Maxisorp) were coated with rMOG (housemade) at a concentration of 10 µg/ml in PBS and incubated overnight at 4 °C. After washing four times with wash buffer (PBS containing 0.05 % Tween20), the plate was blocked with blocking solution (PBS containing 10 % FBS) for 1-2 h at RT, followed by four washing steps. Then, the serum samples and the antibody standard (mouse anti-MOG IgG1; clone 8.18c5; housemade) were diluted in blocking solution, added to the plate and incubated overnight at 4 °C. Following extensive washing, the plate was incubated with biotin-labeled detection

antibody rat anti-mouse IgG1 (clone A85-1; BD Pharmingen) at a concentration of 1 µg/ml diluted in blocking solution for 1 h at RT. Then, the plate was washed again and incubated with avidin-horseradish peroxidase (Av-HRP; eBioscience) diluted 1:1000-1:2000 in blocking solution for 30 min at RT. After extensive washing, TMB Substrate (BioLegend) was used to induce the Av-HRP-dependent color reaction, which was stopped by addition of TMB Stop Solution (BioLegend), and the optical density (OD) was measured at 450 nm. Samples were tested in duplicates and results were reported as mean concentrations according to the standard curve.

3.13 Single-cell RNA sequencing (scRNA-seq)

3.13.1 Fluorescence-activated cell sorting (FACS) of B cells

To analyze the gene expression of B cells by single-cell RNA sequencing, cells were isolated from the CNS, spleen and cervical lymph nodes (cLN) of Th17-EAE mice at the peak of disease, and B cells were sorted based on their expression of CD19. Surface staining was performed using 1×10^6 cells from spleen and cLN or $2.7\text{-}3.7\times10^6$ cells from CNS samples. Cells were washed with T cell medium, and unspecific binding of antibodies to Fc receptors was blocked by incubating the cells with TruStain FcX™ (Biolegend) diluted 1:20 in T cell medium for 15 min at 4 °C. Afterwards, cells were stained with the following antibodies diluted 1:100 in T cell medium for 20 min at 4 °C: anti-CD45.1-FITC (clone A20; Biolegend) or anti-CD45.2-FITC (clone 104; Biolegend), anti-CD11b-PE-Cy7 (clone M1/70; Biolegend), anti-CD19-APC (clone 1D3; eBioscience), anti-CD4-PE (clone GK1.5; BD Pharmingen). In addition, cells of different organs were labeled with anti-mouse hashtag oligonucleotide (HTO) antibodies (TotalSeq™-C0301 anti-mouse Hashtag 1 Antibody, TotalSeq™-C0302 anti-mouse Hashtag 2 Antibody, TotalSeq™-C0303 anti-mouse Hashtag 3 Antibody; Biolegend), which bind the ubiquitously expressed surface proteins CD45 and MHC class I and are conjugated to distinct oligonucleotides, allowing to pool B cells from different organs for multiplex gene expression analysis [174]. The hashtag antibodies were diluted 1:50 and included in the surface staining. After two washing steps, cells were resuspended in T cell medium containing 2 mM EDTA (Sigma), filtered through a 35 µm cell strainer and kept on ice. Sorting was performed using a BD FACSAria™ Fusion No1 in the Core Facility Flow Cytometry at the Biomedical Center of the

Ludwig-Maximilians-Universität München. For each sample, 30.000 B cells were sorted in tubes prefilled with T cell medium and kept on ice. Thereby, the following gating strategy (P1 → P5) was applied:
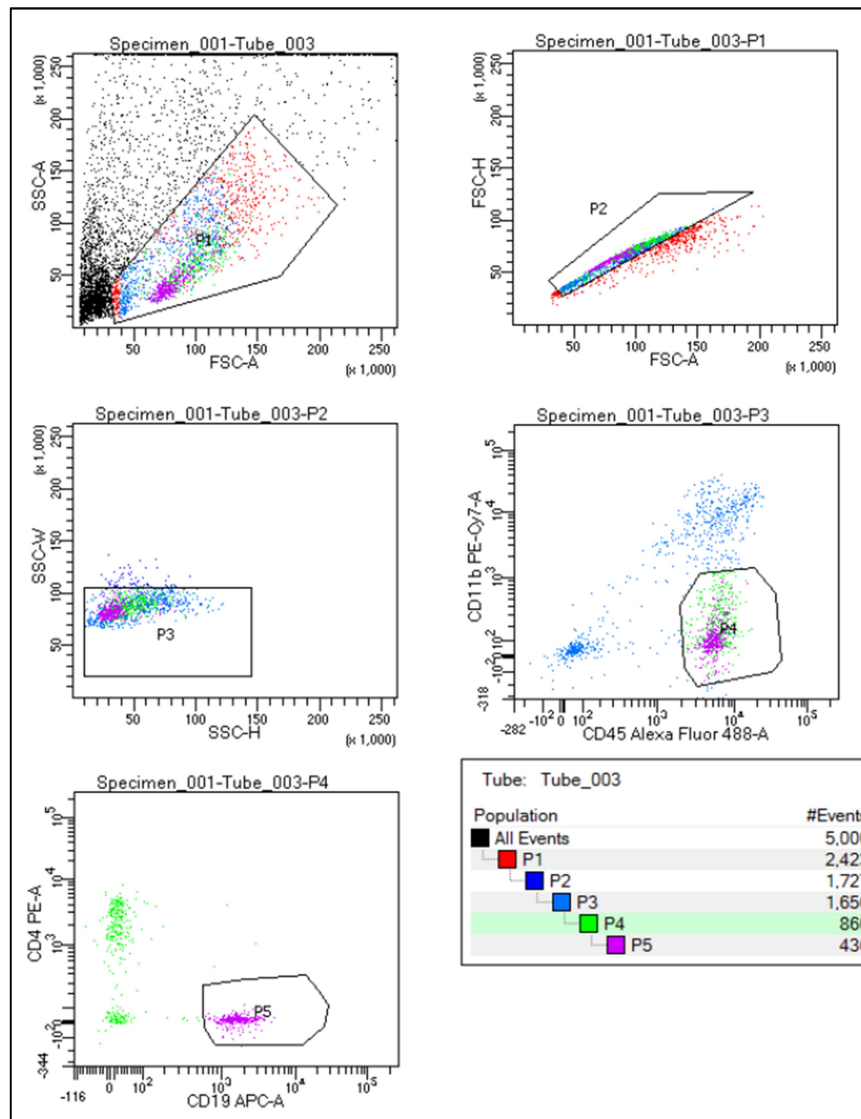
3.13.2 Library construction and sequencing

For each mouse, B cells from CNS, spleen and cLNs were pooled (90.000 B cells in total), centrifuged and, after a washing step, resuspended in PBS containing 0.04 % BSA at a concentration of 1000 cells/µl. The viability of cells was confirmed by staining with trypan blue solution. Further processing of samples was performed using the 10x Chromium Single Cell 5` Solution (Chromium Next GEM Single Cell V(D)J v1.1 with Feature Barcoding technology for Cell Surface Protein, 10x Genomics) according to the

manufacturer`s instructions. In brief, for each mouse, 15.000 B cells (5.000 per organ) were loaded onto the chromium chip (1 lane per mouse). Here, the B cells were mixed with 10x barcoded gel beads and reagents for reverse transcription, and then with partitioning oil to create gel beads in emulsion (GEMs). The cells were delivered in a limiting dilution approach to ensure that every GEM contained not more than one cell and thus, single cell resolution was achieved. In GEMs, the cells` RNA was reverse-transcribed into cDNA, whereby all the cDNA from the same cell was labeled with a shared barcode. Then, the cDNA was pooled, purified, amplified and quantified using the Qubit dsDNA HS kit (Life Technologies). scRNA-seq, scBCR-seq and cell hashing libraries were constructed, followed by quality control using a Bioanalyzer 2100 (Agilent Technologies) and quantification using the Qubit dsDNA HS kit. Next-generation sequencing (NGS) was performed on the Illumina HiSeq 1500 using read lengths of 28 base pairs (bp) read 1, 8 bp i7 index and 91 bp read 2 at the Gene Center Munich.

3.13.3 Data processing

To demultiplex samples, align the reads to the reference mouse mm10 genome, and process the raw data, we used the Cell Ranger Software (10X Genomics, v. 3.1.0). Following this, the unique molecule identifiers (UMIs) were summarized and the single-cells were filtered by the number of UMI counts identified. Then, we processed the gene matrices with R (v. 4.0.5) and the R package Seurat (v. 4.0.6) [175, 176]. Cell hashing raw counts were normalized using centered log-ratio (CLR) transformation by comparing the counts of single cells to the geometric mean of the HTOs signal with subsequent logarithmic transformation. Cells with missing HTO signals or containing two different HTO-identifiers were removed from the further analysis. Further, the scRNA-seq count matrices were log-normalized and scaled by passing through only the cells containing more than 200 and less than 5000 genes with mitochondrial gene fractions below 5 %. Subsequently, the highly variable genes were identified with the vst method, and cells from each compartment were integrated using the canonical correlation analysis (CCA) method. The aligned BCR sequencing information was added into the metadata file of the Seurat object with subsequent removal of cells with missing BCR sequences. The cells were considered as expanded if more than 2 cells belonged to the same B cell clonotype. In the next step, 18413 cells were recovered

and the corresponding PCA was computed using the previously identified highly variable genes. Based on the first 15 PCA dimensions, we constructed the Shared Nearest Neighbor (SNN) graph and clustered the cells by using the FindNeighbours and FindClusters functions of the Seurat R package. The following dimensional reduction was performed with the help of the Uniform Manifold Approximation and Projection (UMAP) method. For identification of differentially upregulated genes per cluster, compartment, or expansion condition we used the FindMarkers function based on the log-transformed count matrices of each single cell by applying the Wilcoxon test and subsequent p-value adjustment with the Bonferroni correction.

3.13.4 Clonotype analysis

Clonotypes with an expansion factor of 4 or higher were analyzed using the IMGT/V.QUEST tool. Here, the variable regions of both heavy and light chain were compared to germline sequences to identify the utilized V, D, and J genes, acquired mutations and the nucleotide and amino acid sequence of the CDR3 region.

3.14 Intravital two-photon microscopy

3.14.1 Animal preparation

Prior to surgery, the mice were anesthetized with MMF anesthesia consisting of midazolam (5 mg/kg bodyweight (bw)), medetomidine (500 µg/kg bw) and fentanyl (50 µg/kg bw). Subsequently, they were tracheotomized and ventilated with 1.5-2 % isoflurane, which was supplied throughout the surgery and the entire imaging session. Thereby, the mice were placed on a custom-made microscope stage, while their body temperature was stabilized at 37.5 °C using a heated pad. During imaging, breathing parameters, including concentrations of inspiratory and expiratory gases as well as ventilation pressure, and electrocardiograms were constantly monitored.

The experimental procedure of spinal cord imaging has been described previously by the lab of our collaboration partner Dr. Naoto Kawakami [123, 177]). In brief, a small imaging window at level Th12/L1 of the spinal cord was prepared. First, a midline incision of about 2 cm was placed to open the skin and, subsequently, to detach the

paravertebral musculature. To reduce artefacts caused by breathing and thereby ensure stable imaging conditions, a custom-made stage was used in order to fix three spines. Then, a laminectomy on the central vertebra was performed using a dental drill (Foredom). Finally, low-melting agarose was used to build a ring-shaped surrounding, which was filled with PBS to keep the tissue of the opened spine hydrated and to allow using the water immersion objective.

3.14.2 Image acquisition

Time-lapse two-photon laser-scanning microscopy was performed using a SP8 multi-photon microscope (Leica) at the Core Facility Bioimaging at the Biomedical Center of the Ludwig-Maximilians-Universität München. The SP8 system was equipped with a pulsed InSight DS+ laser (Spectra Physics). The emission wavelength was tuned to 841 nm and the fluorescent signal was collected using a water immersion objective (25x, NA 1, Leica) and detected with external, non-descanned hybrid photo detectors (HyDs) featuring 483/32 nm, 535/30 nm, 585/40 nm and 650/50 nm bandpass filters. Images were recorded using a 1-2x zoom, whereby areas of 221x221 µm, 295x295 µm or 443x443 µm were scanned, and 49-115 µm z-stacks with 2.5-4.3 µm step size were acquired with an acquisition rate of 21-22 s per z-stack.

3.14.3 Image processing and analysis

Time-lapse images were acquired using the LAS X software (Leica), followed by processing and analysis using ImageJ (NIH). Before the stacks were z-projected with maximum intensity to obtain two-dimensional movies, a Gaussian blur filter was applied. For Twitch-2B-expressing cells, the cpVenus^{CD} (FRET) channel was divided by the mCerulean3 (CFP) channel and, by changing to a fire lookup table, ratiometric pseudocolor images were generated. In each time frame of the two-dimensional maximum intensity projection, the cell shapes were outlined manually to create a region of interest (ROI) for analyzing the calcium ratios. Since the bleed-through of CFP into the YFP channel was determined to account for 44 %, the FRET signal was corrected as follows: YFP = FRET – 0.44 x CFP. In order to calculate the calcium ratio in every time frame, the average signal intensities of all pixels in each ROI were used.

Cell coordinates over time were used to calculate motility parameters by using ImageJ. T:B cell contact analysis was performed by monitoring the movement of each Twitch-2B+ T cell and its interaction with tdTomato+ B cells in the 3D follicle structure using the LAS X software.

3.15 Statistical analysis

Statistical analysis was performed using GraphPad Prism software (version 7). The statistical test chosen is described in the figure captions. For comparison of two groups, statistical differences were calculated using the unpaired Student`s *t*-test for normally distributed data, including Welch`s correction in case of unequal variances, or the Mann-Whitney U test if Gaussian distribution could not be determined. For comparison of three groups, the one-way ANOVA with Tukey`s test for multiple comparisons was applied.

4. Results

4.1 Establishment and characterization of adoptive transfer EAE

4.1.1 Adoptively transferred MOG-specific Th1 and Th17 cells can induce EAE and maintain their cytokine profile in the inflamed CNS

In active and spontaneous EAE models, both Th1 and Th17 responses contribute to the pathogenic cascade targeting the CNS, rendering it impossible to differentiate between Th1- and Th17-mediated aspects of disease. To investigate whether and how Th1 and Th17 cells cooperate with B cells to induce and propagate EAE, it is a key requirement to use an animal model that exhibits Th1-driven or Th17-driven disease, respectively. Therefore, according to Jäger et al. [72], we established adoptive transfer EAE, a model that employs the *in vivo* transfer of *in vitro* differentiated pure T helper cell subsets into wildtype recipient mice (Figure 5A). Here, naïve CD4$^+$ T cells were isolated from 2D2 mice, which carry a transgenic TCR specific for the MOG$_{35-55}$ peptide, and *in vitro* differentiated with polarizing cytokines into Th1 or Th17 cells in the presence of anti-CD3 antibody and irradiated APCs. After four days of differentiation, Th1 and Th17 cultures were analyzed by intracellular cytokine staining and flow cytometry for polarization. Primary Th1 and Th17 cells strongly produced their signature cytokine IFNγ and IL-17A, respectively, while being devoid of cytokine secretion associated with the other subset (Figure 5B). Since these primary cells did not induce EAE upon adoptive transfer (data not shown), a second round of stimulation was required. After five to eight days of primary culture, Th1 and Th17 cells reached a resting state and were restimulated with anti-CD3 and anti-CD28 antibodies for two days. These maximally activated cells were then transferred into immunocompetent recipient animals, whereupon EAE developed after eight to 15 days (Figure 5A). Both Th1 and Th17 cells were able to induce EAE with comparable disease course and severity. Representative disease courses are depicted in Figure 5C. EAE incidence ranged between 75 and 100 % (Figure 5C, upper panel). The mice were affected by ascending paralysis, starting at the tail and progressing to hindlimbs and sometimes even forelimbs. While Th1 recipients mainly showed classical EAE symptoms, some Th17 recipients also developed atypical signs of EAE, such as extensive weight loss, ataxia and imbalance. In contrast to active and spontaneous models, adoptive transfer

EAE mice did not recover from the disease and remained on high scores for several days before analysis (Figure 5C, lower panel).

To investigate whether transferred Th1 and Th17 cells maintain their original cytokine profile *in vivo*, infiltrating mononuclear cells were recovered from the CNS at the peak of disease. Transferred T cells could be distinguished from endogenous (recipient-
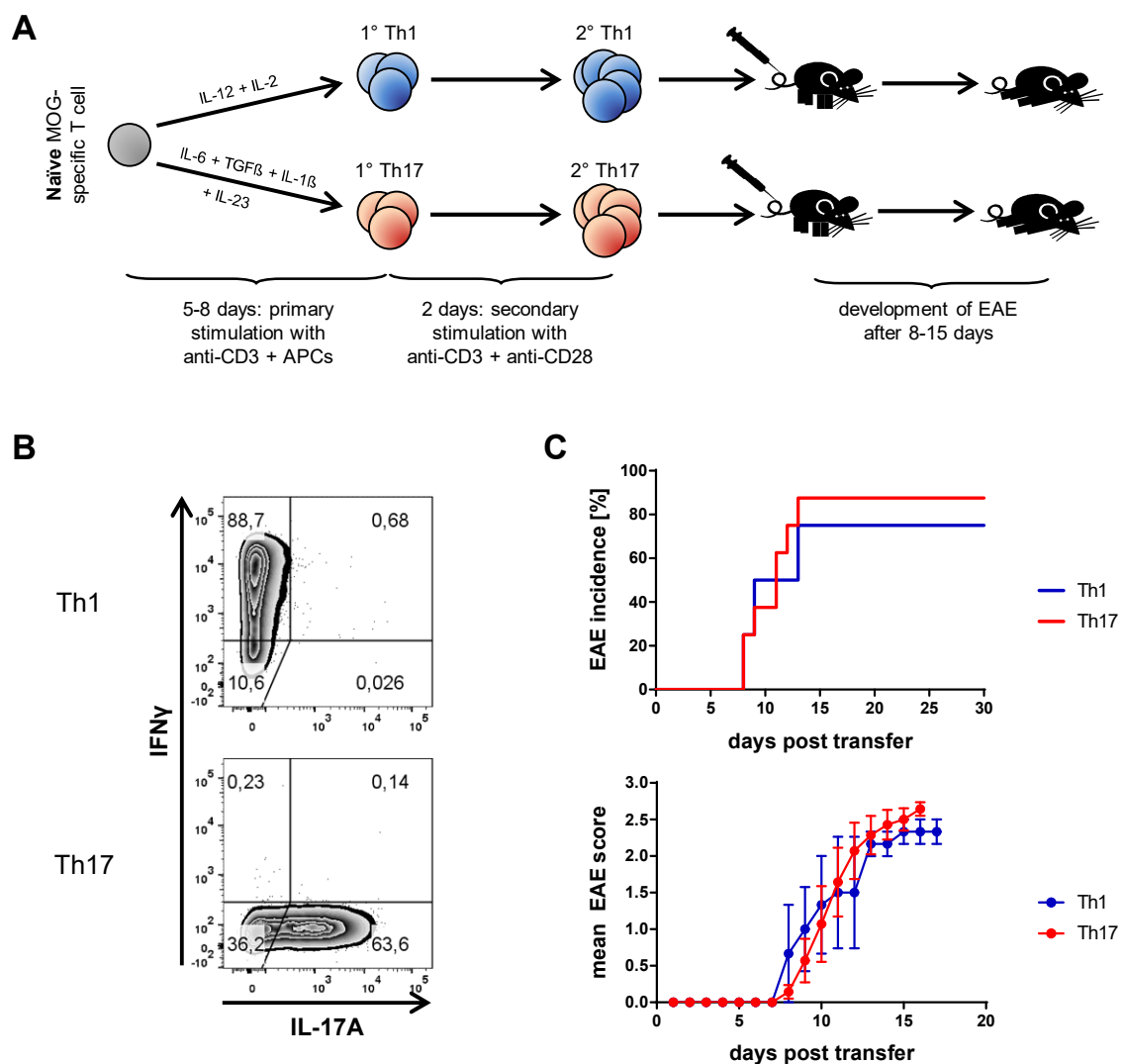
Figure 5. Th1 and Th17 adoptive transfer EAE. (**A**) Experimental outline. Naïve MOG-specific T cells isolated from 2D2 mice are differentiated with polarizing cytokines into Th1 or Th17 cells in the presence of anti-CD3 and APCs. After 5-8 days, the cells are restimulated with anti-CD3 and anti-CD28 for 2 days before they are transferred i.v. or i.p. into recipient animals. Clinical disease develops after 8-15 days post transfer. (**B**) After 4 days under Th1 or Th17 polarizing conditions, cultures were analyzed for IL-17A and IFNγ expression by intracellular cytokine staining. Representative flow cytometry plots are shown. (**C**) EAE incidence (upper panel) and mean EAE scores (lower panel) of Th1 and Th17 recipients that developed clinical disease. Mean ± SEM. Clinical data of one experiment (n_{Th1} = 4 mice; n_{Th17} = 8 mice) is shown. Similar results were obtained in four (Th1-EAE) or 14 (Th17-EAE) independent experiments.

derived) T cells based on their expression of the Vα3.2 chain, which is part of the transgenic MOG-specific TCR of 2D2 mice and is only rarely expressed in wildtype C57BL/6 mice. The cytokine expression of T cells was analyzed by intracellular cytokine staining and flow cytometry. In both Th1- and Th17-EAE mice, transferred T cells constituted the majority of the CD4$^+$ T cell population in the CNS (Figure 6). The frequency of infiltrating endogenous T cells was higher in Th1-EAE mice (14.3 %) compared to Th17-EAE mice (7.41 %). The majority of transferred Th1 cells produced IFNγ but no IL-17A in the CNS, indicating that the Th1 phenotype is very stable *in vivo*. Infiltrating endogenous T cells mainly produced IFNγ (Figure 6A). In contrast, Th17 cells maintained expression of IL-17A (27.7 %), but could also adopt production of IFNγ *in vivo*, either alone (14.5 %) or together with IL-17A (5.87 %). Endogenous T cells mainly produced IFNγ also in Th17-mediated EAE (Figure 6B). Taken together, these findings indicate that both Th1 and Th17 cells maintain expression of their signature cytokines in the inflamed CNS, with Th17 cells showing a more plastic phenotype.
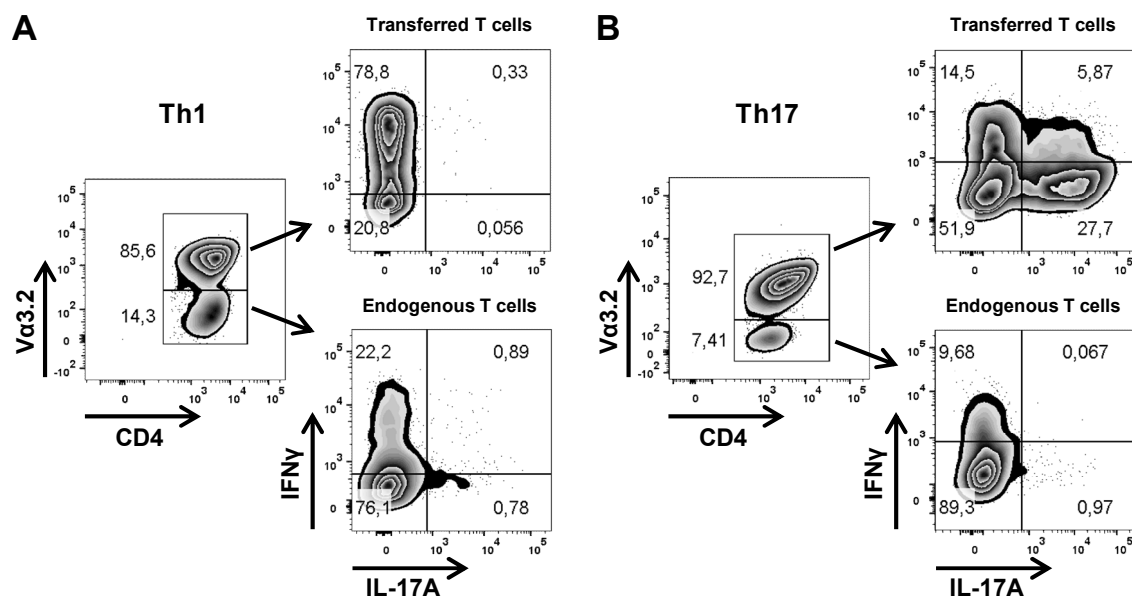
Figure 6. Transferred Th1 and Th17 cells maintain their cytokine profile in the inflamed CNS. At the peak of disease, cells were isolated from the CNS of (**A**) Th1 and (**B**) Th17-EAE mice and analyzed by flow cytometry. Transferred T cells were identified by their expression of the transgenic MOG-specific Vα3.2 TCR. Transferred and endogenous (Vα3.2$^-$) T cells were analyzed for expression of IL-17A and IFNγ by intracellular cytokine staining. Flow cytometry plots are representative of (**A**) three independent experiments with two to three mice or (**B**) seven independent experiments with two to five mice.

4.1.2 Th17 cells are superior to Th1 cells in recruiting B cells into the CNS

Encephalitogenic Th cells are known to migrate to the CNS, where they cross the BBB, become reactivated by local APCs and orchestrate the inflammatory response by recruiting other immune cells. In Th17-EAE, B cells were reported to become recruited to the CNS as part of a second wave of infiltration following Th17 cell accumulation [178]. To compare the extent of B cell recruitment between Th1 and Th17-EAE, CNS-infiltrating cells were isolated from the CNS of mice, which had been on a high score for several days to allow for continued immune cell infiltration, and were analyzed for the presence of B cells by flow cytometry. Representative plots (Figure 7A) show a larger B cell population in the CNS of Th17-EAE mice (27.6 %) compared to Th1-EAE mice (13.6 %). Quantitative analysis revealed a significant increase in the frequency of B cells within the CD45^{high} CD11b^{low} population (Figure 7B) as well as higher absolute numbers of B cells (Figure 7C) in the CNS of Th17 recipients compared to Th1 recipients. These data suggest Th17 cells to be better equipped than Th1 cells to recruit B cells into the CNS.
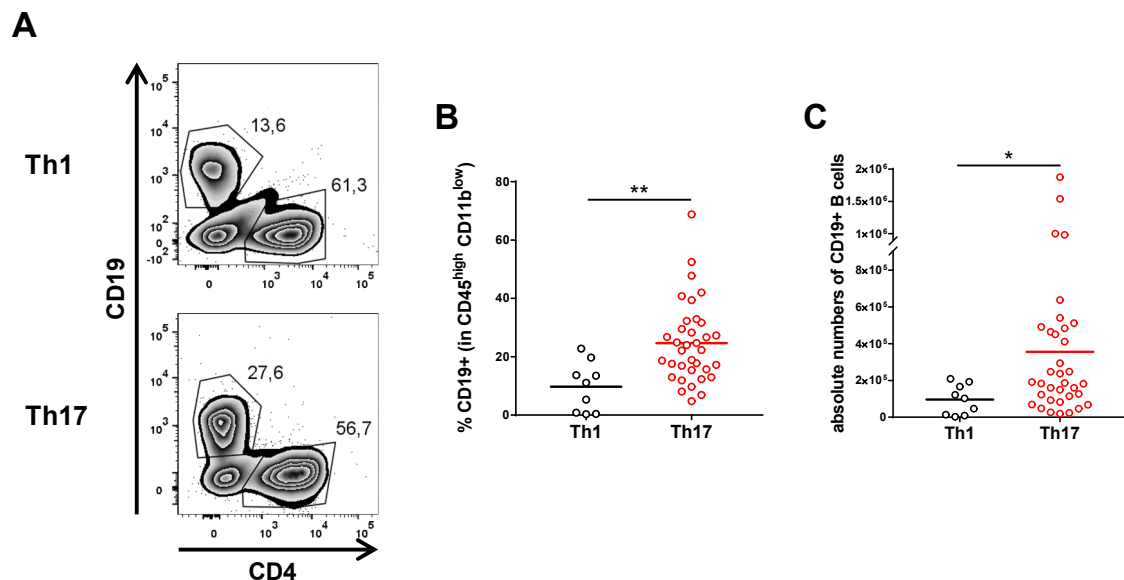
Figure 7. Th17 cells are superior to Th1 cells in recruiting B cells into the CNS. At the peak of disease, cells were isolated from the CNS of Th1 and Th17-EAE mice and analyzed for the presence of CD19$^+$ B cells. (**A**) Representative flow cytometry plots (pre-gated on CD45^{high} CD11b^{low} cells) and quantification of the (**B**) frequency of CD19$^+$ B cells in CD45^{high} CD11b^{low} cells and (**C**) absolute numbers of infiltrating CD19$^+$ B cells in the CNS. Graphs show cumulative data from three (Th1-EAE) or eight (Th17-EAE) independent experiments. Mann-Whitney U test. *P < 0.05; **P < 0.01. Horizontal lines indicate means. Dots represent individual mice.

4.1.3 Large ectopic lymphoid follicle-like structures form in association with the meninges in Th17-mediated EAE

Adoptive transfer studies found ectopic lymphoid follicle-like structures (eLFs) in the leptomeninges of the spinal cord predominantly in Th17 recipients, but not upon transfer of other Th cell subsets [109]. Since we detected abundant infiltration of B cells in the CNS of Th17-EAE mice, we next performed histological analysis of CNS lesions to investigate the structural organization and composition of cellular infiltrates. Th17 recipients, which had been on a high score for several days, were perfused and the CNS was carefully dissected to keep the leptomeninges intact. From the entire spinal cord, longitudinal cryosections were prepared. Every 15th sections was stained with Giemsa stain and inspected for aggregates of small round dark blue cells by light microscopy to identify regions with lymphoid infiltrates (Figure 8A). Neighboring sections were stained for T cells (CD3), B cells (B220) and laminin, which nicely visualized the basal lamina of blood vessels and the pia mater, and analyzed by confocal microscopy. These ectopic lymphoid structures displayed a wide range of organization and size, with some of them being only loose aggregates of a few cells, while others contained large amounts of both T and B cells and extended over wide areas, even up to several millimeters (Figure 8B-D). All aggregates showed prominent clustering of B cells, which was considered as a defining criterion for eLFs. Interestingly, eLFs often comprised separate T and B cell zones, similar to the structural organization of secondary lymphoid organs (SLOs). While B cells were almost exclusively located in these meningeal clusters, T cells were found to also broadly invade the underlying parenchyma. Identified based on their unique morphology and expression of CD11b, considerable amounts of macrophages were detected in close vicinity, but also within the follicle structure (Figure 8E). In all five mice analyzed, large eLFs were found distributed throughout the spinal cord. The individual localization is different in each mouse and the spatial distribution of the largest eLFs is depicted in Figure 8F.

Similar to histological analysis of spinal cords, also the brain of Th17-EAE mice was screened for the presence of eLFs. From the entire brain, coronal cryosections were prepared and, following evaluation by Giemsa staining, stained for T cells (CD3), B cells (B220) and laminin. In all five mice analyzed, massive infiltration of immune cells

Figure 8. Large lymphocytic aggregates form in association with the meninges of the spinal cord in Th17-EAE mice. At the peak of disease, the spinal cord of Th17-EAE mice was dissected and longitudinal cryosections were prepared. (**A**) Every 15th section was stained with Giemsa stain to identify regions with lymphocytic infiltrates. (**B**) Neighboring sections were stained for T cells (CD3, red), B cells (B220, green) and laminin (blue). (**C**) Zoom of red highlighted area in B. (**D**) Zoom of yellow highlighted area in B. (**E**) Cryosections were stained for T cells (CD3, red), B cells (B220, green) and macrophages (CD11b, cyan). (**F**) Scheme shows the spatial distribution of the largest ectopic lymphoid aggregates (red stars) in the spinal cord of the five mice analyzed. Scale bars: 200 µm except (**E**) 100 µm. *V, ventral; D, dorsal.*

was found in many different areas of the brain, including the cortex, the subarachnoid space at the base of the brain, the brainstem and the medial preoptic area of the hypothalamus (Figure 9). These aggregates formed structures of considerable size and organization, and they appeared to arise from the meninges and disperse inwardly towards the underlying parenchyma. Similar to spinal cord eLFs, T cells were found to egress from the follicle area and invade the subpial tissues, and some aggregates exhibited separated T and B cell zones. Taken together, our Th17 adoptive transfer EAE model features formation of very large eLFs in association with the meninges of brain and spinal cord, and thus, is well suited to investigate the unique relationship of Th17 cells and B cells and, in particular, their functional interplay in eLFs.

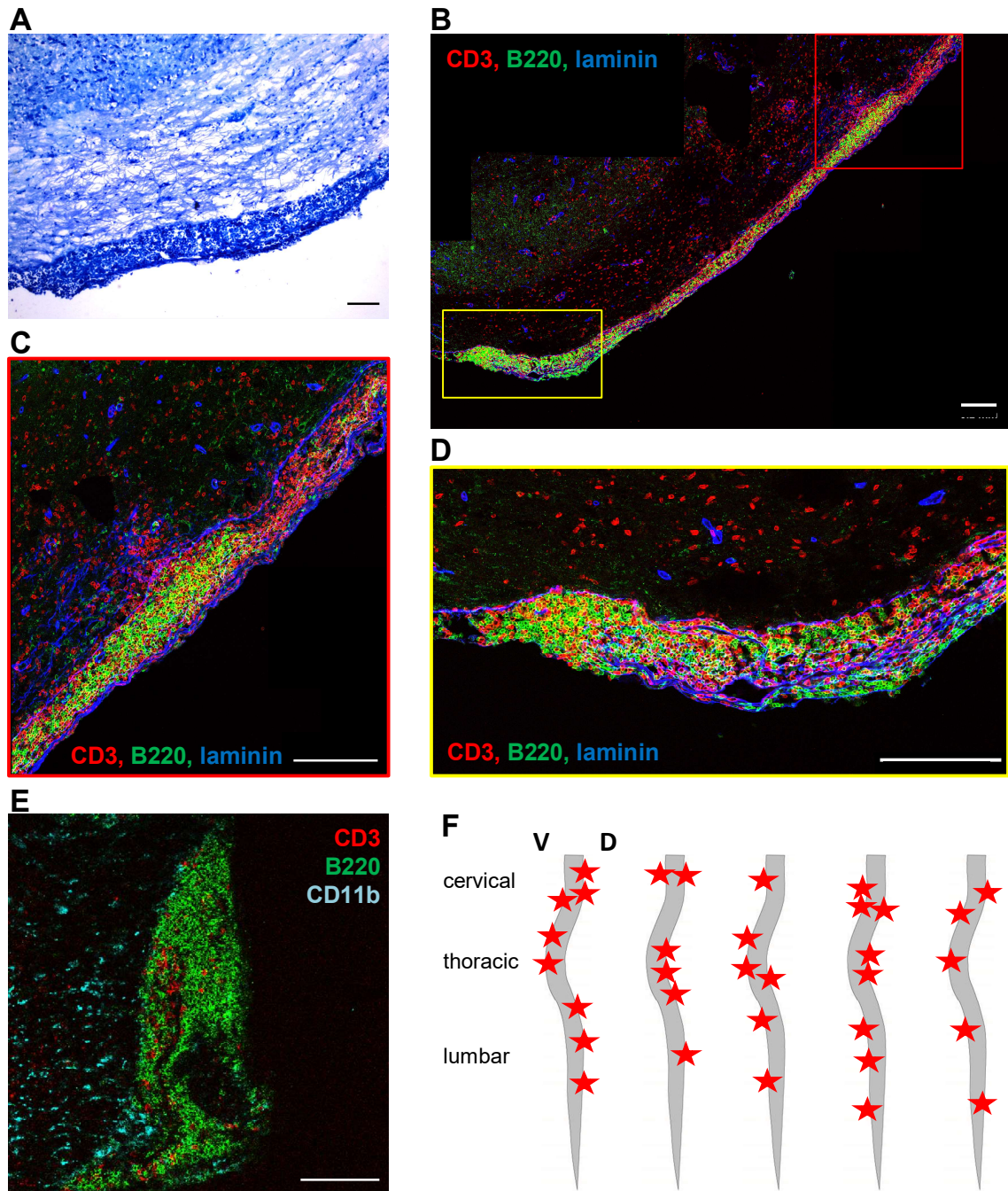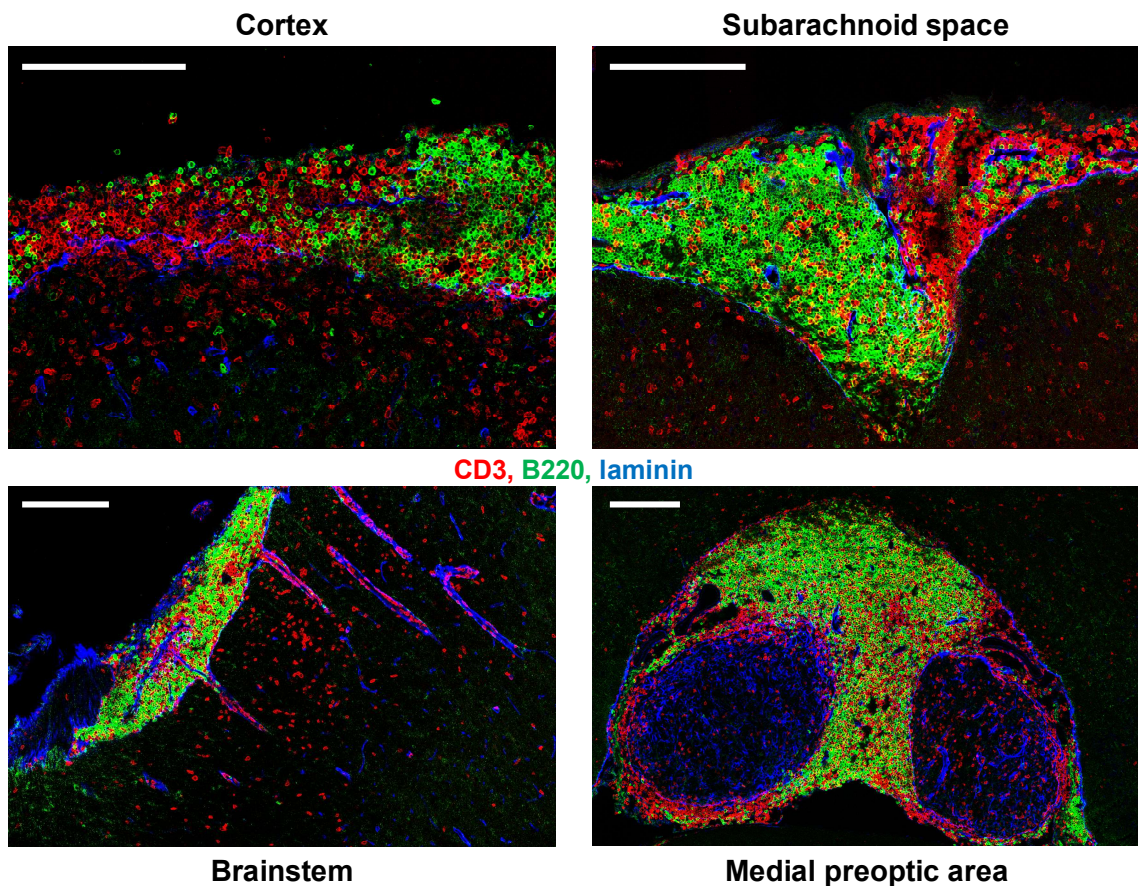**Figure 9. Large lymphocytic aggregates form in association with the meninges of the brain in Th17-EAE mice.** At the peak of disease, the brain of Th17-EAE mice was dissected, and coronal cryosections were prepared and stained for T cells (CD3, red), B cells (B220, green) and laminin (blue). Scale bars: 200 μm.

4.1.4 Ectopic lymphoid follicles are sites of T and B cell proliferation and show expression of germinal center markers

In MS patients, the presence of eLFs was reported to correlate with a more severe disease course, and highly organized eLFs were shown to contain follicular dendritic cells, T cells, proliferating B cells as well as plasma cells, which indicates formation of ectopic germinal centers (GC) in the CNS meninges [56, 148, 151-153]. In GC reactions, antigen-specific follicular T helper (Tfh) cells and B cells intensely interact with each other, inducing B cells to undergo somatic hypermutation (SHM) and clonal selection, eventually giving rise to high affinity plasma cells or memory B cells. Thus, these follicles have been postulated to maintain or exacerbate chronic inflammation directly in the CNS. EAE studies have yielded heterogeneous results regarding the expression of GC markers in eLFs. Since induction of enormous eLFs, often with separated T and B cell zones, appears to be a characteristic feature of our Th17-mediated EAE model, the degree of maturation of eLFs was further investigated by confocal microscopy. By staining CNS cryosections for T cells (CD3), B cells (B220) and the proliferation marker Ki67, proportions of both T and B cells were found to be positive for Ki67, which suggests that eLFs are sites of T and B cell proliferation (Figure 10A). In addition, sections were stained with peanut agglutinin (PNA), which is commonly used to identify GC B cells due to their expression of ligands for PNA, and some PNA$^+$ B cells were found within eLFs (Figure 10B). Sections were also stained for the enzyme activation-induced cytidine deaminase (AID), which is involved in somatic hypermutation and class-switch recombination, and in many eLFs, scattered AID$^+$ B cells could be detected (Figure 10C). On the other hand, in some eLFs, there was extensive clustering of AID$^+$ B cells, strongly resembling GC formation in SLOs (Figure 10D). Furthermore, the expression of GC markers was also confirmed by flow cytometric analysis of CNS-infiltrating cells from Th17-EAE mice at the peak of disease. Around 8 % of B cells were positive for PNA (Figure 10E). As part of their maturation process, B cells undergo isotype switching of their antibodies in GC reactions, leading to production of IgG, IgE and IgA instead of IgM and IgD. About 8 % of CNS B cells were negative for both IgM and IgD, which indicates that they had switched their isotypes (Figure 10F). Additionally, staining for the plasma cell marker CD138 revealed a small population of plasma cells (around 3 %) among CNS B cells Figure 10G). Together, these data support our hypothesis that eLFs are sites of

maturation of antigen-specific B cells. However, it is also possible that some B cells mature in the periphery, before they migrate to the CNS. Similarly, CNS T cells were
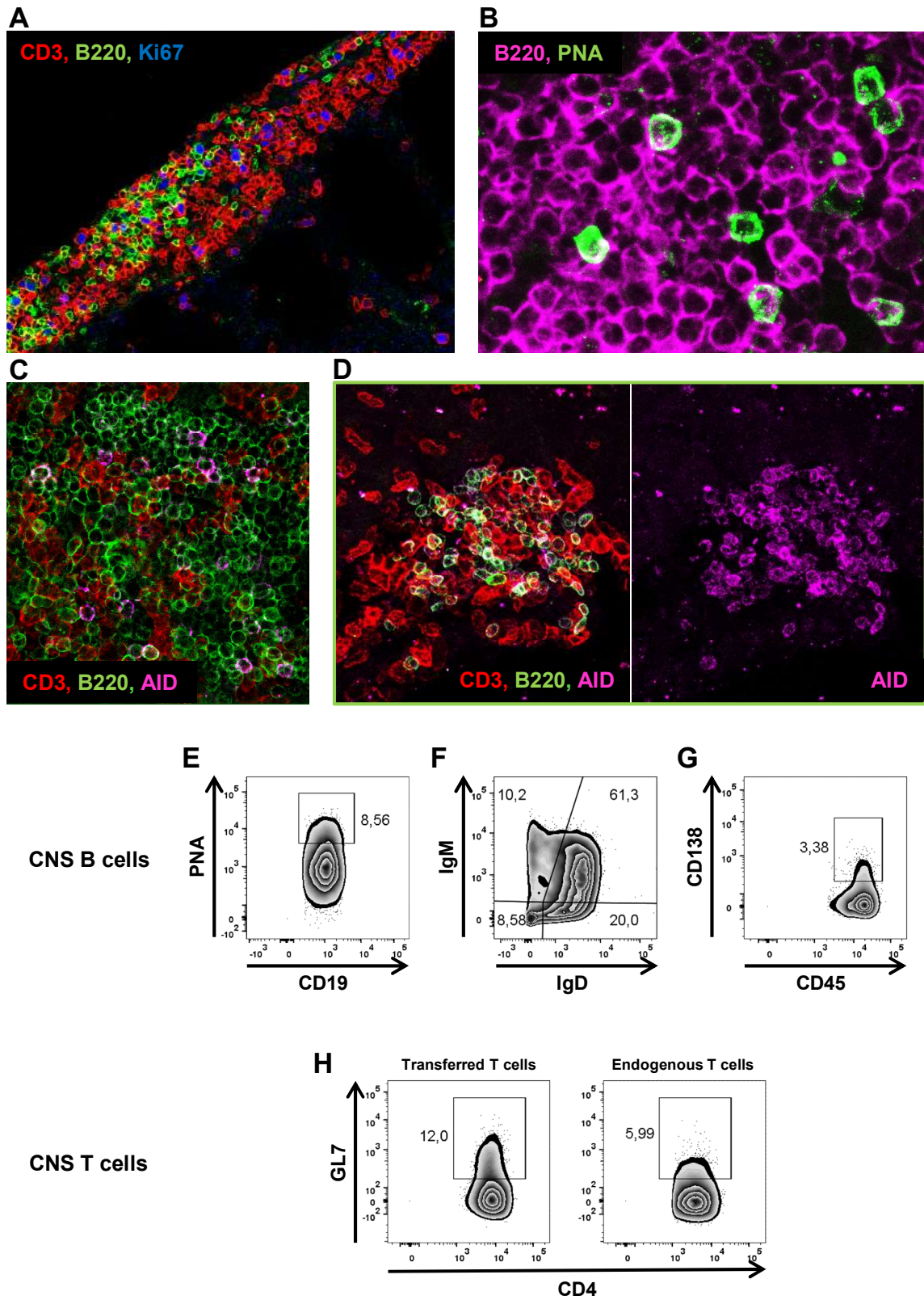
Figure 10. T and B cells express germinal center markers in the CNS of Th17-EAE mice. (**A-D**) CNS cryosections of Th17-EAE mice at the peak of disease were stained for (**A**) T cells (CD3, red), B cells (B220, green) and the proliferation marker Ki67 (blue); (**B**) B cells (B220, magenta) and the germinal center marker peanut agglutinin (PNA, green); (**C**, **D**) T cells (CD3, red), B cells (B220, green) and the enzyme activation-induced cytidine deaminase (AID, magenta), which is important for germinal center reactions in B cells. For better visualization, the AID staining is shown separately in D. (**E-H**) CNS-infiltrating cells isolated at the peak of disease were investigated by flow cytometry. B cells were analyzed for expression of (**E**) PNA, (**F**) IgM and IgD (pre-gated on CD19+ cells) and (**G**) the plasma cell marker CD138 (pre-gated on $CD45^{high}$ $CD11b^{low}$ cells). (**H**) Transferred (pre-gated on $V\alpha3.2^{+}$ $CD4^{+}$) and endogenous (pre-gated on $V\alpha3.2^{-}$ $CD4^{+}$) T cells were analyzed for expression of the germinal center marker GL7. Flow cytometry plots are representative of (**E**) 7 mice from two independent experiments, (**F**) 17 mice from four independent experiments, (**G**) 9 mice from two independent experiments and (**H**) 17 mice from five independent experiments.

tested for expression of the germinal center and activation marker GL7. Transferred 2D2 T cells showed higher frequency as well as higher expression levels compared to endogenous T cells (Figure 10H). Collectively, eLFs were found to contain clusters of proliferating T cells and B cells, and express GC markers, thereby indicating eLFs to be sites of functional GC formation and show resemblance to follicle-like structures in MS patients.

4.2 Characterization of the B cell response in Th17-mediated EAE

4.2.1 CNS-infiltrating B cells are phenotypically different from peripheral B cells

Since massive accumulation of B cells in the CNS is a hallmark of Th17-mediated EAE, we next examined whether Th17 cells shape a pathogenic B cell response. To characterize the phenotype of CNS-infiltrating B cells, single-cell RNA sequencing was performed using the 10x Genomics` chromium technology. In brief, cells were recovered from the CNS, spleen and cervical lymph node (cLN) of three Th17-EAE mice at the peak of disease and B cells were sorted. In addition, cells were labeled with hashtag antibodies, which bind ubiquitously expressed surface proteins (CD45 and MHC-I) and are conjugated to distinct oligonucleotides, allowing to pool B cells from different organs for multiplex analysis. Importantly, the three mice analyzed showed prominent B cell infiltration into the CNS, with the B cell frequency ranging between 42 and 69 % of CD45^{high} CD11b^{low} cells. For each mouse, B cells from the different organs were pooled and 15.000 B cells (5.000 per organ) were loaded onto the chromium chip. Here, the B cells were mixed with 10x barcoded gel beads and reagents for reverse transcription, and then with partitioning oil to create gel beads in emulsion (GEMs). The cells were delivered in a limiting dilution approach to ensure that every GEM contained not more than one cell and thus, single cell resolution was achieved. In GEMs, the cells` RNA was reverse-transcribed into cDNA, whereby all the cDNA from the same cell was labeled with a shared barcode. Then, the cDNA was pooled, purified, amplified and - following library construction - analyzed by Illumina sequencing. The aim of this gene expression analysis was to investigate whether there are differences in B cell phenotype between the CNS and peripheral organs, and, in particular, whether CNS-infiltrating B cells have a pro-inflammatory function driving disease pathogenesis. In addition to antibody production and cytokine secretion, B cells could reactivate T cells in the CNS by upregulating their capacity to present antigen and provide costimulatory stimuli. In addition to splenic B cells, B cells from cLNs were included as peripheral compartment since the CNS-draining cLNs could be a site where B cells are recruited before they enter the CNS. In fact, in the RR model, the recruitment of MOG-specific B cells from the endogenous pool by transgenic MOG-specific T cells was suggested to

take place in the cLN [179]. Furthermore, B cells in CNS and cLN were shown to be clonally related in MS [180].

Combining the analysis of the three Th17-EAE mice, the single cell transcriptomes of 18413 B cells were obtained and displayed as a UMAP (Uniform Manifold Approximation and Projection) plot for dimension reduction to show the global structure of the data, whereby the distance between clusters reflects their difference. The transcriptomic data were either plotted separately for CNS, spleen and cLN (Figure 11A) or plotted together for all three compartments (Figure 11B). In general, twelve different B cell clusters were identified, containing cells of all three compartments. While some clusters were very large, for example cluster 0 and 1, others like cluster 9, 10 and 11 contained only very few cells. By comparing the UMAP plots of spleen and cLN, B cells were found to possess a similar distribution of distinct subsets and corresponding phenotypes in these two peripheral compartments. In contrast, CNS B cells showed a distinct clustering with some clusters being enriched, for example cluster 6 and 7, while others comprised fewer cells, for example cluster 3 and 4. For each of the twelve clusters, the fraction of cells belonging to the three different compartments was calculated (Figure 11C). In cluster 6 to 10, the fraction of B cells from the CNS was increased, most pronounced for cluster 6, where 93 % of cells were CNS B cells.

As CNS B cells were found to form a distinct pattern of cell clustering compared to peripheral B cells, we next investigated the most prominent differences in gene expression. Figure 12A (Supplementary Table 1) shows the top 10 upregulated genes in the CNS compartment, with *Nr4a1* being the most highly expressed gene in CNS B cells. Nr4a1, also called Nur77, is an orphan nuclear receptor which is an important regulator of inflammatory responses, and is rapidly upregulated in B cells following BCR stimulation [181, 182]. In fact, Nr4a1 represents one of the most highly induced transcription factors in response to BCR engagement [183] and its expression was shown to scale with affinity and dose of antigenic stimulation via the BCR [184, 185]. *Nr4a1* was highly expressed in cluster 7, and also in cluster 6 (Figure 12B, left panel), which were enriched for B cells from the CNS. Another highly expressed gene was *Egr1* (early growth response protein 1), an immediate early gene, which encodes a transcription factor that is rapidly induced upon B cell activation and modulates the

Figure 11. CNS-infiltrating B cells show distinct clustering from peripheral B cells. At the peak of disease, B cells were sorted from indicated organs of Th17 recipients (n = 3 mice) based on their expression of CD19, and their gene expression was characterized by 10x genomics whole transcriptome analysis. Single cell transcriptomes are depicted in UMAP plots representing twelve color-coded cell clusters, either shown (**A**) separately for CNS, spleen and cervical lymph node (cLN) or (**B**) plotted together for all three compartments. (**C**) For each cluster, the fraction of cells belonging to CNS, spleen or cLN was calculated.

expression of target genes such as CD44, IL-2, and TNFα [186]. Upon BCR engagement, mature B cells start to proliferate with an increase in *Egr1* expression [187]. EGR1 has been indicated to be important for B cell survival, differentiation and maturation [188]. Similar to *Nr4a*1, *Egr1*-high expressing cells were predominantly located in cluster 7, but also in cluster 6 (Figure 12B, middle panel). CNS B cells also showed upregulation of *Socs3* (suppressor of cytokine signaling 3), which is induced upon stimulation by cytokines such as IL-21, a T cell-derived cytokine important for B cell proliferation and maturation in GC reactions. Socs3 is part of a negative feedback loop regulating the intracellular transduction of cytokine signaling and its deletion was suggested to negatively affect the GC response of B cells [189]. An accumulation of *Socs3*-expressing B cells was found in cluster 6 (Figure 12B, right panel). The

remaining of the top 10 upregulated genes in the CNS included proteins important for gene transcription and translation, intracellular signal transduction, proliferation and differentiation, and their precise role in CNS B cells still needs to be clarified. Interestingly, CNS-infiltrating B cells also showed increased expression of the activation markers *Cd69* and *Cd83* compared to peripheral B cells (Figure 12C). CD69 is involved in retention of activated lymphocytes in SLOs [190], and is rapidly upregulated upon internalization of antigen [191]. CD83 is implicated in B cell activation, antigen presentation and GC responses [192]. In addition, *Cd86* was upregulated, which, as ligand for CD28, plays an important role in costimulation of T cells [193]. Together, upregulation of these genes renders B cells well equipped to engage in B:T cell interactions in the CNS. Besides, the expression of the chemokine receptors *Ccr6* and *Ccr7* was induced in CNS B cells, which could be involved in
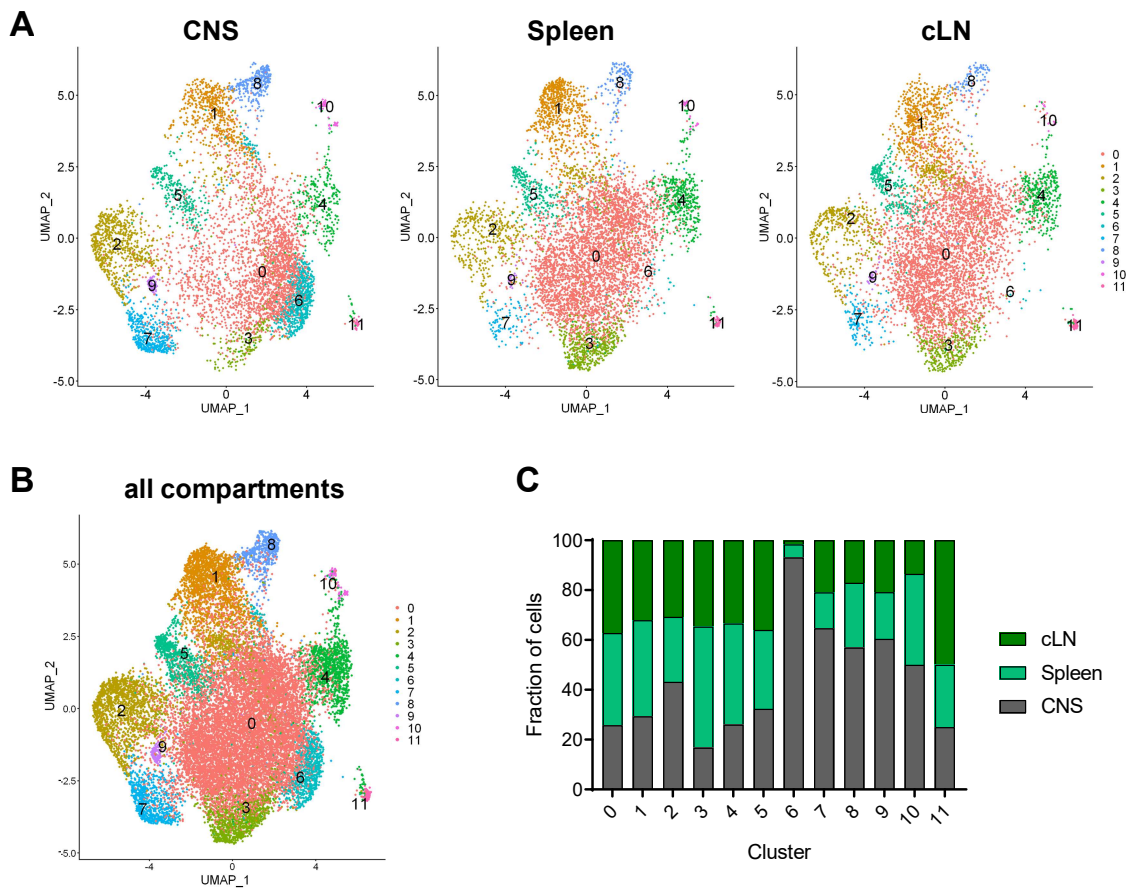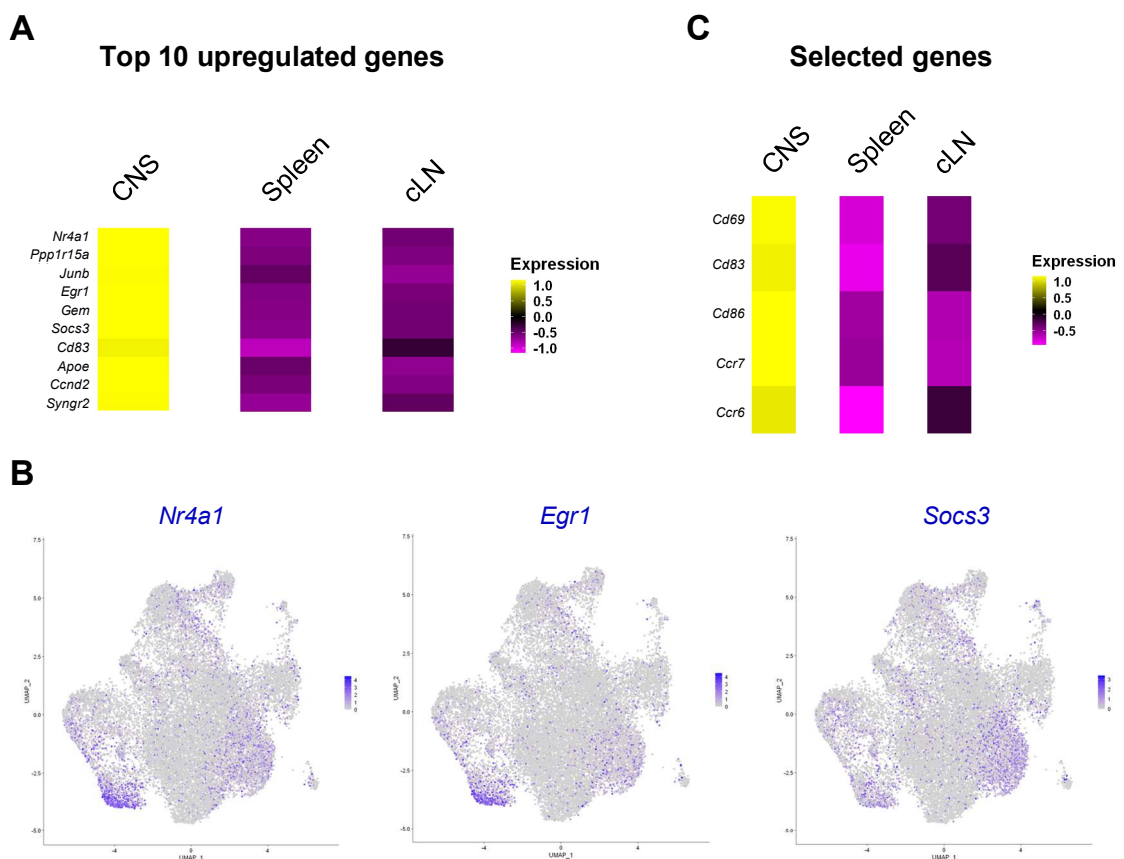

Figure 12. CNS-infiltrating B cells are phenotypically different from peripheral B cells. At the peak of disease, B cells were sorted from indicated organs of Th17 recipients (n = 3 mice) based on their expression of CD19, and their gene expression was characterized by 10x genomics whole transcriptome analysis. (**A**) Top ten upregulated genes in CNS B cells compared to peripheral B cells. (**B**) Feature plots depicting distribution of *Nr4a1*, *Egr1* or *Socs3*-expressing B cells among B cell clusters (see Figure 11). (**C**) Selected upregulated genes in CNS B cells compared to peripheral B cells.

recruitment of cells to the CNS and in case of *Ccr7* - as receptor for CCL19 and CCL21 - important for migration to T cell zones within the eLFs. Next, the upregulated and downregulated genes as well as associated pathways need to be analyzed in detail to unravel the phenotype and function of the different B cell clusters, especially the ones enriched for CNS B cells. The top 10 upregulated genes for each cluster are listed in Supplementary Table 2. So far, our preliminary transcriptomic analysis provides evidence for enhanced APC function as well as ongoing B cell maturation in the CNS, and points towards recently BCR-stimulated B cells in cluster 7 and pre-GC/GC B cells in cluster 6.

4.2.2 CNS-infiltrating B cells express markers associated with marginal zone B cells

By analyzing the distinct markers of the individual B cell clusters, expression of genes associated with marginal zone (MZ) B cells, *Fcrl5* and *Cd9*, was found in cells of cluster 1 and 8 (Figure 13A, Supplementary Table 2). Being primarily localized in the MZ of the spleen, MZ B cells are well positioned to respond to blood-borne pathogens [13]. Due to their high expression of MHC-II, CD80 and CD86, MZ B cells are potent antigen presenters and activators of CD4$^+$ T cells [17, 18]. MZ B cells are also thought to be innate-like cells that can develop into short-lived plasma cells without BCR stimulation [15]. Fcrl5 (Fc receptor-like protein 5) has been indicated as a discrete marker of peritoneal B-1 B cells and MZ B cells. Fcrl5 is an IgG receptor, which was reported to inhibit BCR signaling and B cell activation. However, by associating with CD21, a complement receptor highly expressed in MZ B cells, Fcrl5 was implicated to strongly boost B cell activation when both receptors bind ligands in form of immune complexes [14, 194]. Secondly, CD9 represents a marker for MZ B cells, B-1 B cells and plasma cells [195]. *Fcrl5* (Figure 13A, left panel) and *Cd9* (Figure 13A, right panel) expressing cells were predominantly found in cluster 1 and 8, with *Fcrl5* being more abundantly produced. In contrast, transcripts of the MZ marker *Cd1d1* were mainly found in cluster 1, but not in cluster 8 (Figure 13B). Within cluster 1, *Cd1d1* was only expressed by B cells from spleen, whereas *Cd1d1* mRNA could not be detected in CNS B cells (Figure 13C). Next, we aimed to confirm the presence of MZ-like B cells in the CNS by analyzing CD1d protein levels using flow cytometry (Figure 13D). From Th17-EAE

mice, cells were isolated from the CNS and investigated for IgM^{high} IgD^{low} CD21^{high} CD1d$^+$ MZ B cells. In six out of seven mice, a small MZ B cell population was found (Figure 13D, left panel), whereas one mouse contained substantial accumulation of MZ B cells in the CNS (26 % of IgM^{high} IgD^{low} B cells) (Figure 13D, right panel). In addition, spinal cord cryosections of Th17-EAE mice were stained for T cells (CD3), B cells (B220) and CD1d for confocal microscopy, thereby confirming the presence of some CD1d$^+$ B cells in eLFs in the CNS (Figure 13E). Taken together, combining transcriptomic, flow cytometric and microscopic analyses, our data indicate that there is a MZ-like B cell population among CNS-infiltrating B cells.
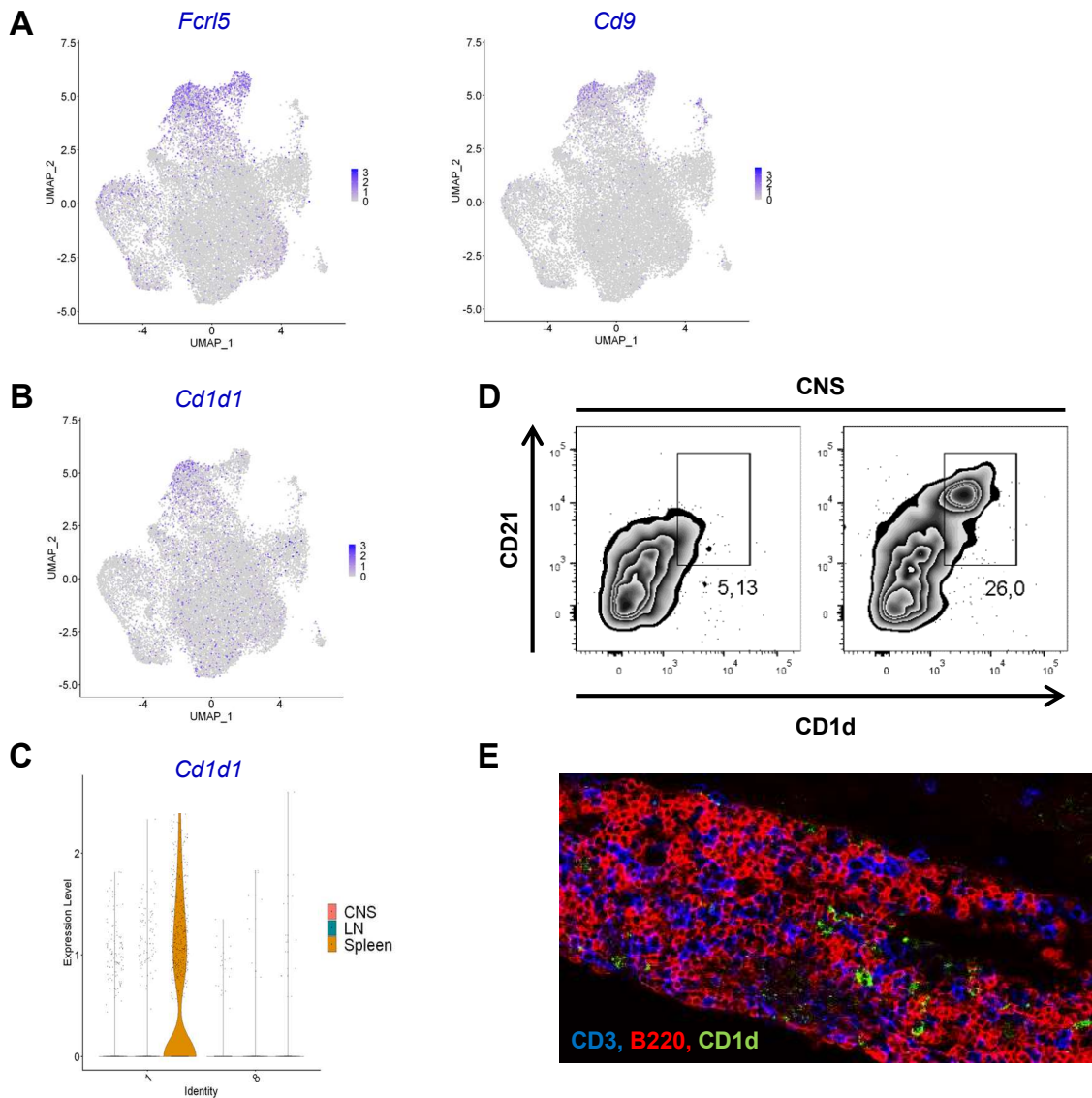
Figure 13. CNS-infiltrating B cells express markers associated with marginal zone (MZ) B cells. (**A-C**) At the peak of disease, B cells were sorted from indicated organs of Th17 recipients (n = 3 mice) based on their expression of CD19, and their gene expression was characterized by 10x genomics whole transcriptome analysis. (**A**, **B**) Feature plots depicting distribution of (**A**) *Fcrl5* or *Cd9* or (**B**) *Cd1d1*-expressing B cells among B cell clusters (see Figure 11). (**C**) Violin plot showing expression of *Cd1d1* in cluster 1 and 8. (**D**) Cells were isolated from the CNS of Th17 recipients and analyzed for expression of CD21 and CD1d by flow cytometry. A pre-gate on CD19+ IgM^{high} IgD^{low} B cells was applied. (Left panel) One representative plot of two independent experiments (n = 6 mice). (Right panel) One plot from a mouse with substantial CD21^{high} CD1d^{+} population (n = 1 mouse). (**E**) Spinal cord cryosections of Th17 recipients were stained for T cells (CD3, blue), B cells (B220, red) and CD1d (green).

4.2.3 Clonal expansion of infiltrating B cells in the CNS

In addition to the single cell whole transcriptome analysis (explained in section 4.2.1), the BCR repertoire of 18413 B cells, pooled from CNS, spleen and cLN of Th17-EAE mice at the peak of disease, was analyzed using the 10x Genomics` chromium technology. In brief, from amplified cDNA, V(D)J segments were enriched via PCR amplification using primers specific to Ig constant regions prior to library construction and Illumina sequencing. First, we investigated the BCR repertoire for evidence of clonal expansion. B cells were classified as expanded if more than two cells per clonotype could be detected, whereby the clonotype assignment was performed based on V(D)J sequence alignment. In total, 180 cells were found to belong to expanded clones, corresponding to around 1 % of all cells analyzed. In the CNS, 1.7 % of cells were expanded, showing that the repertoire of CNS B cells is largely polyclonal. The spatial distribution of expanded cells among the formerly defined twelve B cell clusters (Figure 11) is depicted in Figure 14A. The majority of expanded cells were located in cluster 8, which was enriched for CNS B cells. In this cluster, 16.8 % of cells were expanded ones. Some expanded cells belonged to cluster 4, constituting 4.7 % of all cells. In the remaining clusters, only a few expanded cells could be detected (cluster 0, 1, 2, 3, 5, 7, 9) or none at all (cluster 6, 10, 11) (Figure 14B). For each expanded B cell clone, the expansion factor, i.e. the number of cells per clone, and the distribution among B cell clusters was determined (Figure 14C). While cluster 4 mainly contained clones with three or four cells, cluster 8 comprised larger clones consisting of six, twelve, 20 or 22 cells. Figure 14D shows the expanded cells (Figure 14A) separately for each compartment, and the fraction of expanded cells belonging to CNS, spleen and cLN was calculated (Figure 14E). Importantly, 56 % of expanded cells represented B cells from the CNS, whereas 29 % or 16 % were derived from spleen or cLN,

respectively. This preferential localization of expanded clones may indicate that infiltrating B cells undergo clonal expansion in the inflamed CNS. Interestingly, the majority of expanded cells in the CNS were located in cluster 8, which contained the most expanded clones and was suggested to comprise MZ-like B cells (section 4.2.2). Since B cells were sorted based on their expression of CD19, plasma cells, which do not express CD19 anymore, were not included in this analysis. Therefore, the expanded CNS B cells in cluster 8 could be in the process of maturation into plasma cells. Indeed, by comparing the transcriptome of non-expanded and expanded cells in this cluster, the expanded cells were found to upregulate the expression of genes associated with plasma cell differentiation and MZ B cells or B-1 B cells, for example *Fam46c, Emb* and *Gpx4* (Figure 14F). The non-canonical poly(A) polymerase Fam46C
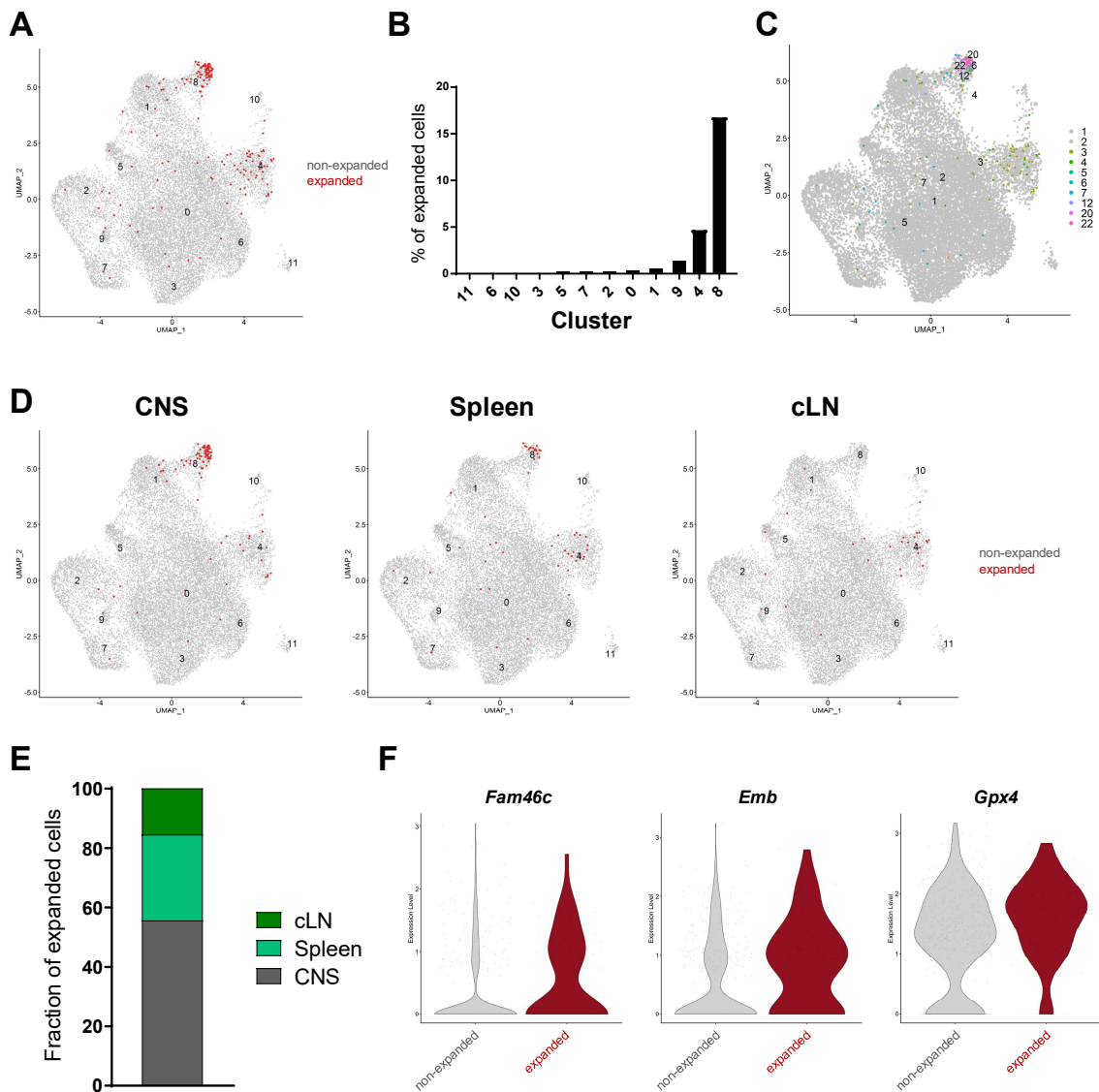
Figure 14. Clonal expansion of infiltrating B cells in the CNS. At the peak of disease, B cells were sorted from indicated organs of Th17 recipients (n = 3 mice) based on their expression of CD19, and characterized by BCR repertoire analysis. (**A**) Feature plot depicting distribution of non-expanded (grey) and expanded (red) B cells among B cell clusters (see Figure 11). (**B**) Frequency of expanded cells in each cluster. (**C**) Feature plot depicting distribution of color-coded B cell clones among B cell clusters. The color code indicates the number of cells per clone. (**D**) Expanded cells from (A) plotted separately for CNS, spleen and cLN. (**E**) Fraction of expanded cells belonging to CNS, spleen and cLN. (**F**) Violin plots showing expression of *Fam46c, Emb and Gpx4* in non-expanded and expanded cells in cluster 8.

was found to be induced during plasma cell differentiation and to target Ig mRNAs, leading to their polyadenylation and stabilization, and consequently, increasing antibody production [196]. *Emb* encodes the adhesion molecule embigin, which was reported to be restricted to MZ B cells in the splenic B cell compartment. In addition, peritoneal B-1 B cells and plasma cells were found to be embigin[+] [197]. *Gpx4* encodes the glutathione peroxidase-4, which is crucial for preventing lipid peroxidation. MZ and B-1 B cells consume large amounts of fatty acids to maintain their metabolic functions, and are therefore more prone to lipid peroxidation. In contrast to follicular B cells, both subsets depend on Gpx4 during antibody responses and homeostasis [198].

As next step, the more expanded clones, consisting of at least four cells, were further investigated, including their distribution across the different organs, antibody isotype and mutations in the variable region of heavy and light chain to examine whether expanded B cells further mature in the CNS. A detailed overview is given in Table 3, which also contains the amino acid (AA) sequence of the FR3 (framework region 3) - CDR3 (complementarity determining region 3) junction, the V-gene of both the heavy and light chain, as well as their affiliation with the formerly defined B cell clusters. Notably, the expanded clones were mainly shared between CNS and spleen with a preferential accumulation in the CNS compartment, supporting our hypothesis that infiltrating B cells expand in eLFs in the CNS. However, the majority of clones did not undergo isotype switching of their antibodies, but maintained expression of IgM. In addition, only three out of 20 clonotypes showed mutations in the nucleotide sequence of their variable regions: clonotype 6 contained two mutations in the heavy chain (HC), clonotype 9 two mutations in both heavy and light chain (LC) and clonotype 10 two mutations in the HC. The fact that the most expanded clones are devoid of mutations may be explained by the short disease course of Th17-mediated EAE, whereby the B cells spend maximally a few days in the CNS tissue. However, some striking

similarities were found in the AA sequence of the CDR3 region, which is the most variable CDR and the key determiner of antigen specificity. Completely matching sequences between different clones are highlighted in color and may point towards shared clones between different animals, possibly indicating an antigen-driven process. Summing up, this BCR repertoire analysis provides evidence for clonal expansion of infiltrating B cells in the CNS, with expanded B cells showing upregulation of genes associated with the innate-like B cell subsets MZ B cells and B-1 B cells. By analyzing the specificity of these expanded B cell clones in the future, we may be able to answer the question whether education and expansion of CNS-specific B cells takes place in CNS eLFs.

4.2.4 Transferred T cells recruit endogenous autoreactive B cells

Since our transcriptomic analysis provides evidence for enhanced APC function, ongoing maturation and clonal expansion of B cells in the CNS, we next investigated whether CNS B cells are MOG-specific and thereby share antigen-specificity with the transferred Th17 cells. First, CNS-infiltrating cells were isolated from Th17-EAE mice, and MOG-specific B cells were labeled using MOG tetramer staining and analyzed by flow cytometry. Only very few MOG tetramer-reactive B cells (< 1 % of all B cells) were detected (Figure 15A). In addition, an induced germinal center B cell (iGB) culture of CNS B cells was performed, where the B cells were grown on a fibroblastic feeder cell layer expressing CD40L and BAFF. These stimulation and survival signals, together with exogenous IL-4 and IL-21, allowed massive expansion and isotype switching of B cells [199]. Then, the culture supernatant was analyzed for the presence of anti-MOG IgG1 via ELISA, but the antibody level was below the detection limit (not shown). One reason could be that MOG tetramer$^+$ B cells might not survive the culture very well, probably due to activation-induced cell death, as was indicated by another project in our lab. To determine whether CNS eLFs contain MOG-specific B cells, the MOG tetramer staining was optimized for immunohistochemistry and applied to CNS cryosections. Lymph node cryosections from a Th mouse, carrying MOG-specific B cells, were used as positive control and showed a nice staining of MOG tetramer$^+$ B cells (B220) (Figure 15B). Staining of CNS cryosections from Th17-EAE mice revealed that most eLFs contained only very few MOG tetramer$^+$ B cells (Figure 15C, left panel).

Table 3. Clonotype analysis of expanded clones in Th17-EAE mice

Mouse	Clonotype	Expansion factor	Organ	Isotype	Mutations	AA junction (heavy chain)	V-gene (heavy chain)	AA junction (light chain)	V-gene (light chain)	Cluster
M1	clonotype 1	12	9x CNS 3x SP	IgM	HC: 0; LC: 0	CMRYGSSYWYFDVW	IGHV11-2*01 F	CLQHGESPWTF	IGKV14-126*01 F	8; 1x 1 (CNS)
M1	clonotype 2	6	5x CNS 1x SP	IgM	HC: 0; LC: 0	CMRYDGYYYFDYW	IGHV11-2*01 F	CLQHGESPYTF	IGKV14-126*01 F	8
M2	clonotype 3	4	3x CNS 1x SP	IgD (3) IgM (1)	HC: 0; LC: 0	CARFGYGRTFAYW	IGHV1-19*01 F	CQQDYSSPLTF	IGKV6-32*01 F	3x 0; 1x7 (SP)
M2	clonotype 4	4	2x CNS 1x SP	IgM	HC: 0; LC: 0	CMRYSNWWYFDVW	IGHV11-2*01 F	CLQHGESPFTF	IGKV14-126*01 F	8
M2	clonotype 5	4	1x CNS	IgM	HC: 0; LC: 0	CARSYGNSGAMDYW	IGHV1-19*01 F	CSQSTHVPPTF	IGKV1-110*01 F	4
M2	clonotype 6	4	4x CNS	IgG3 (3) IgA (1)	HC: 2; LC: 0	CARYIGGYGSSDWYFNVW	IGHV7-3*01 F	CLQYDNLYTF	IGKV19-93*01 F	3x 1; 1x 8
M3	clonotype 7	22	14x CNS 3x SP	IgM	HC: 0; LC: 0	CMRYSNYWYFDVW	IGHV11-2*01 F	CLQHGESPYTF / CQQWSGYPYTF#	IGKV14-126*01 F / IGKV4-51*01 F#	8; 1x 2 (SP)
M3	clonotype 8	20	13x CNS 6x SP	IgM	HC: 0; LC: 0	CMRYGSSYWYFDVW	IGHV11-2*01 F	CLQHGESPYTF	IGKV14-126*01 F	8
M3	clonotype 9	7	5x CNS	IgM (4) IgA (1)	HC: 2; LC: 2	CTDPPWFPYW	IGHV6-3*01 F	CAQNLELPFTF	IGKV2-109*01 F	8
M3	clonotype 10	5	1x SP 1x LN	IgG2b (1?)	HC: 2; LC: 0	CTRYGNYGFAYW	IGHV1-69*01 F or IGHV1-69*02 F	CLQSDNMYTF	IGKV17-127*01 F	1x 0 (SP); 1x 9 (LN)
M3	clonotype 11	5	1x CNS	IgD (4) IgM (1)	HC: 0; LC: 0	CARLGLGYDYDGPYAMDYW	IGHV9-3*01 F	CQNGHSFPFTF	IGKV5-39*01 F	0
M3	clonotype 12	4	2x LN	IgM (3) IgD (1)	HC: 0; LC: 0	CARSSRFDYW	IGHV1-64*01 F	CQNVLSTPYTF	IGKV12-89*01 F	4
M3	clonotype 13	4	2x LN	IgM	HC: 0; LC: 0	CARTSTTVVAPTYW	IGHV1-34*01 F	CQQHYSTPWTF	IGKV6-17*01 F	4
M3	clonotype 14	4	1x CNS	IgM	HC: 0; LC: 0	CARHEDSGYAMDYW	IGHV1-62-2*01 F or IGHV1-71*01 F	CKQSYNLWTF	IGKV8-21*01 F	4
M3	clonotype 15	4	1x SP	IgM	HC: 0; LC: 0	CARHEDYGSSHAMDYW	IGHV2-6*03 F	CQQLYSTPYTF	IGKV12-98*01 F	4
M3	clonotype 16	4	2x LN	IgM (3) IgD (1)	HC: 0; LC: 0	CARDYYGSRGYFDVW	IGHV1-12*01 F	CWQGTHFPRTF	IGKV1-135*01 F	1x 4; 1x 0
M3	clonotype 17	4	2x SP	IgM	HC: 0; LC: 0	CARSHTTVVAGAMDYW	IGHV1-81*01 F	CLQSDNLPYTF	IGKV17-121*01 F	1x 4; 1x 0
M3	clonotype 18	4	3x CNS 1x SP	IgM	HC: 0; LC: 0	CARELYGNYLYYYAMDYW	IGHV1-39*01 F	CALWYSTHYVF	IGLV2*02 F	8
M3	clonotype 19	4	2x CNS	IgM	HC: 0; LC: 0	CARGGYDGYYDYYAMDYW	IGHV5-16*01 F	CALWYSTHYVF	IGLV2*02 F	1x 0; 1x 8
M3	clonotype 20	4	3x CNS 1x SP	IgM	HC: 0; LC: 0	CARREGYGNYVDYYAMDYW	IGHV9-4*01 F	CALWYSNHWVF	IGLV1*01 F	8

found additionally in seven cells

In contrast, some eLFs displayed massive accumulation of MOG tetramer^{+} B cells (Figure 15C, right panel). Furthermore, the presence of a MOG-specific IgG1 response in the serum of Th17 and Th1 recipients was determined via ELISA at different time points after adoptive transfer (Figure 15D). At peak of clinical disease, many Th17 recipients showed high levels of MOG-specific IgG1 antibodies compared to very low levels before EAE onset. Similarly, some Th1 recipients exhibited elevated antibody titers at the peak of disease compared to very low levels in mice, which were analyzed
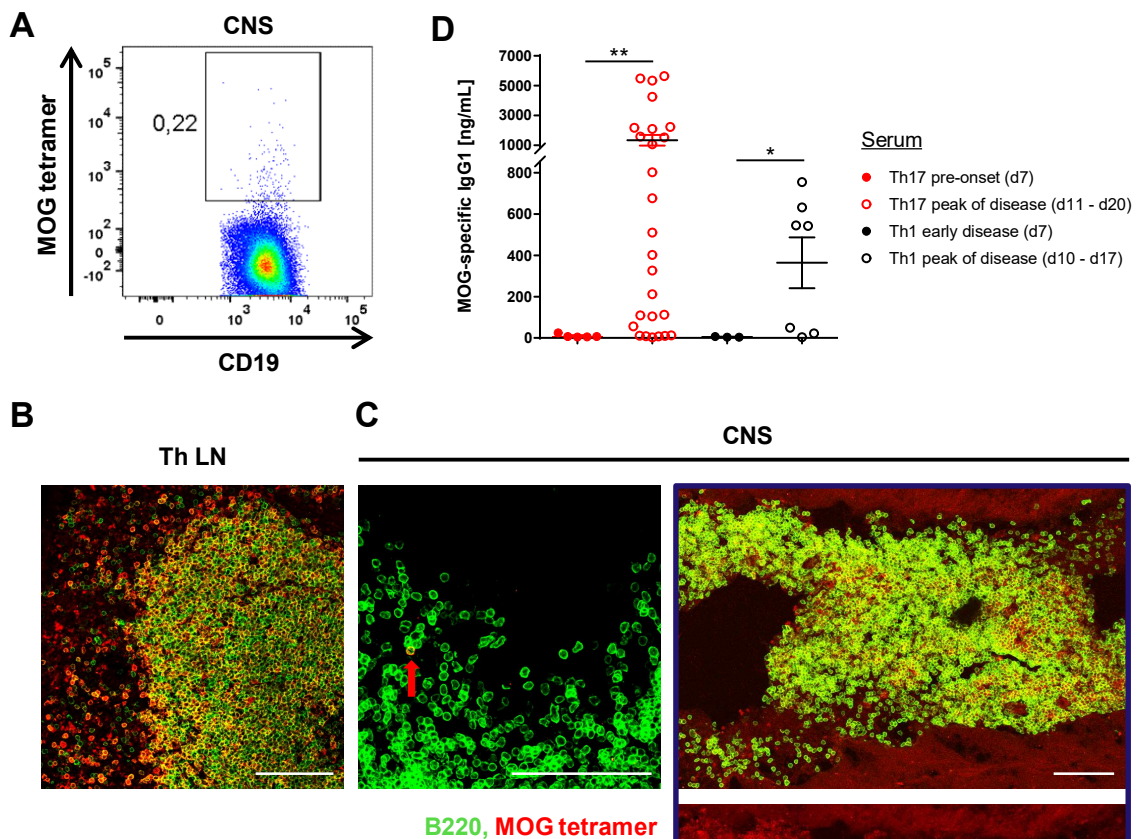
Figure 15. Transferred T cells recruit endogenous MOG-specific B cells. (**A**) Cells were isolated from the CNS of Th17- EAE mice and MOG-specific B cells were labeled using MOG tetramer staining and flow cytometry. A pre-gate on CD19^{+} B cells was applied. One representative plot for n = 5 mice. (**B**) As positive control, lymph node cryosections from a Th mouse were stained for B cells (B220, green) and MOG tetramer (red). (**C**) CNS cryosections from Th17-EAE mice at the peak of disease were stained for B cells (B220, green) and MOG tetramer (red). (Left panel) While most eLFs contain only very few MOG tetramer^{+} B cells (arrow), (right panel) some eLFs show massive accumulation of MOG tetramer^{+} B cells. Box in left lower corner shows zoom of MOG tetramer staining. (**D**) MOG-specific IgG1 antibodies were measured via ELISA in the serum of Th17 and Th1 recipients at different time points (days) after adoptive transfer. Dots represent individual mice. Mean ± SEM, Mann-Whitney U test (Th17 pre-onset vs. peak of disease), Welch`s t-test (Th1 early disease vs. peak of disease). *p < 0.05; **p < 0.01. Scale bars: 100 μm.

at an early disease stage before B cells are starting to infiltrate into the CNS. However, the highest MOG-specific IgG1 titers were found in Th17-EAE mice. Together, data indicate that transferred MOG-specific Th17 cells recruit B cells with the same antigen specificity from the endogenous pool.

4.3 The role of B cells in reactivating T cells in the CNS

4.3.1 T cells depend on B cells to sustain pro-inflammatory functions in the CNS

Since abundant infiltration of B cells into the CNS is a characteristic feature of Th17-mediated EAE, and CNS B cells were found to upregulate markers of GC reactions, costimulation and antigen presentation, we next investigated whether B cells are required for Th17 cells to maintain their full pathogenic potential in the CNS. Previously, the disease severity was indicated to depend on the presence of B cells in Th17-EAE mice suggesting a pro-inflammatory function in this context [178]. To learn more about the contribution of B cells in disease development, Th17 cells were transferred into B cell-deficient Mb1-KO or WT mice for EAE induction. There was no significant difference in EAE development, neither in EAE incidence (Figure 16A) nor in maximum EAE scores (Figure 16B). On the contrary, Mb1-KO mice even showed a slightly earlier disease onset. Thus, in our hands clinical severity in Th17-mediated EAE does not depend on the presence of B cells. A possible reason could be that the transferred Th17 cells are maximally activated and, upon infiltration into the CNS, may strongly drive the pathogenic cascade leading to massive neuroinflammation, rendering B cells dispensable for disease development. To compare the T cell response in the presence and absence of B cells, infiltrating cells were recovered from the CNS of WT and Mb1-KO mice at the peak of disease, and T cells were analyzed by intracellular cytokine staining and subsequent flow cytometry. Transferred T cells could be distinguished from endogenous T cells due to their expression of the transgenic MOG-specific Vα3.2 TCR chain. Interestingly, the frequency of transferred T cells in the CNS was elevated and, correspondingly, the frequency of endogenous T cells was decreased in Mb1-KO mice compared to WT mice (Figure 16C, D). By analyzing transferred and endogenous T cells for the expression of cytokines, substantial differences in T cell responses in the CNS were revealed. For transferred T cells, the frequency of IL-17A$^+$, IFNγ$^+$ and IL-17A$^+$IFNγ$^+$ producers was strongly decreased in Mb1-KO mice compared to WT mice (Figure 16E left panel, F). Similarly, endogenous T cells, which mainly produced IFNγ, showed lower levels of IL-17A$^+$, IFNγ$^+$ and IL-17A$^+$IFNγ$^+$ cells in Mb1-KO mice (Figure 16E right panel, G). In contrast, there were no significant differences in the frequency of Foxp3$^+$, IL-10$^+$ and Foxp3$^+$IL-10$^+$ cells (not
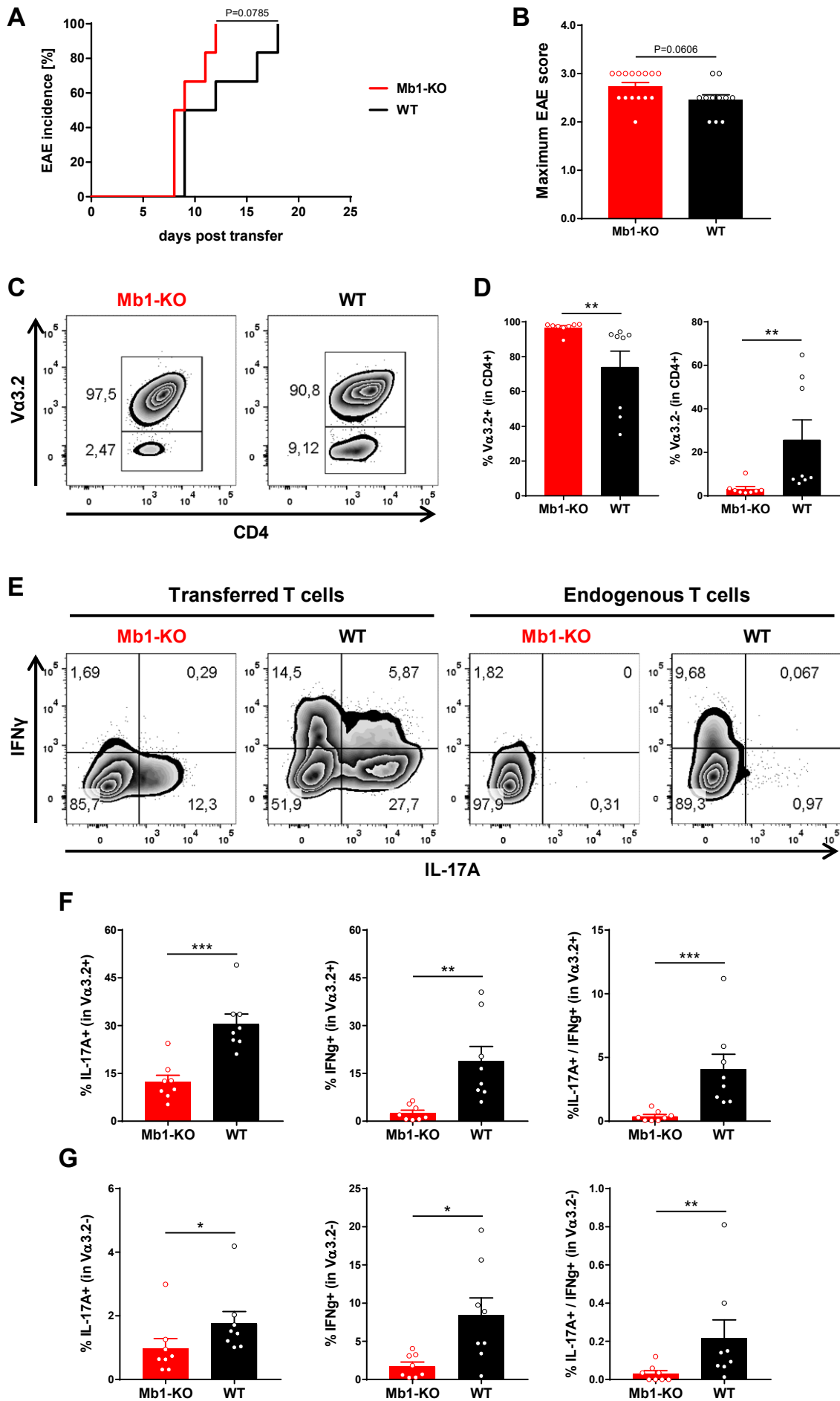
Figure 16. T cells depend on presence of B cells to maintain a highly pro-inflammatory cytokine profile in the CNS. Comparison of Th17-mediated EAE in B cell-deficient Mb1-KO mice and WT mice. (**A**) EAE incidence (n = 6 mice per group). Graph is representative of three independent experiments with three to six mice per group. Mantel-Cox Log rank test. P = 0.0785 (**B**) Maximum scores of mice that developed clinical disease. Graph shows cumulative data from three independent experiments. Mann-Whitney U test. P = 0.0606 (**C-G**) At the peak of disease, cells were isolated from the CNS and analyzed by flow cytometry. (**C**) Representative flow cytometry plots and (**D**) quantification of the frequency of transferred ($V\alpha3.2^+$) and endogenous ($V\alpha3.2^-$) T cells. Mann-Whitney U test. **P < 0.01 (**E-G**) Transferred and endogenous T cells were analyzed for IL-17A and IFNγ expression by intracellular cytokine staining. (**E**) Representative flow cytometry plots and quantification of IL-17A$^+$, IFNγ$^+$ and IL-17A$^+$IFNγ$^+$ producers of (**F**) transferred ($V\alpha3.2^+$) and (**G**) endogenous ($V\alpha3.2^-$) T cells. Graphs show cumulative data from two independent experiments. (F) unpaired *t*-test (left), Welch`s t-test (middle), Mann-Whitney U test (right). (G) Mann-Whitney U test (left and right), Welch`s t-test (middle). *P < 0.05; **P < 0.01; ***P < 0.001. Mean ± SEM. Dots represent individual mice.

shown). Taken together, CNS T cells express lower levels of pro-inflammatory cytokines in the absence of B cells. We propose that in our model, B cells are dispensable for EAE development, but they are required for T cells to maintain their highly pro-inflammatory cytokine profile in the CNS. However, the short acute disease course of only up to six days may prevent us from observing clinical effects caused by decreased effector functions of CNS T cells in the absence of B cells.

4.3.2 Observing T:B cell interactions in meningeal eLFs by intravital microscopy

Meningeal eLFs have been proposed to fuel chronic inflammation directly in the CNS by providing a good microenvironment for the interaction of T and B cells. Indeed, our previous results argue for intense T:B cell communication in the CNS and support a role of B cells in antigen presentation and restimulation of T cells. In the final part of the project, we investigated what exactly happens in eLFs by observing the interaction of T and B cells in real-time using intravital two-photon microscopy. In particular, we aimed to clarify whether B cells are able to reactivate Th17 cells in eLFs, thereby supporting inflammatory processes within the CNS.

Compared to confocal microscopy, two-photon microscopy provides increased penetration depth and reduced phototoxicity, thereby allowing imaging of live tissues. During imaging, the animal needs to be anesthetized, intubated and mechanically stabilized [110]. Intravital imaging does not only enable visualizing cellular movement, but also monitoring cellular function. Here, we used the genetically-encoded calcium indicator Twitch-2B, which allows for studying T cell activation in real-time by

measuring the increase of the intracellular calcium concentration upon TCR ligation [110]. An overview of the experimental set-up is given in Figure 17A. During their differentiation into Th17 cells, MOG-specific T cells from 2D2 mice were transduced with a retrovirus containing Twitch-2B, and adoptively transferred into Mb1Cre x ROSA26 tdTomato mice, which expressed tdTomato specifically in B cells under control of the *Cd79a* promoter. EAE developed after eight to 15 days, and using mice, which had been on a high score for several days to allow massive infiltration of B cells and eLF formation, intravital two-photon microscopy of spinal cord eLFs was performed to visualize interactions of transferred Twitch-2B$^+$ Th17 cells and tdTomato$^+$ B cells and subsequent activation events of the Th17 cells. To establish the experimental procedure, the optimal time point for retroviral transduction, which is only successful in proliferating cells, during the differentiation process was determined. T cells were infected with the Twitch-2B sensor either after two days in Th17 conditions (primary phase) or one day after restimulation with anti-CD3 and anti-CD28 (secondary phase), and the frequency of Twitch-2B$^+$ T cells was determined two days after transduction by flow cytometry (Figure 17B). The transduction efficiency was considerably higher during the secondary phase with up to 60 % Twitch-2B-expressing Th17 cells. In addition, T cells that were transduced during the primary phase did not survive the restimulation with anti-CD3 and anti-CD28 well, emphasizing the secondary phase as best time point for retroviral transduction. Two days after restimulation, which corresponds to one day after transduction, Th17 cells were adoptively transferred into recipient mice, and it was confirmed that the transduction did not impair their ability to induce EAE. From the CNS, infiltrating cells were isolated and the transferred T cells were analyzed for expression of Twitch-2B by flow cytometry. Transduced T cells survived very well *in vivo* and infiltrated the CNS, as indicated by almost identical fractions of Twitch-2B$^+$ cells in the CNS compared to the *in vitro* culture (Figure 17C). Moreover, transduced T cells were confirmed to be fully functional *in vivo*, since they showed the same cytokine profile as Twitch-2B$^-$ T cells in the CNS (Figure 17D). To image interactions of T and B cells, also the B cells need to be fluorescently labeled. Therefore, we crossed Mb1.Cre mice to ROSA26 tdTomato mice to obtain mice expressing tdTomato specifically in B cells. First, we performed flow cytometry of blood samples to confirm that tdTomato expression is restricted to B cells (not shown). Next, it was tested *in vitro* whether tdTomato$^+$ B cells loose tdTomato expression, when they

proliferate strongly. By performing an iGB culture, highly proliferating B cells were shown to maintain tdTomato expression (not shown). In addition, tdTomato expression in CNS-infiltrating B cells in Mb1.Cre x ROSA26 tdTomato Th17-EAE mice was detected by flow cytometry as well as confocal microscopy of CNS cryosections stained for T cells (CD3) and B cells (B220) (Figure 17E). In contrast, other CNS-infiltrating APCs such as CD11b$^+$ macrophages showed frequencies of tdTomato$^+$ cells below 4 % (not shown). Summing up, the successful labeling of CNS T and B cells with fluorescent reporters paved the way for observing their interactions by intravital two-photon microscopy.

In the first set of intravital microscopy experiments, we imaged three Th17-EAE mice, which had exhibited clinical symptoms for four to seven days and an EAE score of at least 2.5 at the day of analysis. The long disease duration with a high clinical score is crucial to maximize B cell infiltration and results in a more advanced developmental stage of eLFs. In the thoracic part of the spinal cord, a small window of the size of one vertebra was carefully dissected, leaving the leptomeninges completely intact. In all three mice, massive accumulation of Twitch-2B$^+$ T cells and tdTomato$^+$ B cells was found in the meninges, revealing eLFs of substantial size and structure. A representative image of the dorsal view onto a large eLF is shown in Figure 18A. In the central area, there was strong clustering of B cells with infiltrating T cells, whereas in the outer region, there were mainly T cell aggregates. Since in this experiment, the transduction rate of T cells ranked at 58 %, it can be assumed that the accumulation of transferred T cells was even underestimated in this image. The histological evaluation of CNS lesions in Th17-EAE mice (section 4.1.3) revealed that the localization of eLFs in the spinal cord is different in each mouse. Therefore, it was quite unexpected to find enormous T:B cell aggregates in the very small imaging window of all three mice, suggesting that substantial parts of the leptomeninges might be lost during dissection and preparation of CNS tissues for histological analysis. Then, we zoomed inside the eLFs and found that many T cells have contact with one or more B cells (Figure 18B). Exemplary images of extensive T:B cell contacts are also shown (Figure 18C).
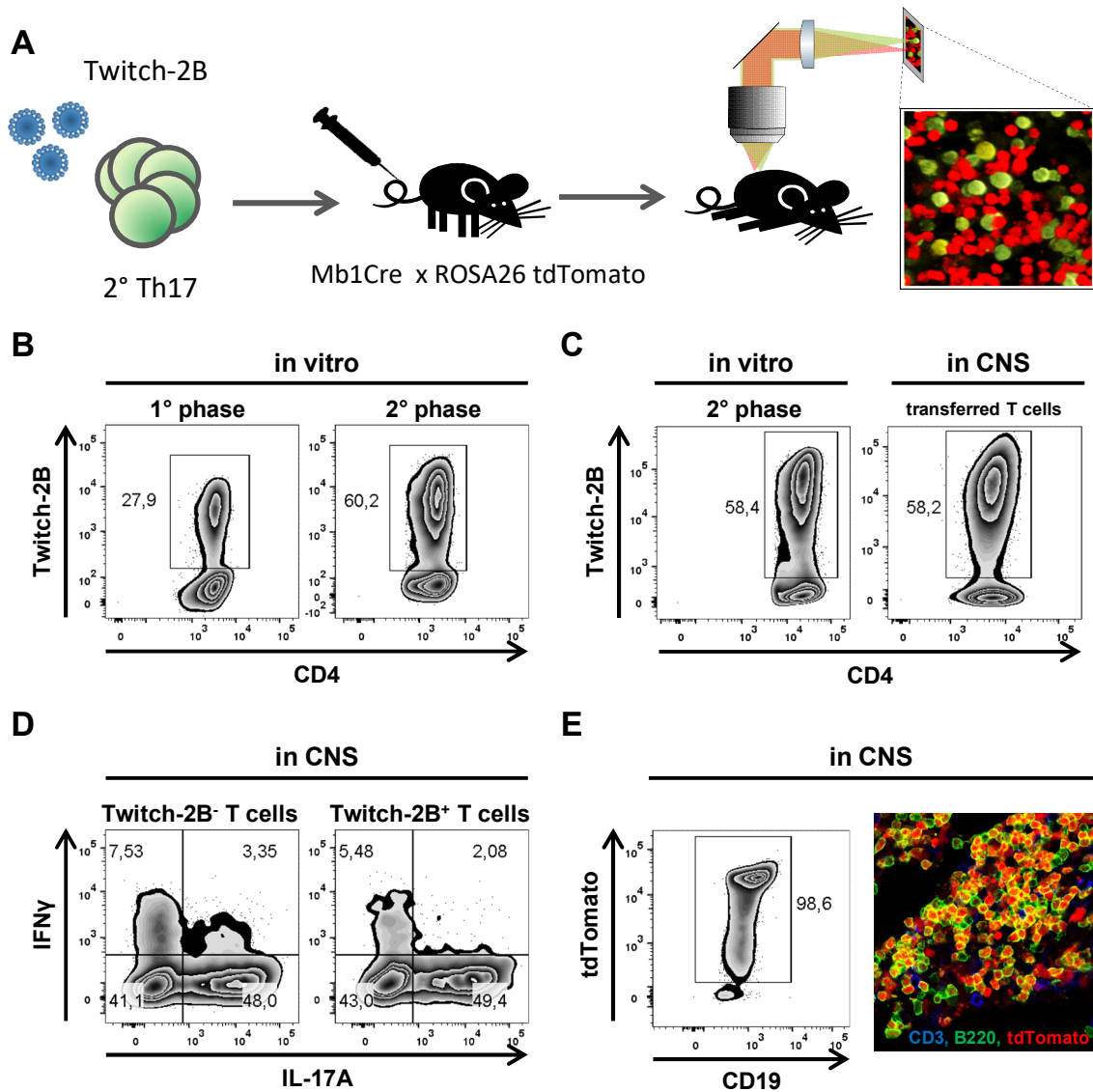
Figure 17. Studying interactions of Th17 cells expressing the calcium indicator Twitch-2B and B cells expressing tdTomato in meningeal eLFs by intravital microscopy. (**A**) Experimental outline. MOG-specific T cells from 2D2 mice are retrovirally transduced with the Twitch-2B construct during their differentiation into Th17 cells. Upon adoptive transfer in Mb1.Cre x ROSA26 tdTomato mice, intravital two-photon microscopy of spinal cord eLFs in EAE mice can be performed to visualize interactions of Th17 cells (green) and B cells (red) as well as subsequent activation events of Th17 cells. (**B**) During *in vitro* differentiation, T cells were either transduced after two days in Th17 conditions (primary phase) or one day after restimulation (secondary phase) and tested for transduction efficiency after two days. Flow cytometry plots are representative of four independent experiments. (**C**) The frequency of Twitch-2B$^+$ T cells before adoptive transfer (secondary phase) and in the CNS of Th17-EAE mice was compared. For the CNS sample, a pre-gate on transferred (Vα3.2$^+$) T cells was applied. Flow cytometry plots are representative of nine mice from four independent experiments. (**D**) Twitch-2B$^-$ and Twitch-2B$^+$ T cells from the CNS of Th17-EAE were analyzed for expression of IL-17A and IFNγ by intracellular cytokine staining. A pre-gate on transferred (Vα3.2$^+$) T cells was applied. Flow cytometry plots are representative of four mice from two independent experiments. (**E**) CNS CD19$^+$ B cells from Mb1.Cre x ROSA26 tdTomato Th17-EAE mice were analyzed for tdTomato expression by flow cytometry (left) and confocal microscopy of a CNS cryosection stained for T cells (CD3, blue) and B cells (B220, green) (right). The shown flow cytometry plot is representative of six mice from 3 independent experiments.
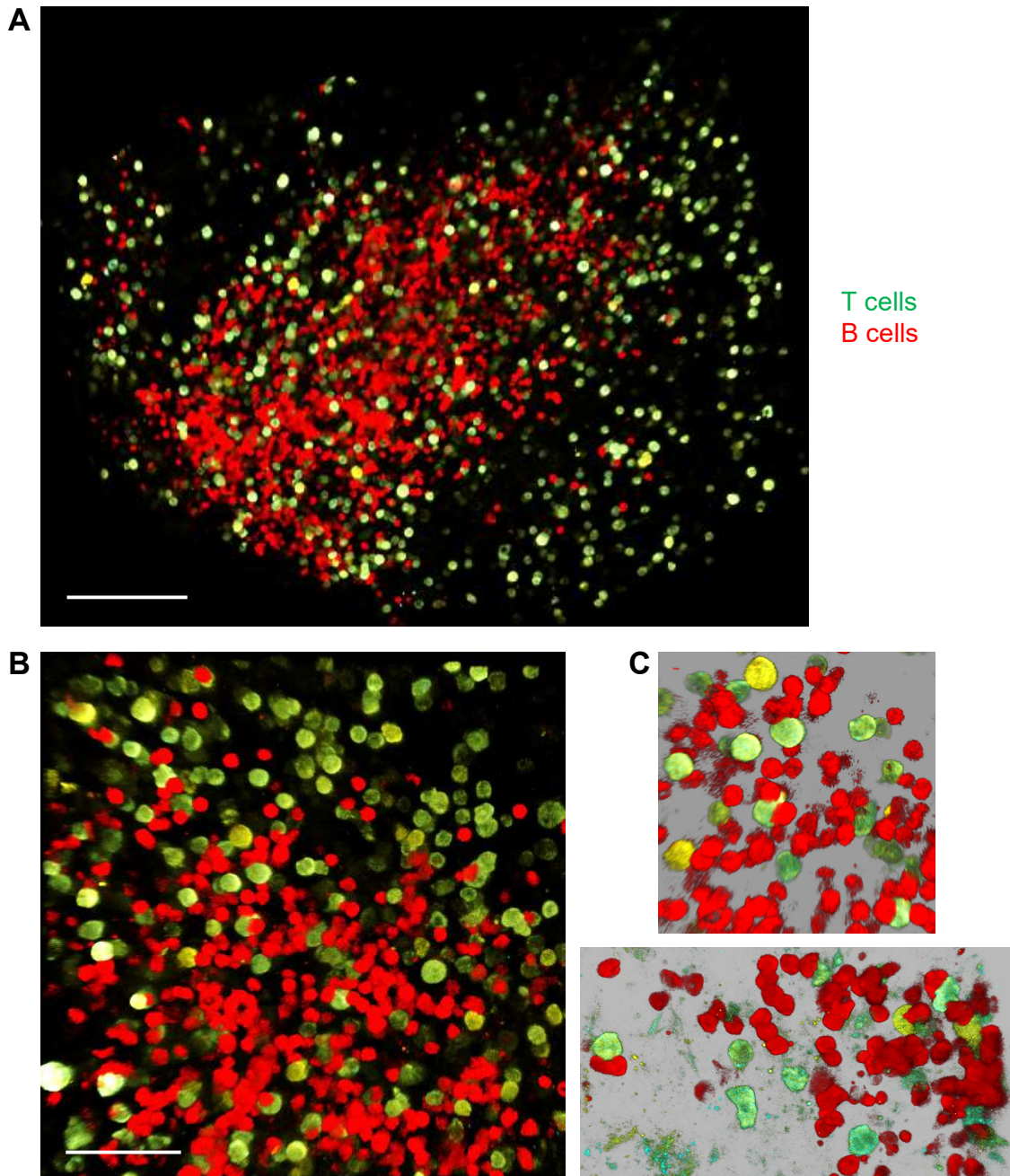
Figure 18. Meningeal eLFs are sites of massive T and B cell accumulation with extensive T:B cell contacts. Intravital microscopy of Twitch-2B$^+$ T cells and tdTomato$^+$ B cells in spinal cord eLFs of Th17-EAE mice. (**A**) Dorsal view onto and (**B**) zoom into eLF containing Twitch-2B$^+$ T cells (green) and tdTomato$^+$ B cells (red). (**C**) Exemplary images of T:B cell contacts. Scale bar: (**A**) 100µm, (**B**) 50µm.

To investigate whether eLFs are sites of T cell activation, T:B cell aggregates were imaged at different locations to examine the T cell behavior. The FRET- based Twitch-2B sensor represents a powerful tool to visualize intracellular calcium signaling in activated T cells. When the calcium concentration increases, the calcium-binding domain causes a conformational change bringing the two fluorophores mCerulean3

and cpVenus in close proximity, and the resulting FRET leads to a drop in blue fluorescence and an increase in yellow fluorescence. Thereby, the ratio of yellow and blue fluorescence directly reflects the change in the intracellular calcium concentration [123, 124]. In general, both T and B cells were found to be quite stationary within eLFs, whereby the T cells appeared very blastic, indicating that they are highly activated. Figure 19 depicts a single time point of a representative video, with the left and right part showing a fluorescence overlay of Twitch-2B^{+} T cells and tdTomato^{+} B cells and a pseudocolor calcium ratio image indicating calcium signaling in T cells, respectively. Importantly, many T cells showed elevated calcium levels, indicating eLFs to be sites where CNS-infiltrating T cells can become reactivated.

T cells
B cells

Low   Ca²⁺   High
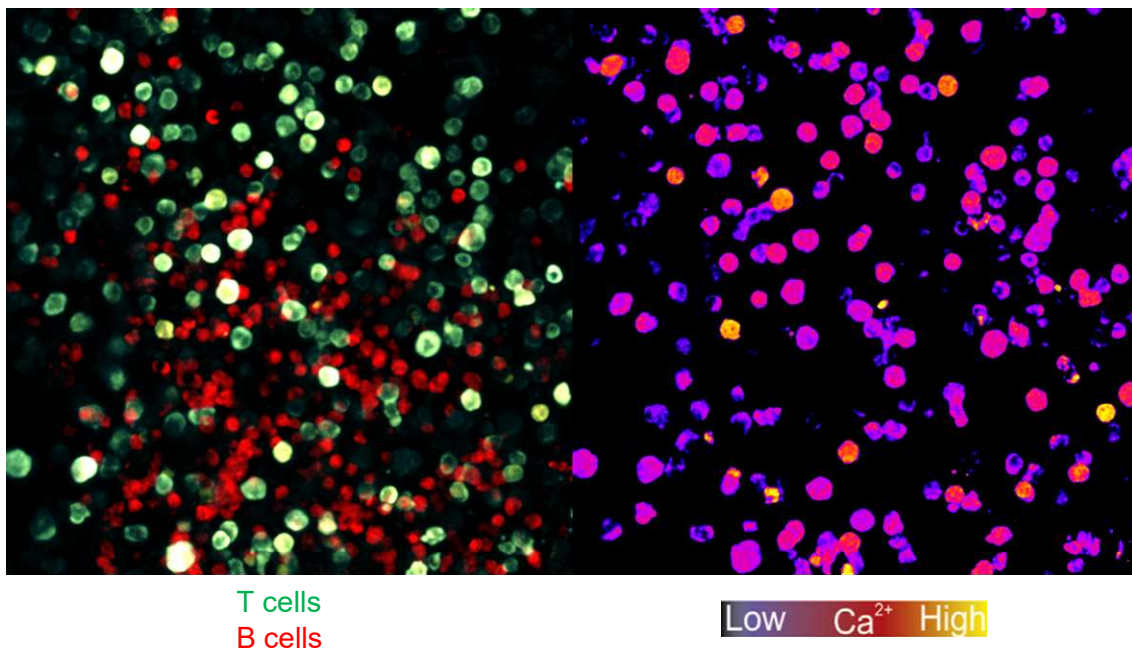
Figure 19. Many T cells show elevated calcium levels in meningeal eLFs. Intravital microscopy of Twitch-2B^{+} T cells and tdTomato^{+} B cells in spinal cord eLFs of Th17-EAE mice. (Left) Fluorescence overlay of Twitch-2B^{+} T cells (green) and tdTomato^{+} B cells (red) and (right) pseudocolor calcium ratio image showing calcium levels of T cells.

4.3.3 T cells can form long-lasting contacts with B cells in meningeal eLFs

As control, a second set of intravital microscopy experiments was performed, whereby ovalbumin (OVA, a chicken egg white protein)-specific T cells were adoptively transferred in addition to MOG-specific T cells. Naïve OVA-specific T cells were isolated from OT-II mice, which express the TCR Vα2 and Vβ5 chains recognizing the

ovalbumin 323-339 peptide on the C57Bl/6J background [166], and, in parallel to MOG-specific T cells from 2D2 mice, differentiated into Th17 cells. In contrast to previous experiments, OT-II Th17 cells were infected with the Twitch-2B sensor (with a transduction rate of 75 %) instead of 2D2 Th17 cells, and they were transferred together into Mb1.Cre x Rosa26 tdTomato mice. The aim of this experiment was to compare the T cell response of 2D2 T cells to OT-II T cells, which as non-CNS-specific T cells should not find their antigen in the meninges in contrast to 2D2 T cells and can therefore be considered as control cells. Importantly, OT-II T cells infiltrated the CNS together with 2D2 T cells. In total, 128 2D2 T cells and 101 OT-II T cells, recorded in three independent experiments for both groups, were investigated regarding their interaction with B cells by monitoring the movement of each individual cell in the 3D follicle structure during the entire length of the acquired videos. Notably, around half of the 2D2 T cells formed contacts with B cells, whereas only 14 % of OT-II T cells interacted with B cells (Figure 20A). Next, the duration of T:B cell contacts was
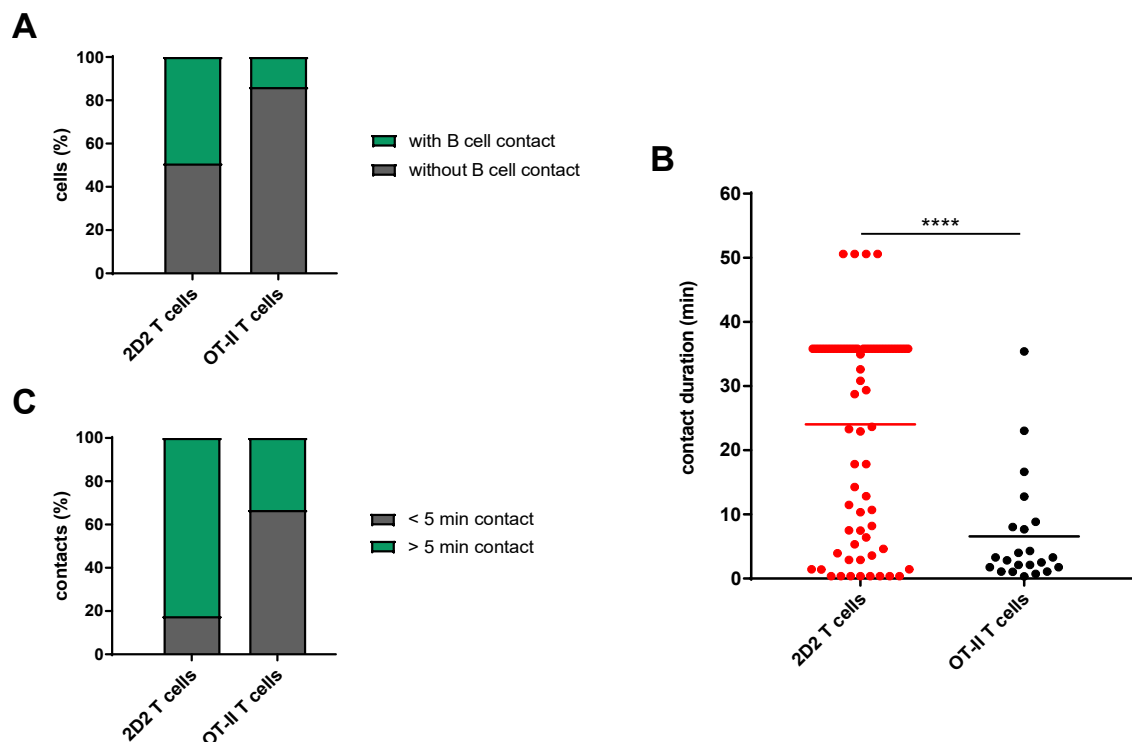
Figure 20. 2D2 T cells form long-lasting contacts with B cells compared to OT-II T cells. Intravital microscopy of Twitch-2B^{+} T cells and tdTomato^{+} B cells in spinal cord eLFs of Th17-EAE mice. (**A**) Proportion of 2D2 (n = 128 cells from three independent experiments) and OT-II T cells (n = 101 cells from three independent experiments) forming contact with B cells. (**B**) Quantification of T:B cell contact duration. Tied values result from maximum video length (15-50 min for both experimental groups). Dots represent individual contacts. Horizontal lines indicate means. Mann-Whitney U test. ****P < 0.0001. (**C**) Proportion of long (> 5 min) and short (< 5 min) T:B cell contacts.

quantified. 2D2 T cells can form very long contacts with B cells, which could often be observed during the entire observation period of up to 50 minutes. In comparison, OT-II T cells formed B cell contacts of much shorter duration (Figure 20B). Setting a threshold of five minutes to define short and long contacts, as was suggested by measuring the contact length of B cells and Tfh cells in regular GC reactions [200], we found that the majority of 2D2 T cells (82 %) engage in long T:B cell contacts compared to only a third of OT-II T cells (Figure 20C). Thus, this contact analysis points towards an antigen-specific interaction of 2D2 T cells with B cells in meningeal eLFs.

4.3.4 B cells are able to reactivate T cells in meningeal eLFs

Next, it was investigated whether 2D2 T cells become activated during B cell contact. For all 128 recorded 2D2 T cells, the velocity was plotted against the calcium indicator ratio (YFP/CFP) of the Twitch-2B sensor in each time frame (Figure 21A). In this graph, each data point represents a single time point for a particular cell. The calcium ratio was found to negatively correlate with the velocity. Therefore, increased calcium ratios were associated with lowered motility of the respective T cell, as was shown in previous studies [123, 201]. To correctly interpret increased intracellular calcium concentrations as calcium signaling, a threshold for the calcium ratio needs to be defined. Formerly, the threshold was set to the maximal calcium ratio level reached spontaneously by 95 % of cells of a chosen control group [201]. In our study, the threshold was defined based on T cells, whose velocity was higher than 5 µm/min since these cells are moving too fast to become activated via cellular contact. According to this criterion, the threshold was calculated using 351 calcium ratios, which corresponded to 3.2 % of the fastest 2D2 T cells. Since 95 % of these calcium ratios were below a value of 1.289, calcium ratios above this threshold were defined as calcium signaling. Interestingly, in 2D2 T cells, 12.5 % of calcium ratios were found to exceed the threshold (Figure 21A). To compare the calcium signaling in T cells without and with B cell contact, calcium ratios (n = 10851) were sorted into two groups, depending on whether the T cell has contact with a B cell in this time frame ($n_{without\ contact}$ = 6081; $n_{with\ contact}$ = 4770). Notably, 17.4 % of calcium ratios in T cells with B cell contact were above the threshold compared to 8.7 % of calcium ratios in T cells without

A

B

C
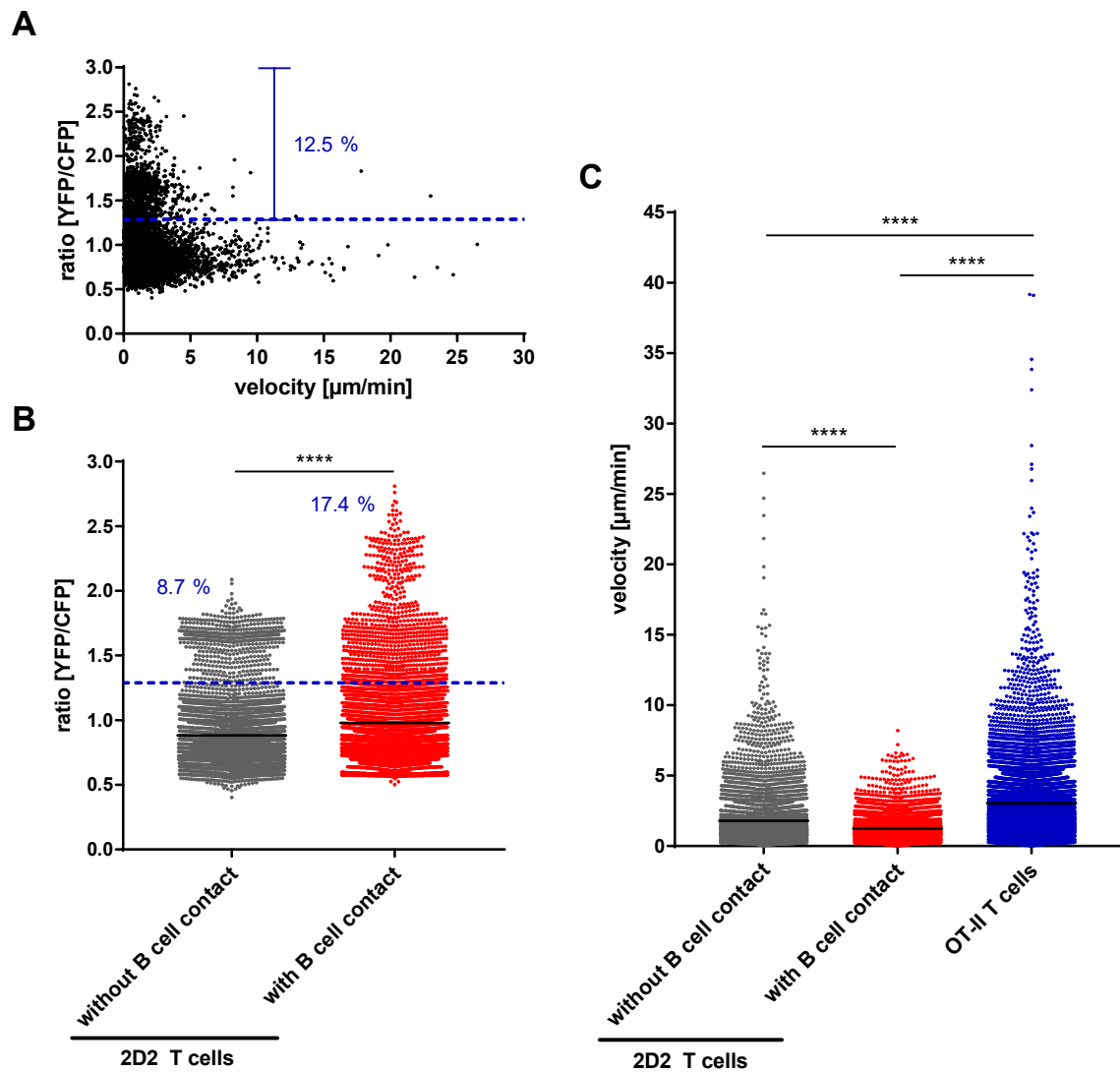
Figure 21. B cells are able to reactivate T cells in eLFs. Intravital microscopy of Twitch-2B^{+} T cells and tdTomato^{+} B cells in spinal cord eLFs of Th17-EAE mice. (**A**) Scatterplot showing velocity versus calcium indicator ratio (YFP/CFP) of 2D2 T cells. Each dot represents a single time point for a particular cell. (**B**) Quantification of the calcium indicator ratio (YFP/CFP) and comparison between 2D2 T cells without B cell contact (n = 6081 ratios) and 2D2 T cells with B cell contact (n = 4770 ratios). Mann-Whitney U test. ****$P < 0.0001$. (**C**) Quantification of the velocity of 2D2 T cells without B cell contact (n = 6013 velocities), 2D2 T cells with B cell contact (n = 4705 velocities) and OT-II T cells (n = 8879 velocities). One-way ANOVA with Tukey post-test. ****$P < 0.0001$. (**A**), (**B**) The blue dashed line indicates the ratio threshold (1.289). (**B**), (**C**) Horizontal lines indicate means. All graphs show cumulative data from three independent experiments.

B cell contact, indicating more pronounced calcium signaling in T cells during B cell contact. Very high calcium ratios exceeding a value of 2.0 were almost exclusively found in the group with B cell contact (Figure 21B). Consistently, T cells with B cell contact showed significantly lower velocity compared to T cells without B cell contact ($n_{without\ contact}$ = 6013 velocities; $n_{with\ contact}$ = 4705 velocities). In comparison, OT-II T cells displayed significantly higher motility than both 2D2 T cell groups (n = 8879 velocities

from 101 cells recorded in three independent experiments) (Figure 21C), indicating that the non-CNS-specific OT-II T cells are being arrested less often due to lack of cognate interaction with B cells and other APCs. This quantitative analysis supports our hypothesis that T cells can become reactivated by B cells in eLFs. However, threshold-exceeding calcium ratios in T cells without B cell contact may result from reactivation by other APCs such as macrophages or interaction with B cells prior to the imaging period.

For better visualization of T:B cell interaction and the resulting T cell response, Figure 22A depicts snapshots of a representative 2D2 T cell, which becomes activated during B cell contact. The left and right part show a fluorescence overlay of Twitch-2B⁺ T cells
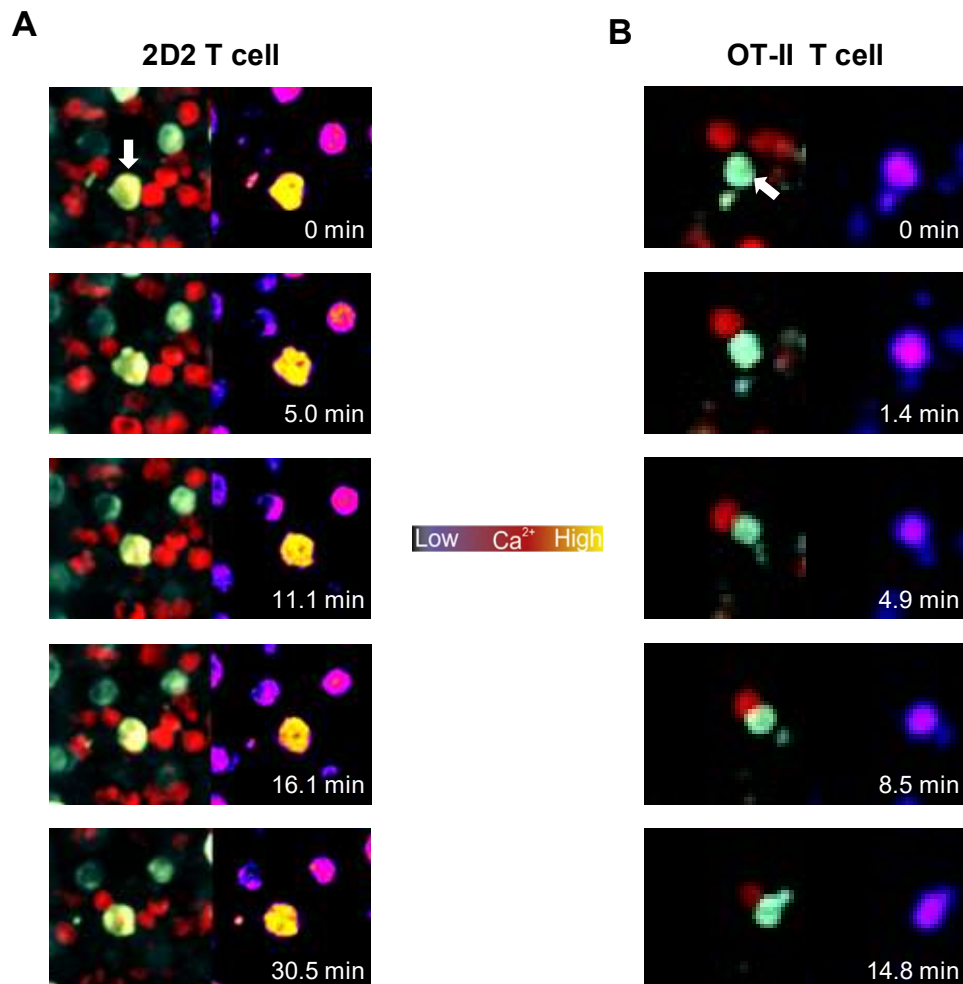
Figure 22. 2D2 T cells, but not OT-II T cells become reactivated during B cell contact – exemplary microscopic images. Intravital microscopy of Twitch-2B⁺ (**A**) 2D2 or (**B**) OT-II T cells and tdTomato⁺ B cells in spinal cord eLFs of Th17-EAE mice. (Left) Fluorescence overlay of Twitch-2B⁺ T cells (green) and tdTomato⁺ B cells (red) and (right) pseudocolor calcium ratio image showing calcium levels of T cells. White arrow indicates cell of interest. (**A**) 2D2 T cell has B cell contact at all indicated time points. (**B**) 0 min: before B cell contact; 1.4 min – 14.8 min: with B cell contact.

and tdTomato+ B cells and a pseudocolor calcium ratio image indicating calcium signaling in T cells, respectively. The indicated T cell formed a long-lasting contact with one and later two B cells. While the cell appeared to be arrested and only underwent minor changes in cell shape, it displayed high calcium signaling for over 30 min. To further investigate whether OT-II T cells, which were found to form only rare and predominantly short contacts with B cells (Figure 20), become activated during B cell contact, we also analyzed their calcium ratios, with a representative cell being depicted in Figure 22B. The indicated OT-II T cell did not show a difference in calcium levels before (0 min) and during contact with a B cell (1.4 min – 14.8 min). The difference in T cell response upon B cell contact became even more evident by comparing single cell tracks of 2D2 and OT-II T cells. The four representative 2D2 T cells formed B cell contact during the entire or a part of the observation period. In the upper left and right

A 2D2 T cells
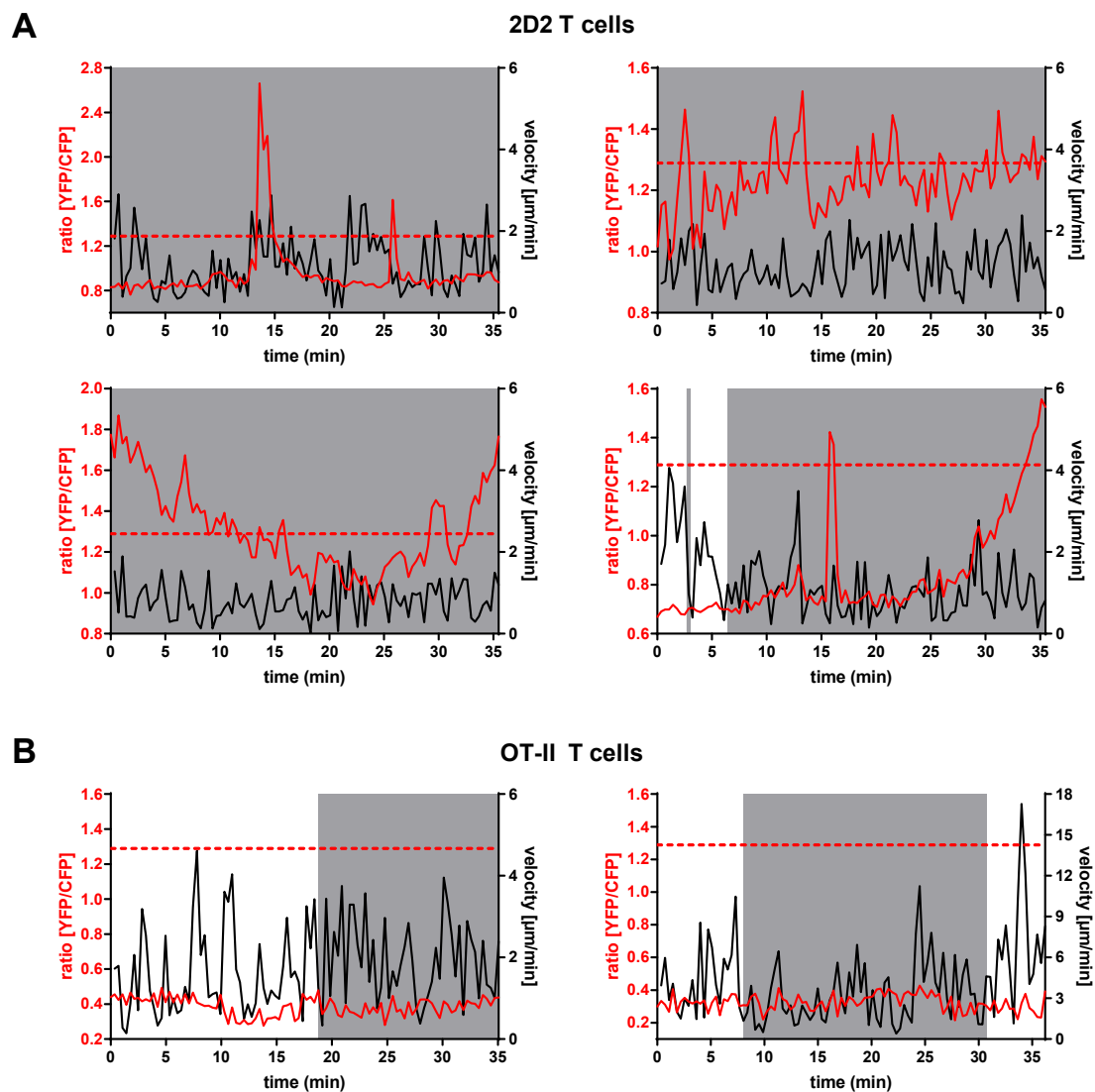
B OT-II T cells

Figure 23. 2D2 T cells, but not OT-II T cells, become reactivated during B cell contact – time course analysis of T cell behavior. Intravital microscopy of Twitch-2B^{+} T cells and tdTomato^{+} B cells in spinal cord eLFs of Th17-EAE mice. Representative tracks of (**A**) 2D2 T cells (n = 128 cells from three independent experiments) and (**B**) OT-II T cells (n = 101 cells from 3 independent experiments) showing calcium indicator ratio (YFP/CFP, red) and velocity (black) in each time frame. The red dashed line indicates the ratio threshold (1.289). Grey shading highlights time frames with B cell contact.

track, the T cell showed two calcium spikes and several consecutive ones, respectively. In the lower left track, the T cell displayed high calcium ratios, which then decreased below the threshold before they increased again. In the lower right track, the T cell showed a single spike and increasing calcium ratios at the end of the observation period (Figure 23A). In contrast, the calcium ratios of the two representative OT-II T cells remained unchanged during B cell contact (Figure 23B). Together, these data indicate that 2D2 T cells, but not OT-II T cells can become reactivated by B cells, pointing towards an antigen-specific interaction. This finding was supported by analyzing 2D2 and OT-II T cell responses in the CNS by intracellular cytokine staining and subsequent flow cytometry. While both strongly produced IL-17A during the *in vitro* culture, OT-II T cells failed to maintain IL-17A production *in vivo* in contrast to 2D2 T cells. Instead, they adopted secretion of the anti-inflammatory cytokine IL-10 (Figure 24), indicating that OT-II T cells do not become reactivated by APCs in the CNS. Summing up, our intravital microscopy study provides evidence for a role of B cells in antigen presentation and reactivation of T cells in meningeal eLFs.
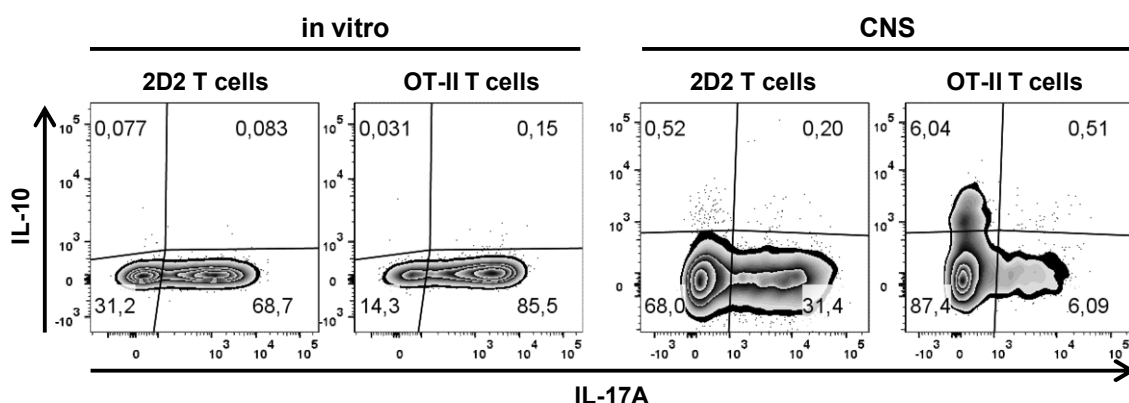
Figure 24. In contrast to 2D2 T cells, OT-II T cells fail to maintain IL-17A production and start secreting IL-10 in the CNS. 2D2 and OT-II T cells were analyzed for expression of IL-17A and IL-10 by intracellular cytokine staining. (Left panel) 2D2 and OT-II cultures after four days under Th17 polarizing conditions. (Right panel) At the peak of disease, cells were isolated from the CNS of a Th17-EAE mouse (n = 1). Transferred 2D2 and OT-II T cells were identified based on their expression of the transgenic Vα3.2 and Vβ5.1/5.2 TCR chain, respectively.

5. Discussion

5.1 The role of Th17 cells in recruiting B cells into the CNS

In addition to pathogenic T cells, which have long been accepted as crucial disease drivers in CNS autoimmunity, a pivotal role has also been suggested for B cells. In the present study, we aimed to investigate whether and how different T cell subsets cooperate with B cells in disease induction and propagation. To discriminate between Th1- and Th17-mediated pathology, we established adoptive transfer EAE according to Jäger et al. [72]. In this model, disease is induced by *in vivo* transfer of *in vitro* differentiated pure MOG-specific Th cell subsets into wildtype recipient mice (Figure 5A). In previous and still common protocols, adoptive transfer EAE was performed by isolating myelin-antigen primed T cells from immunized mice, which were then *in vitro* restimulated under Th1- or Th17-skewing conditions before transfer [70, 71, 202]. Since these CNS-specific T cells have already been primed and possibly exposed to differentiation-inducing cytokine environments *in vivo*, they could comprise precursors of different subsets. Therefore, our more rigorous method of generating and transferring pure Th1 and Th17 cell populations represents a powerful approach to study their pathogenicity independently of each other and dissect their distinct pathogenic properties *in vivo*. Consistent with the previous study by Jäger et al. [72], Th1 and Th17 cells were demonstrated to transfer EAE independently of each other, with Th1 and Th17 recipients showing a comparable disease course and similar severity (Figure 5C). Both Th cell subsets required two rounds of stimulation *in vitro* to be able to confer disease upon adoptive transfer since the secondary restimulation is crucial for generating a largely homogeneous population of highly activated T cells. Interestingly, Th1 recipients mainly showed classical EAE symptoms, whereas some Th17 recipients also developed atypical signs of EAE, such as extensive weight loss, ataxia and severe balance problems. Adoptive transfer of Th17 cells into IL-17 receptor A (RA)-deficient mice revealed that the development of atypical disease may be caused by the Th17 signature cytokine IL-17 since these mice exhibit only classical symptoms in contrast to WT recipients [109]. Earlier studies have indicated that cerebellum and brainstem are especially sensitive to inflammation induced by IL-17, and that lesions in these areas appear to be associated with atypical signs of EAE. In contrast, the Th1 signature cytokine IFNγ seems to protect cerebellum and brainstem

from inflammation, while inducing lesions mainly in the spinal cord, which are associated with classical signs of EAE [203-205]. In addition, adoptive transfer studies in RAG2-KO mice, which are deficient for mature B and T cells, showed that Th1 cells predominantly transferred classical EAE, whereas around half of Th17 recipients exhibited atypical disease signs [206]. In line with these data, we found abundant inflammatory infiltrates not only in the spinal cord, but also in the brainstem and cerebellum of Th17 recipients (Figure 8 + Figure 9). To investigate whether transferred Th1 and Th17 cells stably express their signature cytokines upon adoptive transfer, T cell responses in the CNS were analyzed by flow cytometry. Th1 cells were found to be very stable *in vivo,* since they robustly expressed IFNγ, but no IL-17A (Figure 6A). In contrast, Th17 cells maintained production of IL-17A, but they could also adopt expression of IFNγ, whereby both IFNγ$^+$ single and IFNγ$^+$IL-17A$^+$ double producers could be detected (Figure 6B). As comparison, primary Th17 cells were almost devoid of IFNγ-producing cells *in vitro* (Figure 5B). These results are consistent with previous observations by Jäger et al. [72] and highlight the plasticity of the Th17 cell subset. Interestingly, fate-mapping experiments with MOG/CFA-immunized mice demonstrated that also *in vivo*-generated Th17 cells exclusively express or co-express IFNγ in the CNS, suggesting that this adoption is part of the normal effector mechanisms of Th17 cells in the target organ [101, 102]. However, considering that our Th17 culture also contains some non-IL17A-producing cells, it cannot be excluded that a proportion of IFNγ producers among transferred T cells in the CNS originate from these formerly uncommitted T cells, which then acquire a Th1 phenotype *in vivo*. Summing up, in our model, both transferred Th1 and Th17 cells maintain expression of their original cytokines in the inflamed CNS, and Th17 cells represent a more plastic T cell subset that is able to modulate its effector functions *in vivo*.

Several lines of evidence argue for a special relationship of Th17 cells and B cells. Th17 cells were shown to trigger strong proliferation of B cells *in vitro* and promote B cell responses in GC reactions *in vivo*, providing help for isotype class switching and antibody production [160]. On the other hand, B cells are efficient APCs for the activation of T cells with the same antigen specificity [163]. They also produce IL-6 [137], an important cytokine for pathogenic Th17 cell differentiation in EAE [138]. Importantly, several studies reported substantial infiltration of B cells into the CNS in Th17-mediated EAE [109, 157, 178]. Quinn et al. [178] performed a time course

analysis by quantifying the extent of B cell accumulation in the CNS before EAE onset, at early disease as well as at the peak of disease. They found increasing B cell infiltration in brain and spinal cord with disease progression, with the highest number of B cells detected at the peak of disease, and reported B cell recruitment to the CNS to be part of a second wave of immune cell infiltration following Th17 cell accumulation. In our study, we aimed to verify whether B cell invasion of the CNS is a central feature in our Th17-EAE model, and compared the ability of Th1 and Th17 cells to recruit B cells into the CNS. Notably, Th17 recipients showed both a higher frequency as well as increased absolute numbers of infiltrating B cells in the CNS at the peak of disease compared to Th1 mice. Th17 recipients displayed considerable variation in B cell frequencies, with some mice even containing more than 40 % B cells within the CD45^{high} CD11b^{low} population and more than 1x10^6 B cells in the CNS (Figure 7). Comparison of B cell numbers in the CNS revealed markedly higher B cell infiltration (~60 % more) in our model compared to the study by Quinn et al. [178]. Accordingly, they reported rather small clusters of accumulated B cells shown by immunohistochemical analysis of spinal cord sections. In both studies, Th17 recipients were analyzed at the peak of disease and exhibited clinical disease for up to seven days. Therefore, differences in disease duration can likely be excluded as a reason for the reduced B cell accumulation in the study by Quinn et al. A possible explanation could be that they induced EAE by transferring T cells which were isolated from MOG/CFA-immunized mice and cultured in Th17-skewing conditions instead of *in vitro* differentiated Th17 cells, as in our more stringent protocol. In consequence, the purer Th17 response might account for the enhanced B cell infiltration in our model. Consistently, a recent study employing our protocol also reported high frequencies of accumulating B cells and large eLFs in spinal cord meninges [207]. Since massive accumulation of B cells in the CNS is a characteristic feature of Th17-, but not Th1-mediated EAE, we can conclude that Th17 cells are superior to Th1 cells in recruiting B cells into the CNS. Consistent with this finding, CNS lesions in Th1 and Th17 recipients were reported to display distinct histopathological phenotypes. While Th1 recipients show typical mononuclear cell infiltrates in the parenchyma and meninges of the spinal cord, Th17 recipients exhibit very large aggregates of small lymphocytes in the leptomeninges [72]. In a follow-up study, these meningeal eLF-like structures were further described as sites of enormous T and B cell accumulations, which are

abundantly found in Th17 recipients, but not in recipients of other Th cell subsets [72, 109]. To investigate the structural organization and cellular components of CNS lesions in our Th17-EAE model, we performed a detailed histological analysis by light and confocal microscopy. Large accumulations of T and B cells were found distributed throughout the meninges of the spinal cord and showed varying degrees of organization and size. While some contained loose aggregates of a few cells, others were composed of large amounts of T and B cells and extended over wide distances of up to several millimeters. Moreover, eLFs were often found to exhibit separate T and B cell zones in our model, thereby mimicking the structural organization of SLOs. In addition, macrophages were detected in close vicinity, but also within these follicle structures (Figure 8). Furthermore, enormous eLFs were found in many different areas of the brain, such as the cortex, brainstem, cerebellum, basal ganglia, hippocampus, hypothalamus and the subarachnoid space at the base of the brain, and appeared to originate from the meninges and invade the underlying parenchyma (Figure 9). As the histological analysis in the previous study by Peters et al. focused on the spinal cord [109], we here reported for the first time that large eLFs also form in the meninges of the brain in our model. Notably, all eLFs were characterized by prominent B cell clustering, with B cells being almost exclusively located in these meningeal aggregates. In contrast, T cells seemed to egress from the eLF structure in large numbers and infiltrate the subpial parenchymal tissues. Strong clustering of B cells in eLFs was also observed in other EAE models and is considered as a defining criterion [147]. However, it is still under investigation, which factors are responsible for the attraction and retention of B cells in meningeal eLFs. One possibility is the chemokine CXCL13, which attracts CXCR5-expressing Tfh and B cells into follicles in SLOs. Several studies have provided evidence for enhanced *Cxcl13* expression during EAE [109, 157, 207, 208], and CXCL13 protein could be detected in CNS eLFs [109, 208]. In MS patients, the majority of B cells and a proportion of CD4^{+} T cells in the CSF express CXCR5 [209], and CXCL13-expressing cells were identified in CNS eLFs [56], pointing towards a role of the CXCL13-CXCR5 axis in attraction of lymphocytes to the CNS and eLF formation. To test the involvement of CXCR5 in CNS invasion of B cells, we induced Th17-mediated EAE in mice with CXCR5-deficient B cells. Preliminary analysis did not reveal a significant difference in B cell frequencies in the CNS compared to control mice, as measured by flow cytometry (not shown), indicating CXCR5 to be dispensable

for B cell recruitment to the CNS. However, histological analysis of CNS infiltrates might answer the question whether chemoattraction via CXCL13 is required for aggregation of B cells in eLFs. Summing up, Th17 cells are potent inducers of eLFs in both spinal cord and brain in our model, with eLFs providing a good microenvironment for the interaction of T and B cells. Accumulating evidence underpins the vital role of Th17 cells in the induction of eLFs. Intriguingly, the Th17 cytokines IL-17, IL-21 and IL-22 have all been linked to eLF formation [210, 211] and an ancestral connection with lymphoid tissue inducer (LTi) cells has been suggested, especially since they share expression of the master transcription factor RORγt and several cytokines [212, 213]. Indeed, a study by Pikor et al., employing Th17-mediated EAE on the SJL genetic background, indicates that IL-17 and IL-22 can stimulate meningeal fibroblasts to start remodelling the extracellular matrix, thereby providing the structural basis for eLF formation [157]. This could suggest an LTi-like function of Th17 cells in the meninges.

Since our Th17-mediated EAE model features abundant meningeal T:B cell aggregates of substantial size and organization, eLFs were further characterized regarding their functionality and maturation status by confocal microscopy. Staining for Ki67 revealed eLFs to be sites of T and B cell proliferation (Figure 10A), consistent with studies in several EAE models [155-157, 208] and MS [56, 148]. In many eLFs, only scattered B cells expressing the GC marker PNA or AID were found (Figure 10B+C), however, some eLFs exhibited clusters of AID$^+$ B cells, strongly indicative of GC formation (Figure 10D). GC marker-expressing B cells in CNS eLFs have also been identified in other studies, both in EAE [155, 156, 158] and MS [153]. In addition, flow cytometric analysis of CNS-infiltrating cells confirmed the presence of PNA$^+$ B cells (Figure 10E) and isotype-switched IgM$^-$ IgD$^-$ B cells (Figure 10F), which points towards an ongoing GC reaction in the CNS. Also, a small population of plasma cells could be detected (Figure 10G). However, it cannot be excluded that the plasma cells matured in the periphery and then infiltrated instead of differentiating inside the CNS. Additionally, a fraction of CNS T cells expressed the GC and activation marker GL7. Thereby, transferred 2D2 T cells showed higher frequency of GL7$^+$ cells as well as higher expression levels compared to endogenous T cells (Figure 10H), which might be due to their difference in antigen-specificity. Since transferred T cells recognize the CNS-antigen MOG, they can become reactivated by interacting with local APCs in contrast to endogenous T cells, which presumably contain only a minor fraction of CNS-reactive

T cells. Although T cells are found in large numbers in eLFs, they also egress from these aggregates and broadly infiltrate the underlying tissues. Therefore, it is not clear whether all GL7$^+$ T cells are localized in eLFs. The presence of GC marker-expressing B and T cells as well as class-switched B cells in the CNS of Th17-EAE mice was also shown by Peters et al. [109]. Interestingly, a recent study by Quinn et al. reported the amount of class-switched B cells in the spinal cord to correlate with disease severity, measured by weight loss of mice, in Th17-mediated EAE [178], indicative of ongoing B cell maturation. Correspondingly, transferred Th17 cells were demonstrated to express CXCR5, ICOS and Bcl6 – markers associated with Tfh cells – in the CNS [109] and therefore, may perform Tfh functions supporting B cell maturation in GC reactions. In fact, Bcl6 expression in Th17 cells was recently shown to be crucial for their ability to induce severe disease, meningeal eLF formation, and to support B cell responses in the CNS [207]. Taken together, we propose that Th17 cells are uniquely equipped to recruit B cells to CNS eLFs, where at least some of these cells interact with each other in a GC reaction, possibly fueling inflammation within the CNS. Combined flow cytometric and immunohistochemical analysis showed that eLFs appear in different stages of maturation, also within the same animal, whereby many eLFs were not fully matured at the time point of investigation, probably due to the rather short disease duration in our model.

5.2 The role of B cells in Th17-mediated EAE

As second part of the project, we aimed to investigate whether Th17 cells not only recruit B cells, but also shape a pathogenic B cell response contributing to smoldering inflammation in the CNS. Therefore, we performed a detailed phenotypical analysis of CNS-infiltrating B cells by single-cell RNA sequencing. To dissect the properties of CNS B cells and determine whether and how they perform a pro-inflammatory function, their transcriptome was compared to peripheral B cells from spleen and cLN. Since lymph fluid from the CNS containing cells and antigens drains into cLNs [214-216], they could be a site where recruitment of B cells for CNS invasion takes place. Of note, in the spontaneous RR mouse model, endogenous autoreactive B cells were indicated to be recruited by transgenic encephalitogenic T cells in the cLN [179]. Unbiased clustering of the single cell transcriptomes revealed twelve individual B cell clusters

(Figure 11B) varying substantially in size and containing B cells of all three compartments (Figure 11A). Overall, peripheral B cells from spleen and cLN displayed a similar distribution of cells among the different clusters and corresponding phenotypes, whereas CNS B cells showed a distinct clustering, indicating them to be phenotypically different from peripheral B cells. Clusters 6 to 10 are enriched for CNS B cells, most pronounced for cluster 6, in which 93 % of cells belong to the CNS fraction (Figure 11C). Comparative gene expression analysis revealed prominent differences between CNS and peripheral B cells (Figure 12). Intriguingly, the orphan nuclear receptor *Nr4a1* was the most highly upregulated gene in the CNS. Nr4a1 is known to be one of the most highly induced transcription factors in response to BCR ligation [183], yet its precise function in B cells is still under investigation. Of note, *Nr4a1* expression is correlated with the strength of BCR stimulation via antigen [184, 185]. Transcriptional profiling revealed that Nr4a1 represses a set of BCR signaling-responsive genes and thereby dampens the expansion of strongly BCR-stimulated B cells when sufficient costimulation by T cells is missing. Some of these target genes are associated with T:B cell interaction, including *Icam1, Cd69* and *Cd86*, and limit the ability of B cells to receive T cell help [184]. Nr4a1 upregulation is also found in GC B cells located in the light zone [217, 218], where B cells capture antigen via their BCRs and may become positively selected. In a recent study, Nr4a1 was proposed to prevent high-affinity (and thus highly stimulated) clones from dominating the GC niche in order to preserve clonal diversity [219]. In BCR transgenic mouse models, Nr4a1 expression was found to correlate with the degree of autoreactivity of B cells and restrain their survival, possibly representing a mechanism of peripheral tolerance [220]. In our study, *Nr4a1* was highly expressed in cluster 7, and also in cluster 6, both of which are highly enriched for CNS B cells. High expression of *Nr4a1* indicates that at least a proportion of B cells received strong antigenic stimulation via their BCRs in the CNS and could even raise the possibility that these B cells are autoreactive. Further analysis of up- and downregulated pathways in these cells is necessary to determine the function of Nr4a1, for example whether it restricts survival and expansion of highly stimulated cells in the CNS. In addition, expression of the transcription factor *Egr1* was upregulated in the CNS, which is known to be rapidly induced upon B cell activation and increasingly expressed during subsequent proliferation [186, 187]. EGR1 was indicated to be important for B cell survival, differentiation and maturation [188]. Together, high

expression of *Nr4a*1 and *Egr1* suggests cluster 7 to comprise recently BCR-stimulated B cells. Besides, cluster 6, which is almost exclusively formed by CNS B cells, showed upregulation of *Socs3* which is induced upon stimulation by cytokines, e.g. IL-21, a cytokine important for B cell responses in GC reactions and produced by Tfh and Th17 cells. Conversely, its deletion was suggested to negatively affect the GC response of B cells [189]. Moreover, B cells in this cluster upregulated the transcription factor Bhlhe40 (Supplementary Table 2), which is rapidly induced upon BCR stimulation and T cell help, and reported to negatively regulate the GC reaction [221]. In humans, Bhlhe40 is highly expressed in pre-GC B cells in tonsils [222]. In addition, cluster 6 showed high expression of ribosomal proteins (Supplementary Table 2). Increased ribosome biogenesis was reported in positively selected GC B cells [223], possibly supporting their subsequent expansion and maturation which comes with increased translational demands. Therefore, we can speculate that cluster 6 is composed of pre-GC or GC B cells. To definitely assign a function to each of the individual B cell clusters, gene ontology analysis needs to be performed to identify up- and downregulated pathways and associated cellular phenotypes. Another scRNA-seq study found a follicular rather than GC phenotype of meningeal B cells in Th17-mediated EAE. However, a much smaller number of B cells was analyzed leading to a lower resolution compared to our study, indicated by the fact that they found only five B cell subclusters [207]. Furthermore, CNS B cells showed increased expression of the activation markers *Cd69* and *Cd83,* which is involved in antigen presentation and expressed by light zone GC B cells [192], the costimulatory molecule *CD86,* and the chemokine receptors *Ccr6* and *Ccr7* (Figure 12C). Hence, these data suggest an enhanced APC function of B cells in the CNS. In fact, the importance of B cells as APCs in neuroinflammation has been reported in several EAE studies [67, 68, 138, 144, 145]. In a mouse model of rheumatoid arthritis (RA), expression of CD80/CD86 in B cells is crucial for aberrant activation of autoreactive T cells and disease development [224]. In MS patients, a subset of pro-inflammatory GM-CSF[+] memory B cells was found to be increased, which - in healthy donors - showed elevated expression of CD80 and CD86 compared to other B cell subsets following *in vitro* activation [225]. CCR6 is essential for mediating the migration of Th17 cells into the CNS and required for EAE induction [226]. Since its ligand CCL20 is upregulated in MS [227, 228], where plasma levels are associated with disease severity [229], and EAE [230], it can be speculated that CCR6 supports

infiltration of both Th17 cells and B cells into the CNS. A recent study using a B cell-dependent EAE model revealed that CCR6 is upregulated on CNS B cells; however, this receptor is dispensable for their entry into the CNS [231]. Interestingly, CCR6 is also involved in GC responses [232, 233] and highly expressed in cluster 6 (Supplementary Table 2), which we proposed to represent pre-GC or GC B cells. Lastly, CCR7 guides B cells into T cell zones, and its ligands CCL19 and CCL21 are increased in the CNS in MS and EAE [234, 235]. In SLOs, CCR7 mediates migration of antigen-primed B cells to the border of the B and T cell zone [236, 237]. Interestingly, a correlation of CCL19 levels in the CSF and intrathecal IgG production was found in MS [234]. Hence, upregulation of CCR7 in CNS-infiltrating B cells might promote their migration to meningeal T cell accumulations and foster T:B cell interactions.

Transcriptomic, flow cytometric and microscopic analysis revealed a population of MZ-like B cells in the CNS (Figure 13). Due to their expression of polyreactive BCRs, high sensitivity to TLR stimulation and production of low affinity natural antibodies, recognizing both self and foreign molecules, and being important for clearing cell debris and pathogens, they are well equipped to contribute to autoimmunity. Indeed, mouse models of autoimmune diseases such as rheumatoid arthritis (RA), systemic lupus erythematosus (SLE), diabetes and Sjögren`s syndrome (SS) exhibit expansion and/or activation of MZ B cells [238]. In EAE, expansion of the MZ B cell subset has so far only been described following MOG_{35-55}/CFA immunization [137]. Importantly, in several autoimmune settings, MZ-like B cells infiltrate the target tissue, e.g. the thyroid gland [239], the pancreas [240] or the salivary glands [241]. In CNS autoimmunity, recruitment of MZ-like B cells into the CNS has not yet been reported. As MZ B cells are known to transport antigen into B cell follicles, thereby facilitating GC reactions, and express high levels of MHC-II and CD80/CD86 [17, 18], it can be speculated that MZ-like B cells present antigen and induce T cell activation in eLFs. In fact, in collagen-induced arthritis (CIA), the mouse model of RA, MZ B cells were demonstrated to present autoantigen to T cells, thereby inducing their activation and proliferation [242, 243]. Similar results were obtained in models of SLE and diabetes [240, 244]. Interestingly, in a mouse model of SS, MZ B cells, which are superior IL-6 producers among B cell subsets [137], show increased IL-6 expression [245], which is consistent with accumulation of both MZ B cells and Th17 cells in lacrimal glands [246]. Since a therapeutic approach, which inhibits Th17 cell development, also decreases the

frequency of MZ B cells, Th17 and MZ B cell responses were postulated to be linked in this model [245]. It is important to note that MZ B cells can also perform regulatory functions [247]. They are more potent IL-10 producers compared to other splenic B cell subsets [137] and may play a protective role in autoimmunity [248, 249]. In fact, several upregulated genes in cluster 8, such as Fcrl5, Zbtb20, Cd9 and Apoe (Supplementary Table 2), were recently defined as markers of Bregs by scRNA-seq of B cells from different murine organs [250]. Instead of migration of MZ B cells from the periphery to the CNS, it is also possible that the inflamed CNS provides a microenvironment, which induces infiltrating B cells to adopt a MZ-like phenotype. The origin of the MZ-like B cell population in the CNS, as well as the question whether they primarily fulfill a pro-inflammatory or a regulatory function in our model remains to be addressed in the future via functional assays.

BCR repertoire analysis revealed that around 1 % of cells belong to expanded clones, whereby 56 % of expanded cells are found in the CNS compared to 29 % or 16 % in spleen or cLN, respectively. The majority of expanded cells in the CNS are localized in cluster 8, which was proposed as MZ-like B cell cluster and contains the clones with the highest expansion factors. Correspondingly, expanded cells in this cluster upregulate expression of genes associated with plasma cell differentiation and MZ B cells or B-1 B cells (Figure 14). Further analysis of the different clonotypes (Table 3) revealed that the expanded clones are mainly shared between CNS and periphery with a preferential distribution in the CNS, implying that infiltrating B cells expand in meningeal eLFs. However, the majority of clones do not show mutations in the nucleotide sequence of their variable regions, possibly because of the short disease duration in our model, which probably results in the majority of eLFs being at the very beginning of a GC reaction. Interestingly, some striking similarities in the AA sequences of the CDR3 region may point towards an antigen-driven process. Besides, the majority of clones did not switch the isotype of their antibodies, and express IgM, also the more expanded ones in the MZ-like B cell cluster. MZ B cell are known to mainly produce natural IgM, which can induce complement activation and subsequent tissue damage upon extravasation into tissues; a process often observed in autoimmunity [238]. Studies in CIA showed that the naturally occurring anti-collagen IgM response of MZ B cells is increased upon immunization, followed by anti-collagen IgG production by follicular B cells and disease development. MZ B cells were

suggested to present autoantigen and activate T cells, thereby driving the immune response [242, 251]. Interestingly, increased IgM - but not IgA or IgG - levels in the CSF are already observed in MS patients at time point of diagnosis, and correlate with the degree of disease progression [252]. To determine whether expanded clones are MOG-specific, we are planning to recombinantly produce the antibodies corresponding to the most expanded clones and test their reactivity in the future. In fact, microscopic analysis revealed that some eLFs contain massive accumulations of MOG-specific B cells in Th17-EAE mice. In addition, Th17- and Th1-EAE mice showed elevated titers of MOG-specific IgG1 antibodies in the serum at the peak of disease compared to very low levels before disease onset / early disease. The highest levels were observed in Th17 recipients, as Th17 cells are the better B cell recruiters (Figure 15). These data demonstrate that transferred T cells recruit autoreactive endogenous B cells with the same antigen specificity, a finding similar to the spontaneous RR model featuring MOG-specific transgenic T cells [69]. In this model, the recruitment process was indicated to take place in the CNS-draining cLNs [179]. To test for accumulation of MOG-specific B cells in our model, a MOG tetramer staining of the cLN needs to be performed. However, as formation of large and abundant eLFs, some being MOG tetramer-positive, is a feature of Th17-mediated EAE, it is likely that expansion of autoreactive B cells at least partially happens directly in CNS eLFs. This could be further investigated by comparing the antibody levels in serum and CSF. The presence of a MOG-specific IgG1 response shows that these B cells have undergone a GC reaction. On the contrary, almost none of the expanded B cell clones are IgG1^{+}. For the transcriptome analysis, CD19-sorted B cells were used and therefore, it is possible that due to the excellent cognate T cell help all the highly MOG-specific clones have already developed further into CD19^{-} plasma cells and were not included in the transcriptomic analysis. However, it also cannot be excluded that the MOG-specific IgG1 response arises from B cells in the periphery, since Th17 cells may provide help to MOG-specific B cells in peripheral compartments. Speaking against this hypothesis we did not detect expanded IgG1^{+} clones in the peripheral compartment either.

To investigate the contribution of B cells to disease development, Th17-mediated EAE was induced in B cell-deficient Mb1-KO mice. We did not observe significant clinical differences between Mb1-KO mice and WT mice, as Mb1-KO mice exhibited even a trend towards an earlier disease onset. However, at peak of disease, both transferred

and endogenous T cells showed reduced frequencies of IL-17A$^+$, IFNγ$^+$ and IL-17A$^+$IFNγ$^+$ producers in the CNS in the absence of B cells (Figure 16). These data indicate that B cells are dispensable for disease development in Th17-mediated EAE, but they are required for T cells to maintain their highly pro-inflammatory cytokine profile in the CNS. In contrast to our finding, a recent study by Quinn et al. reported reduced disease severity of Th17-mediated EAE in B cell-deficient μMT mice [178]. However, the authors also included mice, which did not develop EAE, to calculate the disease burden. Since a higher number of μMT mice than WT mice remained healthy, it is likely that B cell deficiency resulted in decreased EAE incidence, rather than reduced disease severity. Still, in our study, we did not detect any differences in EAE incidence. A possible explanation could be that our Th17 cells are maximally activated at transfer and may induce extensive and irreversible tissue damage in the CNS regardless of the presence of B cells. In addition, due to the high severity the disease development can only be monitored for a few days and, therefore, it is difficult to observe clinical effects of the decreased pro-inflammatory effector function of CNS T cells in Mb1-KO mice. The slightly earlier disease onset of Mb1-KO mice may result from the lack of regulatory B cell responses in the periphery prior to or during early disease events. In fact, depletion of B cells by anti-CD20 antibody treatment before EAE induction by MOG$_{35-55}$/CFA immunization aggravates disease and enhances the accumulation of encephalitogenic T cells in the CNS. In contrast, when mice are treated during established EAE, the disease is ameliorated [253]. It is important to note that B cells can also perform regulatory functions in CNS autoimmunity by secreting IL-10, IL-35 and TGFβ [139-143]. However, in our model the data rather point towards a pro-inflammatory role of B cells in reactivating infiltrating T cells in meningeal eLFs.

To investigate whether T cells also form large meningeal clusters in the absence of B cells, we could perform a histological analysis of CNS lesions in Mb1-KO mice. Interestingly, in the spontaneous OSE model, KO of α4 integrins in B cells or treatment with CD19-directed CAR-T cells abrogates the accumulation of B cells in meningeal eLFs, thereby strongly reducing or eliminating the area of these aggregates. In addition, the T cells appear to be more scattered and deeply infiltrate the spinal cord white matter [254]. Another study showed that OSE mice treated with an anti-CD20 antibody exhibit a drastic reduction of B cell aggregation in meninges and, in addition, less strong T cell clustering, whereby the number of T cells remains unchanged [255].

Together, these reports suggest that B cells are important for organizing T cells into meningeal clusters. If this is also true for our model, it would indicate that the retention of T cells in eLFs and their communication with B cells is crucial for sustaining pro-inflammatory T cell functions in the CNS.

5.3 Real-time observation of T:B cell communication *in vivo*

In the final part of the project, we employed intravital two-photon microscopy to monitor the interaction of T and B cells in meningeal eLFs *in situ* to observe what exactly happens in eLFs and, in particular, to determine whether B cells are able to reactivate T cells and thereby support inflammatory processes within the CNS. To fluorescently label T cells, we used the ratiometric calcium indicator Twitch-2B, which allows to study T cell activation in real-time by visualizing the increase of the intracellular calcium concentration upon TCR ligation [110]. In our Th17-mediated EAE model, Th17 cells were transduced with the Twitch-2B sensor during their *in vitro* culture and then adoptively transferred into Mb1.Cre x ROSA26 tdTomato mice expressing tdTomato specifically in B cells, followed by intravital microscopy of spinal cord eLFs (Figure 17A). To our surprise, we found massive accumulations of T and B cells in the very small dissected imaging window in all imaged mice (Figure 18). In contrast, histological analysis of spinal cord lesions (Figure 8) revealed large eLFs only at distinct locations throughout the spinal cord. Therefore, it can be assumed that substantial parts of the leptomeninges are lost during dissection and preparation of CNS tissues for histological analysis. To address this issue and to visualize the full size and spatial distribution of meningeal eLFs, we could perform the whole-body immunolabeling method vDISCO [256] in a future experiment, which should enable us to image Twitch-2B$^+$ Th17 cells and tdTomato$^+$ B cells in the intact mouse body following tissue clearing.

To compare the T cell response of the EAE-inducing MOG-specific (2D2) Th17 cells to non-encephalitogenic Th17 cells, a set of control experiments was performed, whereby OVA-specific (OT-II) Th17 cells were transduced with the Twitch-2B sensor and transferred together with non-transduced MOG-specific Th17 cells into Mb1.Cre x ROSA26 tdTomato mice. Intriguingly, 2D2 T cells interacted more intensely with B cells than OT-II T cells. Around half of the 2D2 T cells formed contacts with B cells

compared to only 14 % of OT-II T cells (Figure 20A). Thereby, 2D2 T cells and B cells engaged in very long contacts, which lasted up to 50 min (Figure 20B). Since these contacts often lasted during the entire observation period, the contact length is probably even underestimated. A recent intravital microscopy study of SLOs revealed that T:B cell contacts at the border of the T cell zone and the B cell follicle are very long-lasting and can be maintained for up to 30 min [200]. Earlier studies reported that cognate T:B cell interactions can even last up to 60 min, whereas non-antigen-specific contacts show a duration of less than 10 min [237, 257]. In the GC, contacts between B cells and Tfh cells can last up to 13 min, however, the majority of T:B cell contact durations are below 5 min [29, 258, 259], whereby application of cognate antigen considerably increased the fraction of long-lasting contacts [29]. In our study, the majority of 2D2 T cells formed long-lived T:B cell contacts compared to a third of OT-II T cells (Figure 20C). Hence, these results strongly suggest that the interaction of T and B cells in eLFs is antigen-specific, i. e. B cells process and present MOG antigen to T cells. Furthermore, many T:B cell conjugates exhibited extensive cell surface contacts (Figure 18C) reminiscent of so called "T:B cell entanglements", which were described as a morphological characteristic of cognate Tfh:B cell interactions in SLOs. Entangled T:B cell contacts were indicated to require stimulation via the TCR since they could not be observed when T cells encountered non-presenting B cells [259]. Next, we investigated whether 2D2 T cells become reactivated in meningeal eLFs by analyzing the calcium ratios of the Twitch-2B sensor. Consistent with previous studies [123, 201], we found that increased calcium levels are associated with lowered motility of the respective T cell. 12.5 % of calcium levels exceeded the threshold level, indicating that a fraction of 2D2 T cells become reactivated in eLFs (Figure 21A). Notably, in T cells with B cell contact, 17.4 % of calcium levels were above the threshold, compared to 8.7 % of calcium levels in T cells without B cell contact (Figure 21B), showing that T cells exhibit more pronounced calcium signaling during T:B cell contacts. Indeed, very high calcium levels exceeding a value of 2.0 were almost exclusively found in T cells forming contact with B cells, indicating that B cells are able to reactivate T cells in eLFs. Calcium signaling in T cells without B cell contact may result from reactivation by other APCs, for example macrophages, which were shown to accumulate within and adjacent to the follicle structure (Figure 8E), but which are not fluorescently labeled in our *in vivo* imaging experimental set-up. In fact, several studies in other EAE models

have reported that macrophages can reactivate T cells in the meninges [123, 177, 260-262]. It is also possible that these T cells were reactivated by B cells just prior to the imaging period. Consistently, T cells engaged in T:B cell contacts showed a reduced velocity (mean 1.24 µm/min) compared to T cells without B cell contact (mean 1.80 µm/min) (Figure 21C). A previous study employing active EAE in mice reported a mean velocity of 2D2 T cells of around 5 µm/min in the meninges [123]. In rat EAE models, encephalitogenic T cells display mean velocities of around 7-11 µm/min in the meninges [177, 201, 260, 263]. In contrast to previous imaging studies, we performed the intravital microscopy at the late peak of disease, at which the T cell behavior might be different compared to earlier disease stages. Therefore, the choice of animal model as well as the stage of disease might account, at least in part, for the discrepancies in T cell velocity. In GCs of SLOs, Tfh cells were demonstrated to exhibit mean velocities of 9-10 µm/min [29, 200]. A reason for the low motility of T cells in our study could be that the cells in eLFs are very densely packed and might therefore not be able to move as freely as in meninges without follicle structures. It is also possible that due to the extensive tissue damage at late peak of disease the area is more saturated with released CNS antigens compared to onset of disease and that T cells without B cell contact are arrested since they are engaged in contacts with other (unlabeled) APCs, such as macrophages. Another reason could be that eLFs are sites where large amounts of immune cells are recruited to and therefore, high concentrations of chemokines could be responsible for retarding T cells in eLFs. During EAE, the chemokines CCL5 and CXCL9-12 could be detected in the meninges, where they were found to be expressed by meningeal phagocytes and to be important for the adhesion of T cells to meningeal structures [263]. Besides, CXCL13 could be detected in CNS eLFs [109, 208] and transferred Th17 cells were demonstrated to express its receptor CXCR5 in the CNS [109]. On the other hand, the presence of the T cell chemokines CCL19 and CCL20 in eLFs has so far not been proven and T cells are also able to leave eLF structures and infiltrate the underlying tissue (Figure 8 + Figure 9). Since the imaging sessions lasted up to several hours and eLFs contain large amounts of cells, we cannot completely exclude that insufficient oxygen supply at least in part contributes to the low motility of T cells. However, OT-II T cells exhibited significantly higher velocity (mean 3.03 µm/min) compared to 2D2 T cells (Figure 21C) under the same experimental conditions. These data suggest that low motility of 2D2 Th17 cells

is primarily a result of their intense cellular interactions, whereas OT-II T cells are being less often arrested due to lack of cognate interactions with B cells and other APCs, and therefore scan their surroundings faster in search of antigen. This finding is in line with previous studies showing that OVA-specific T cells move through the leptomeninges with higher velocity than CNS-specific T cells and do not form clusters around APCs [201, 264]. Time course analysis revealed that 2D2 T cells can exhibit pronounced calcium signaling during B cell contact, whereas OT-II T cells, which form only rare and predominantly short T:B cell contacts, do not show threshold-exceeding calcium levels during B cell contact (Figure 22 + Figure 23). These data indicate that B cells reactivate 2D2 T cells, but not OT-II T cells in eLFs. Further supporting this conclusion, flow cytometric analysis of a Th17-EAE mouse revealed that OT-II T cells do not maintain IL-17A secretion, but adopt production of the anti-inflammatory cytokine IL-10 in contrast to 2D2 T cells, which strongly produce IL-17A but no IL-10 in the CNS (Figure 24). This preliminary result indicates that OT-II T cells do not become reactivated by APCs in the CNS, however, these data need to be confirmed using a larger cohort of mice. Summing up, our intravital microscopy study provides the first real-time observation of T:B cell interactions in meningeal eLFs and demonstrates that T and B cells form long-lasting contacts, whereby B cells can reactivate T cells in an antigen-dependent manner.

In previous intravital microscopy studies in the lab of our collaboration partner Dr. Naoto Kawakami, the threshold for the calcium ratio was set using encephalitogenic T cells in SLOs or non-encephalitogenic T cells in the CNS as a control to correctly interpret elevated calcium levels as calcium signaling. In our study, the threshold was defined based on 2D2 T cells with higher velocity, which can be assumed to be not activated since they are moving too fast for an activation-inducing contact to occur. As OT-II T cells did not show elevated calcium levels, they could be used as control group for setting the threshold, to be consistent with the standard procedure used in the scientific community. In future studies, data from Twitch-2B-transduced 2D2 and OT-II Th17 recipients will have to be acquired in the same set of experiments to prevent inter-experimental variability of calcium ratios. As only one population can be labeled with the Twitch-2B sensor, it is not possible to image 2D2 and OT-II Th17 cells in the same animal. In addition, we will be able to quantitatively analyze the duration of calcium signaling in T cells during B cell contact to learn more about the individual T

cell responses, since the length of calcium signals results in differential effects on T cells. Notably, elevations of intracellular calcium are not exclusively linked to antigenic stimulation of the TCR. In SLOs devoid of cognate antigen, TCR transgenic T cells were demonstrated to exhibit short-lived calcium fluctuations [123, 201]. Longer calcium signals, lasting minutes to hours, result in translocation of the Ca^{2+}-sensitive transcription factors NF-κB or NFAT into the nucleus, which then induce transcription of activation-dependent gene expression required for various functions, including proliferation, maturation and cytokine production [118, 119, 265]. In a rat EAE model, Kyratsous and colleagues showed that long-lasting calcium spikes depend on antigen presentation since they are abolished by MHC-II blockade and, conversely, increased by injection of exogenous antigen [201]. In our study, time course analysis revealed that 2D2 T cells can exhibit different patterns of calcium signals during B cell contact. While some showed isolated or oscillating spikes, others displayed high calcium levels for several minutes (Figure 23A). In contrast, there were also T cells, which did not become activated during B cell contact, likely because the B cell did not present cognate antigen and/or provide proper costimulation. Similarly, the capacity of leptomeningeal phagocytes to activate T cells was found to be quite variable with some APCs inducing full T cell activation, while others hardly showed any stimulatory potential [201]. A possible explanation could be that myelin proteins may not be available in sufficient amounts, especially considering the high density of APCs in eLFs. Indeed, the availability of antigen on DCs was indicated to regulate the duration of DC:T cell contacts and subsequent T cell activation [266]. Intrathecal injection of myelin antigen converts weakly encephalitogenic T cells into highly pathogenic T cells and exacerbated clinical disease [267]. In addition, freshly isolated meningeal phagocytes present myelin antigens in low doses to T cells [177]. *In vivo*, i.v. injected myelin antigen is taken up and presented by local APCs to CNS-infiltrating encephalitogenic T cells leading to enhanced T cell activation and aggravated EAE [268]. In GC reactions, the interaction of Tfh cells with B cells, which is crucial for their selection, depends on the density of cognate peptide:MHC-II complexes [28]. Thereby, the expansion and hypermutation of B cells are proportional to the level of cognate antigen presented to Tfh cells [30]. In addition to antigen presentation, B cells must provide sufficient costimulatory signals to T cells to induce their activation. Costimulation via CD28 is crucial for enhanced and prolonged intracellular calcium

signaling leading to NFAT and NF-κB activation [269-271]. To prove that meningeal B cells reactivate T cells in an antigen-dependent manner, we could perform an *in vitro* co-culture of *ex vivo* isolated meningeal B cells and naïve or memory 2D2 T cells, testing whether B cells induce proliferation of 2D2 T cells. If the stimulatory effect on T cells is abolished by application of an MHC-II blocking antibody, this would confirm that B cells present antigen to T cells. To investigate the contribution of B cells to reactivation of T cells in the CNS and assess the T cell behavior in the absence of B cell follicles, intravital microscopy of 2D2 Th17 cells in B cell-deficient Mb1-KO mice could be performed. In addition, as we demonstrated that Th17 cells are superior to Th1 cells in recruiting B cells into the CNS, it would be interesting to test whether B cells also interact intensely with Th1 cells in the meninges and mediate their reactivation.

5.4 Clinical relevance of eLFs in CNS autoimmunity

Taken together, we propose that meningeal eLFs are sites where infiltrating T cells can receive strong reactivation stimuli by B cells enabling them to maintain a highly pro-inflammatory cytokine profile and thereby continue to propagate inflammatory processes in the CNS. Still, the clinical significance of eLFs requires further investigation. In MS, formation of eLFs is associated with a stronger disease course and subpial cortical as well as spinal cord pathology [56, 148, 150-153]. In fact, the neuronal loss in the cortex displays a gradient from the pia mater to the white matter [152, 272], suggesting that eLFs contribute to the pathogenesis of cortical damage. In our Th17-mediated EAE model, however, we could not observe a clinical impact of eLFs, considering that also B cell-deficient mice did not exhibit reduced disease severity, probably because of the strong and rather short disease course in our model. So far, only in the spontaneous OSE model, featuring both MOG-specific T and B cells, a correlation between eLF presence and a more severe disease course was found [156]. In the same model, a recent study suggested an immunoregulatory function of eLFs since their abrogation resulted in a higher disease burden [254]. It is possible that eLFs predominantly form in severe disease cases as a counter-regulatory process in an attempt to contain the inflammation. In contrast, our imaging study suggests a pro-inflammatory function of eLFs, which is further supported by our preliminary scRNA-

seq analysis and the reduced pro-inflammatory T cell cytokine profile in the B cell-deficient CNS. However, as we also found upregulation of markers associated with regulatory B cell functions, further analysis is required to gain a more detailed understanding of the B cell response in the CNS. In contrast to the OSE model, Th17-mediated EAE employs non-transgenic B cells with an endogenous repertoire and therefore, the B cell response in our model can be assumed to better reflect B cell-related disease aspects in MS. Importantly, our data indicate that eLFs may support the maturation of CNS-specific B cells, which speaks for a pro-inflammatory role since CNS-reactive autoantibodies are known to be pathogenic in CNS autoimmunity [273]. Regarding the T cell response, the OSE model might better recapitulate the disease pathogenesis in humans since such a strong and pure Th17 response as in our model is unlikely to occur in MS patients. Overall, it is unclear, which model better reflects the function of eLFs in human disease and yet, a recent study did not identify regulatory T cells in eLFs of MS patients [274], hinting towards an immunopathological function. However, both models are important to study the role of eLFs in CNS autoimmunity, whereby each of them may represent one end of the spectrum of what can happen within eLFs, ranging from immunoregulation to immunopathology.

6. Conclusion

In this thesis, flow cytometry, single-cell RNA sequencing, confocal and intravital two-photon microscopy were combined to investigate the unique relationship of Th17 cells and B cells and, in particular, to shed light on their communication in meningeal eLFs. First, we established adoptive transfer EAE to study Th1- and Th17-mediated pathology independently of each other. We confirmed that both Th1 and Th17 cells induce EAE with similar severity and maintain expression of their original cytokine profile in the inflamed CNS, whereby Th17 cells represent a more plastic T cell subset that is able to modulate its effector functions *in vivo*. Furthermore, we demonstrated that Th17 cells are superior to Th1 cells in recruiting B cells into the CNS. Performing a detailed histological analysis of Th17-EAE mice, we found abundant and enormous eLFs containing large amounts of T and B cells in the meninges of brain and spinal cord. While B cells were almost exclusively located in these meningeal aggregates, T cells appeared to egress from these structures and infiltrate the underlying parenchyma. In addition, eLFs contained clusters of proliferating T and B cells, showed expression of GC markers and often exhibited separate T and B cell zones, thereby mimicking the structural organization of SLOs and showing resemblance to eLFs in MS patients. Therefore, Th17-mediated EAE represents a very good model to study T:B cell communication in eLFs. As second part of the project, we performed single-cell RNA sequencing to characterize the phenotype of CNS-infiltrating B cells, in an attempt to dissect whether they play a pathogenic role. Our preliminary analysis indicated that CNS B cells are phenotypically different from peripheral B cells and that BCR-stimulated as well as pre-GC/GC B cells are overrepresented in the CNS, and provided evidence for an enhanced APC function. In addition, a population of MZ-like B cells was found in the CNS. Infiltration of MZ-like B cells in target organs has been shown in several autoimmune diseases; however, it has not yet been reported in CNS autoimmunity. Further analysis of the individual B cell clusters in the future will yield a detailed description of the B cell response in the CNS and enable us to compare the data to datasets from MS patients. BCR repertoire analysis provided evidence for clonal expansion in the CNS, supporting our hypothesis that B cells may expand and differentiate in meningeal eLFs. In fact, striking similarities in the CDR3 region may even point towards an antigen-driven process. In addition, transferred MOG-specific T

cells recruited MOG-specific B cells from the endogenous pool and accumulations of MOG-specific B cells were found in eLFs, indicating that expansion of CNS-reactive B cells may happen in these meningeal structures. In the third part of the project, we employed intravital two-photon microscopy of the CNS to monitor the interaction of Twitch-2B-labeled Th17 cells and tdTomato-labeled B cells. Thereby, we provided the first real-time observation of T:B cell communication in eLFs and demonstrated that T and B cells form long-lived contacts, whereby B cells can provide a reactivation stimulus to T cells. Consequently, we showed that lacking this reactivation stimulus from B cells CNS T cells are not able to maintain their highly pro-inflammatory cytokine profile.

Since the discovery of meningeal eLFs in MS patients, their role in CNS autoimmunity has been investigated for the last two decades. Both a pathogenic and a regulatory function have been proposed. The data presented in this thesis indicate that T and B cells can intensely interact with each other in a GC-like reaction resulting in clonal expansion and differentiation of B cells as well as reactivation of T cells, thereby fueling chronic inflammation directly in the CNS. Unraveling the function and clinical significance of eLFs may qualify them as a therapeutic target in MS.

References

1.   Medzhitov, R. and C. Janeway, Jr., *Innate immunity.* N Engl J Med, 2000. **343**(5): p. 338-44.

2.   Kawai, T. and S. Akira, *The role of pattern-recognition receptors in innate immunity: update on Toll-like receptors.* Nat Immunol, 2010. **11**(5): p. 373-84.

3.   Kono, H. and K.L. Rock, *How dying cells alert the immune system to danger.* Nat Rev Immunol, 2008. **8**(4): p. 279-89.

4.   Gasteiger, G., et al., *Cellular Innate Immunity: An Old Game with New Players.* J Innate Immun, 2017. **9**(2): p. 111-125.

5.   Vivier, E., et al., *Innate Lymphoid Cells: 10 Years On.* Cell, 2018. **174**(5): p. 1054-1066.

6.   Bedoui, S., et al., *Parallels and differences between innate and adaptive lymphocytes.* Nat Immunol, 2016. **17**(5): p. 490-4.

7.   Fearon, D.T. and R.M. Locksley, *The instructive role of innate immunity in the acquired immune response.* Science, 1996. **272**(5258): p. 50-3.

8.   Chaplin, D.D., *Overview of the immune response.* J Allergy Clin Immunol, 2010. **125**(2 Suppl 2): p. S3-23.

9.   Gorentla, B.K. and X.P. Zhong, *T cell Receptor Signal Transduction in T lymphocytes.* J Clin Cell Immunol, 2012. **2012**(Suppl 12): p. 5.

10.   Haring, J.S., V.P. Badovinac, and J.T. Harty, *Inflaming the CD8+ T cell response.* Immunity, 2006. **25**(1): p. 19-29.

11.   Jensen, P.E., *Recent advances in antigen processing and presentation.* Nat Immunol, 2007. **8**(10): p. 1041-8.

12.   Saravia, J., N.M. Chapman, and H. Chi, *Helper T cell differentiation.* Cell Mol Immunol, 2019. **16**(7): p. 634-643.

13.   Allman, D. and S. Pillai, *Peripheral B cell subsets.* Current opinion in immunology, 2008. **20**(2): p. 149-157.

14.   Davis, R.S., *FCRL regulation in innate-like B cells.* Ann N Y Acad Sci, 2015. **1362**(1): p. 110-6.

15.   Ferguson, A.R., M.E. Youd, and R.B. Corley, *Marginal zone B cells transport and deposit IgM-containing immune complexes onto follicular dendritic cells.* Int Immunol, 2004. **16**(10): p. 1411-22.

16.   Cinamon, G., et al., *Follicular shuttling of marginal zone B cells facilitates antigen transport.* Nat Immunol, 2008. **9**(1): p. 54-62.

17.   Attanavanich, K. and J.F. Kearney, *Marginal zone, but not follicular B cells, are potent activators of naive CD4 T cells.* J Immunol, 2004. **172**(2): p. 803-11.

18.   Song, H. and J. Cerny, *Functional heterogeneity of marginal zone B cells revealed by their ability to generate both early antibody-forming cells and germinal centers with hypermutation and memory in response to a T-dependent antigen.* J Exp Med, 2003. **198**(12): p. 1923-35.

19.   Zouali, M. and Y. Richard, *Marginal zone B-cells, a gatekeeper of innate immunity.* Front Immunol, 2011. **2**: p. 63.

20.   Cariappa, A., et al., *Perisinusoidal B cells in the bone marrow participate in T-independent responses to blood-borne microbes.* Immunity, 2005. **23**(4): p. 397-407.

21.   Cariappa, A., et al., *Naive recirculating B cells mature simultaneously in the spleen and bone marrow.* Blood, 2007. **109**(6): p. 2339-45.

22.   Pillai, S. and A. Cariappa, *The follicular versus marginal zone B lymphocyte cell fate decision.* Nat Rev Immunol, 2009. **9**(11): p. 767-77.

23.   Batista, F.D. and N.E. Harwood, *The who, how and where of antigen presentation to B cells.* Nat Rev Immunol, 2009. **9**(1): p. 15-27.

24.   Qi, H., et al., *SAP-controlled T-B cell interactions underlie germinal centre formation.* Nature, 2008. **455**(7214): p. 764-9.

25.   Crotty, S., *Follicular helper CD4 T cells (TFH).* Annu Rev Immunol, 2011. **29**: p. 621-63.

26.   Allen, C.D. and J.G. Cyster, *Follicular dendritic cell networks of primary follicles and germinal centers: phenotype and function.* Semin Immunol, 2008. **20**(1): p. 14-25.

27.   Nera, K.P., M.K. Kyläniemi, and O. Lassila, *Regulation of B Cell to Plasma Cell Transition within the Follicular B Cell Response.* Scand J Immunol, 2015. **82**(3): p. 225-34.

28.   Victora, G.D., et al., *Germinal center dynamics revealed by multiphoton microscopy with a photoactivatable fluorescent reporter.* Cell, 2010. **143**(4): p. 592-605.

29.   Shulman, Z., et al., *Dynamic signaling by T follicular helper cells during germinal center B cell selection.* Science, 2014. **345**(6200): p. 1058-62.

30.   Gitlin, A.D., Z. Shulman, and M.C. Nussenzweig, *Clonal selection in the germinal centre by regulated proliferation and hypermutation.* Nature, 2014. **509**(7502): p. 637-40.

31.   Vinuesa, C.G., et al., *Follicular Helper T Cells.* Annu Rev Immunol, 2016. **34**: p. 335-68.

32.   Nicholson, L.B., *The immune system.* Essays Biochem, 2016. **60**(3): p. 275-301.

33.   Hogquist, K.A., T.A. Baldwin, and S.C. Jameson, *Central tolerance: learning self-control in the thymus.* Nat Rev Immunol, 2005. **5**(10): p. 772-82.

34.   Walker, L.S. and A.K. Abbas, *The enemy within: keeping self-reactive T cells at bay in the periphery.* Nat Rev Immunol, 2002. **2**(1): p. 11-9.

35.   Mueller, D.L., *Mechanisms maintaining peripheral tolerance.* Nat Immunol, 2010. **11**(1): p. 21-7.

36.   Domogalla, M.P., et al., *Tolerance through Education: How Tolerogenic Dendritic Cells Shape Immunity.* Front Immunol, 2017. **8**: p. 1764.

37.   Shevyrev, D. and V. Tereshchenko, *Treg Heterogeneity, Function, and Homeostasis.* Front Immunol, 2019. **10**: p. 3100.

38.   Groux, H., et al., *A CD4+ T-cell subset inhibits antigen-specific T-cell responses and prevents colitis.* Nature, 1997. **389**(6652): p. 737-42.

39.   Roncarolo, M.G., et al., *The Biology of T Regulatory Type 1 Cells and Their Therapeutic Application in Immune-Mediated Diseases.* Immunity, 2018. **49**(6): p. 1004-1019.

40.   Nemazee, D., *Mechanisms of central tolerance for B cells.* Nat Rev Immunol, 2017. **17**(5): p. 281-294.

41.   Nemazee, D., *Receptor editing in lymphocyte development and central tolerance.* Nat Rev Immunol, 2006. **6**(10): p. 728-40.

42.   Goodnow, C.C., et al., *Control systems and decision making for antibody production.* Nat Immunol, 2010. **11**(8): p. 681-8.

43.   Fulcher, D.A. and A. Basten, *Reduced life span of anergic self-reactive B cells in a double-transgenic model.* J Exp Med, 1994. **179**(1): p. 125-34.

44. Cyster, J.G., S.B. Hartley, and C.C. Goodnow, *Competition for follicular niches excludes self-reactive cells from the recirculating B-cell repertoire.* Nature, 1994. **371**(6496): p. 389-95.

45. Cyster, J.G. and C.C. Goodnow, *Antigen-induced exclusion from follicles and anergy are separate and complementary processes that influence peripheral B cell fate.* Immunity, 1995. **3**(6): p. 691-701.

46. Ekland, E.H., et al., *Requirements for follicular exclusion and competitive elimination of autoantigen-binding B cells.* J Immunol, 2004. **172**(8): p. 4700-8.

47. Sospedra, M. and R. Martin, *Immunology of multiple sclerosis.* Annu Rev Immunol, 2005. **23**: p. 683-747.

48. Reich, D.S., et al., *Multiple Sclerosis.* New England Journal of Medicine, 2018. **378**(2): p. 169-180.

49. Thompson, A.J., et al., *Multiple sclerosis.* Lancet, 2018.

50. Levin, L.I., et al., *Temporal relationship between elevation of epstein-barr virus antibody titers and initial onset of neurological symptoms in multiple sclerosis.* Jama, 2005. **293**(20): p. 2496-500.

51. Wekerle, H., *Nature, nurture, and microbes: The development of multiple sclerosis.* Acta Neurol Scand, 2017. **136 Suppl 201**: p. 22-25.

52. Ebers, G.C., et al., *A population-based study of multiple sclerosis in twins.* N Engl J Med, 1986. **315**(26): p. 1638-42.

53. Hohlfeld, R., et al., *The search for the target antigens of multiple sclerosis, part 1: autoreactive CD4+ T lymphocytes as pathogenic effectors and therapeutic targets.* Lancet Neurol, 2016. **15**(2): p. 198-209.

54. Sawcer, S., R.J. Franklin, and M. Ban, *Multiple sclerosis genetics.* Lancet Neurol, 2014. **13**(7): p. 700-9.

55. Lassmann, H., W. Brück, and C.F. Lucchinetti, *The immunopathology of multiple sclerosis: an overview.* Brain Pathol, 2007. **17**(2): p. 210-8.

56. Serafini, B., et al., *Detection of ectopic B-cell follicles with germinal centers in the meninges of patients with secondary progressive multiple sclerosis.* Brain Pathol, 2004. **14**(2): p. 164-74.

57. Rivers, T.M., D.H. Sprunt, and G.P. Berry, *OBSERVATIONS ON ATTEMPTS TO PRODUCE ACUTE DISSEMINATED ENCEPHALOMYELITIS IN MONKEYS.* J Exp Med, 1933. **58**(1): p. 39-53.

58. Glatigny, S. and E. Bettelli, *Experimental Autoimmune Encephalomyelitis (EAE) as Animal Models of Multiple Sclerosis (MS).* Cold Spring Harb Perspect Med, 2018. **8**(11).

59. Johns, T.G. and C.C. Bernard, *The structure and function of myelin oligodendrocyte glycoprotein.* J Neurochem, 1999. **72**(1): p. 1-9.

60. Hemmer, B., J.J. Archelos, and H.P. Hartung, *New concepts in the immunopathogenesis of multiple sclerosis.* Nat Rev Neurosci, 2002. **3**(4): p. 291-301.

61. Tuohy, V.K., et al., *Identification of an encephalitogenic determinant of myelin proteolipid protein for SJL mice.* J Immunol, 1989. **142**(5): p. 1523-7.

62. McRae, B.L., et al., *Induction of active and adoptive relapsing experimental autoimmune encephalomyelitis (EAE) using an encephalitogenic epitope of proteolipid protein.* J Neuroimmunol, 1992. **38**(3): p. 229-40.

63. Berger, T., et al., *Experimental autoimmune encephalomyelitis: the antigen specificity of T lymphocytes determines the topography of lesions in the central and peripheral nervous system.* Lab Invest, 1997. **76**(3): p. 355-64.

64. Mendel, I., N. Kerlero de Rosbo, and A. Ben-Nun, *A myelin oligodendrocyte glycoprotein peptide induces typical chronic experimental autoimmune encephalomyelitis in H-2b mice: fine specificity and T cell receptor V beta expression of encephalitogenic T cells.* Eur J Immunol, 1995. **25**(7): p. 1951-9.

65. Bettelli, E., et al., *Myelin oligodendrocyte glycoprotein-specific T cell receptor transgenic mice develop spontaneous autoimmune optic neuritis.* J Exp Med, 2003. **197**(9): p. 1073-81.

66. Litzenburger, T., et al., *B lymphocytes producing demyelinating autoantibodies: development and function in gene-targeted transgenic mice.* J Exp Med, 1998. **188**(1): p. 169-80.

67. Bettelli, E., et al., *Myelin oligodendrocyte glycoprotein-specific T and B cells cooperate to induce a Devic-like disease in mice.* J Clin Invest, 2006. **116**(9): p. 2393-402.

68. Krishnamoorthy, G., et al., *Spontaneous opticospinal encephalomyelitis in a double-transgenic mouse model of autoimmune T cell/B cell cooperation.* J Clin Invest, 2006. **116**(9): p. 2385-92.

69. Pollinger, B., et al., *Spontaneous relapsing-remitting EAE in the SJL/J mouse: MOG-reactive transgenic T cells recruit endogenous MOG-specific B cells.* J Exp Med, 2009. **206**(6): p. 1303-16.

70. Langrish, C.L., et al., *IL-23 drives a pathogenic T cell population that induces autoimmune inflammation.* J Exp Med, 2005. **201**(2): p. 233-40.

71. Kroenke, M.A., et al., *IL-12- and IL-23-modulated T cells induce distinct types of EAE based on histology, CNS chemokine profile, and response to cytokine inhibition.* J Exp Med, 2008. **205**(7): p. 1535-41.

72. Jager, A., et al., *Th1, Th17, and Th9 effector cells induce experimental autoimmune encephalomyelitis with different pathological phenotypes.* J Immunol, 2009. **183**(11): p. 7169-77.

73. Mosmann, T.R. and R.L. Coffman, *TH1 and TH2 cells: different patterns of lymphokine secretion lead to different functional properties.* Annu Rev Immunol, 1989. **7**: p. 145-73.

74. Zhu, J., *T Helper Cell Differentiation, Heterogeneity, and Plasticity.* Cold Spring Harb Perspect Biol, 2018. **10**(10).

75. Kopf, M., et al., *Disruption of the murine IL-4 gene blocks Th2 cytokine responses.* Nature, 1993. **362**(6417): p. 245-8.

76. Baron, J.L., et al., *Surface expression of alpha 4 integrin by CD4 T cells is required for their entry into brain parenchyma.* J Exp Med, 1993. **177**(1): p. 57-68.

77. Das, M.P., et al., *Autopathogenic T helper cell type 1 (Th1) and protective Th2 clones differ in their recognition of the autoantigenic peptide of myelin proteolipid protein.* J Exp Med, 1997. **186**(6): p. 867-76.

78. Gutcher, I. and B. Becher, *APC-derived cytokines and T cell polarization in autoimmune inflammation.* J Clin Invest, 2007. **117**(5): p. 1119-27.

79. Panitch, H.S., et al., *Exacerbations of multiple sclerosis in patients treated with gamma interferon.* Lancet, 1987. **1**(8538): p. 893-5.

80.   Merrill, J.E., et al., *Inflammatory leukocytes and cytokines in the peptide-induced disease of experimental allergic encephalomyelitis in SJL and B10.PL mice.* Proc Natl Acad Sci U S A, 1992. **89**(2): p. 574-8.

81.   Ando, D.G., et al., *Encephalitogenic T cells in the B10.PL model of experimental allergic encephalomyelitis (EAE) are of the Th-1 lymphokine subtype.* Cell Immunol, 1989. **124**(1): p. 132-43.

82.   Traugott, U. and P. Lebon, *Interferon-gamma and Ia antigen are present on astrocytes in active chronic multiple sclerosis lesions.* J Neurol Sci, 1988. **84**(2-3): p. 257-64.

83.   Chitnis, T., et al., *Effect of targeted disruption of STAT4 and STAT6 on the induction of experimental autoimmune encephalomyelitis.* J Clin Invest, 2001. **108**(5): p. 739-47.

84.   Bettelli, E., et al., *Loss of T-bet, but not STAT1, prevents the development of experimental autoimmune encephalomyelitis.* J Exp Med, 2004. **200**(1): p. 79-87.

85.   Kuchroo, V.K., et al., *Cytokines and adhesion molecules contribute to the ability of myelin proteolipid protein-specific T cell clones to mediate experimental allergic encephalomyelitis.* J Immunol, 1993. **151**(8): p. 4371-82.

86.   Ferber, I.A., et al., *Mice with a disrupted IFN-gamma gene are susceptible to the induction of experimental autoimmune encephalomyelitis (EAE).* J Immunol, 1996. **156**(1): p. 5-7.

87.   Becher, B., B.G. Durell, and R.J. Noelle, *Experimental autoimmune encephalitis and inflammation in the absence of interleukin-12.* J Clin Invest, 2002. **110**(4): p. 493-7.

88.   Oppmann, B., et al., *Novel p19 protein engages IL-12p40 to form a cytokine, IL-23, with biological activities similar as well as distinct from IL-12.* Immunity, 2000. **13**(5): p. 715-25.

89.   Cua, D.J., et al., *Interleukin-23 rather than interleukin-12 is the critical cytokine for autoimmune inflammation of the brain.* Nature, 2003. **421**(6924): p. 744-8.

90.   Harrington, L.E., et al., *Interleukin 17-producing CD4+ effector T cells develop via a lineage distinct from the T helper type 1 and 2 lineages.* Nat Immunol, 2005. **6**(11): p. 1123-32.

91.   Bettelli, E., et al., *Reciprocal developmental pathways for the generation of pathogenic effector TH17 and regulatory T cells.* Nature, 2006. **441**(7090): p. 235-8.

92.   Veldhoen, M., et al., *TGFbeta in the context of an inflammatory cytokine milieu supports de novo differentiation of IL-17-producing T cells.* Immunity, 2006. **24**(2): p. 179-89.

93.   Ivanov, II, et al., *The orphan nuclear receptor RORgammat directs the differentiation program of proinflammatory IL-17+ T helper cells.* Cell, 2006. **126**(6): p. 1121-33.

94.   Chung, Y., et al., *Critical regulation of early Th17 cell differentiation by interleukin-1 signaling.* Immunity, 2009. **30**(4): p. 576-87.

95.   Awasthi, A., et al., *Cutting edge: IL-23 receptor gfp reporter mice reveal distinct populations of IL-17-producing cells.* J Immunol, 2009. **182**(10): p. 5904-8.

96.   Lee, Y., et al., *Induction and molecular signature of pathogenic TH17 cells.* Nat Immunol, 2012. **13**(10): p. 991-9.

97.   McGeachy, M.J., et al., *TGF-beta and IL-6 drive the production of IL-17 and IL-10 by T cells and restrain T(H)-17 cell-mediated pathology.* Nat Immunol, 2007. **8**(12): p. 1390-7.

98.   Korn, T., et al., *IL-17 and Th17 Cells.* Annu Rev Immunol, 2009. **27**: p. 485-517.

99.   Blaschitz, C. and M. Raffatellu, *Th17 cytokines and the gut mucosal barrier.* J Clin Immunol, 2010. **30**(2): p. 196-203.

100.   Omenetti, S., et al., *The Intestine Harbors Functionally Distinct Homeostatic Tissue-Resident and Inflammatory Th17 Cells.* Immunity, 2019. **51**(1): p. 77-89.e6.

101.   Kurschus, F.C., et al., *Genetic proof for the transient nature of the Th17 phenotype.* Eur J Immunol, 2010. **40**(12): p. 3336-46.

102.   Hirota, K., et al., *Fate mapping of IL-17-producing T cells in inflammatory responses.* Nat Immunol, 2011. **12**(3): p. 255-63.

103.   Iwakura, Y., et al., *Functional specialization of interleukin-17 family members.* Immunity, 2011. **34**(2): p. 149-62.

104.   Lock, C., et al., *Gene-microarray analysis of multiple sclerosis lesions yields new targets validated in autoimmune encephalomyelitis.* Nat Med, 2002. **8**(5): p. 500-8.

105.   Montes, M., et al., *Oligoclonal myelin-reactive T-cell infiltrates derived from multiple sclerosis lesions are enriched in Th17 cells.* Clin Immunol, 2009. **130**(2): p. 133-44.

106.   Hofstetter, H.H., et al., *Therapeutic efficacy of IL-17 neutralization in murine experimental autoimmune encephalomyelitis.* Cell Immunol, 2005. **237**(2): p. 123-30.

107.   Ishigame, H., et al., *Differential roles of interleukin-17A and -17F in host defense against mucoepithelial bacterial infection and allergic responses.* Immunity, 2009. **30**(1): p. 108-19.

108.   Regen, T., et al., *IL-17 controls central nervous system autoimmunity through the intestinal microbiome.* Sci Immunol, 2021. **6**(56).

109.   Peters, A., et al., *Th17 cells induce ectopic lymphoid follicles in central nervous system tissue inflammation.* Immunity, 2011. **35**(6): p. 986-96.

110.   Kawakami, N., *In vivo imaging in autoimmune diseases in the central nervous system.* Allergol Int, 2016. **65**(3): p. 235-42.

111.   Trebak, M. and J.P. Kinet, *Calcium signalling in T cells.* Nat Rev Immunol, 2019. **19**(3): p. 154-169.

112.   Lewis, R.S., *Calcium signaling mechanisms in T lymphocytes.* Annu Rev Immunol, 2001. **19**: p. 497-521.

113.   Hogan, P.G., R.S. Lewis, and A. Rao, *Molecular basis of calcium signaling in lymphocytes: STIM and ORAI.* Annu Rev Immunol, 2010. **28**: p. 491-533.

114.   Dustin, M.L., *The immunological synapse.* Cancer Immunol Res, 2014. **2**(11): p. 1023-33.

115.   Martin, P.J., et al., *A 44 kilodalton cell surface homodimer regulates interleukin 2 production by activated human T lymphocytes.* J Immunol, 1986. **136**(9): p. 3282-7.

116.   Bromley, S.K., et al., *The immunological synapse and CD28-CD80 interactions.* Nat Immunol, 2001. **2**(12): p. 1159-66.

117.   Tseng, S.Y., et al., *T cell-dendritic cell immunological synapses contain TCR-dependent CD28-CD80 clusters that recruit protein kinase C theta.* J Immunol, 2008. **181**(7): p. 4852-63.

118.   Fracchia, K., C. Pai, and C. Walsh, *Modulation of T Cell Metabolism and Function through Calcium Signaling.* Frontiers in Immunology, 2013. **4**(324).

119.   Joseph, N., B. Reicher, and M. Barda-Saad, *The calcium feedback loop and T cell activation: how cytoskeleton networks control intracellular calcium flux.* Biochim Biophys Acta, 2014. **1838**(2): p. 557-68.

120.   Dolmetsch, R.E., K. Xu, and R.S. Lewis, *Calcium oscillations increase the efficiency and specificity of gene expression.* Nature, 1998. **392**(6679): p. 933-6.

121.   Tomida, T., et al., *NFAT functions as a working memory of Ca2+ signals in decoding Ca2+ oscillation.* Embo j, 2003. **22**(15): p. 3825-32.

122.   Li, W., et al., *Cell-permeant caged InsP3 ester shows that Ca2+ spike frequency can optimize gene expression.* Nature, 1998. **392**(6679): p. 936-41.

123.   Mues, M., et al., *Real-time in vivo analysis of T cell activation in the central nervous system using a genetically encoded calcium indicator.* Nat Med, 2013. **19**(6): p. 778-83.

124.   Thestrup, T., et al., *Optimized ratiometric calcium sensors for functional in vivo imaging of neurons and T lymphocytes.* Nat Methods, 2014. **11**(2): p. 175-82.

125.   Esiri, M.M., *Multiple sclerosis: a quantitative and qualitative study of immunoglobulin-containing cells in the central nervous system.* Neuropathol Appl Neurobiol, 1980. **6**(1): p. 9-21.

126.   Lucchinetti, C., et al., *Heterogeneity of multiple sclerosis lesions: implications for the pathogenesis of demyelination.* Ann Neurol, 2000. **47**(6): p. 707-17.

127.   Fitzner, B., M. Hecker, and U.K. Zettl, *Molecular biomarkers in cerebrospinal fluid of multiple sclerosis patients.* Autoimmun Rev, 2015. **14**(10): p. 903-13.

128.   Obermeier, B., et al., *Matching of oligoclonal immunoglobulin transcriptomes and proteomes of cerebrospinal fluid in multiple sclerosis.* Nat Med, 2008. **14**(6): p. 688-93.

129.   Brandle, S.M., et al., *Distinct oligoclonal band antibodies in multiple sclerosis recognize ubiquitous self-proteins.* Proc Natl Acad Sci U S A, 2016. **113**(28): p. 7864-9.

130.   Bar-Or, A., et al., *Immunopathophysiology of pediatric CNS inflammatory demyelinating diseases.* Neurology, 2016. **87**(9 Suppl 2): p. S12-9.

131.   Keegan, M., et al., *Relation between humoral pathological changes in multiple sclerosis and response to therapeutic plasma exchange.* Lancet, 2005. **366**(9485): p. 579-82.

132.   Hauser, S.L., et al., *B-cell depletion with rituximab in relapsing-remitting multiple sclerosis.* N Engl J Med, 2008. **358**(7): p. 676-88.

133.   Greenfield, A.L. and S.L. Hauser, *B Cell Therapy for Multiple Sclerosis: Entering an Era.* Ann Neurol, 2017.

134.   Guerrier, T., et al., *Proinflammatory B-cell profile in the early phases of MS predicts an active disease.* Neurol Neuroimmunol Neuroinflamm, 2018. **5**(2): p. e431.

135.   Duddy, M., et al., *Distinct effector cytokine profiles of memory and naive human B cell subsets and implication in multiple sclerosis.* J Immunol, 2007. **178**(10): p. 6092-9.

136.   Bar-Or, A., et al., *Abnormal B-cell cytokine responses a trigger of T-cell-mediated disease in MS?* Ann Neurol, 2010. **67**(4): p. 452-61.

137.   Barr, T.A., et al., *B cell depletion therapy ameliorates autoimmune disease through ablation of IL-6-producing B cells.* J Exp Med, 2012. **209**(5): p. 1001-10.

138.   Molnarfi, N., et al., *MHC class II-dependent B cell APC function is required for induction of CNS autoimmunity independent of myelin-specific antibodies.* J Exp Med, 2013. **210**(13): p. 2921-37.

139.   Fillatreau, S., et al., *B cells regulate autoimmunity by provision of IL-10.* Nat Immunol, 2002. **3**(10): p. 944-50.

140.   Matsumoto, M., et al., *Interleukin-10-producing plasmablasts exert regulatory function in autoimmune inflammation.* Immunity, 2014. **41**(6): p. 1040-51.

141.   Shen, P., et al., *IL-35-producing B cells are critical regulators of immunity during autoimmune and infectious diseases.* Nature, 2014. **507**(7492): p. 366-370.

142.   Wang, R.X., et al., *Interleukin-35 induces regulatory B cells that suppress autoimmune disease.* Nat Med, 2014. **20**(6): p. 633-41.

143.   Bjarnadóttir, K., et al., *B cell-derived transforming growth factor-β1 expression limits the induction phase of autoimmune neuroinflammation.* Sci Rep, 2016. **6**: p. 34594.

144.   Weber, M.S., et al., *B-cell activation influences T-cell polarization and outcome of anti-CD20 B-cell depletion in central nervous system autoimmunity.* Ann Neurol, 2010. **68**(3): p. 369-83.

145.   Parker Harp, C.R., et al., *B cell antigen presentation is sufficient to drive neuroinflammation in an animal model of multiple sclerosis.* J Immunol, 2015. **194**(11): p. 5077-84.

146.   Pitzalis, C., et al., *Ectopic lymphoid-like structures in infection, cancer and autoimmunity.* Nat Rev Immunol, 2014. **14**(7): p. 447-62.

147.   Mitsdoerffer, M. and A. Peters, *Tertiary Lymphoid Organs in Central Nervous System Autoimmunity.* Front Immunol, 2016. **7**: p. 451.

148.   lMagliozzi, R., et al., *Meningeal B-cell follicles in secondary progressive multiple sclerosis associate with early onset of disease and severe cortical pathology.* Brain, 2007. **130**(Pt 4): p. 1089-104.

149.   Lucchinetti, C.F., et al., *Inflammatory Cortical Demyelination in Early Multiple Sclerosis.* New England Journal of Medicine, 2011. **365**(23): p. 2188-2197.

150.   Reali, C., et al., *B cell rich meningeal inflammation associates with increased spinal cord pathology in multiple sclerosis.* Brain Pathology, 2020. **30**(4): p. 779-793.

151.   Howell, O.W., et al., *Meningeal inflammation is widespread and linked to cortical pathology in multiple sclerosis.* Brain, 2011. **134**(Pt 9): p. 2755-71.

152.   Magliozzi, R., et al., *A Gradient of neuronal loss and meningeal inflammation in multiple sclerosis.* Ann Neurol, 2010. **68**(4): p. 477-93.

153.   Serafini, B., et al., *Dysregulated Epstein-Barr virus infection in the multiple sclerosis brain.* J Exp Med, 2007. **204**(12): p. 2899-912.

154.   Magliozzi, R., et al., *Intracerebral expression of CXCL13 and BAFF is accompanied by formation of lymphoid follicle-like structures in the meninges of mice with relapsing experimental autoimmune encephalomyelitis.* J Neuroimmunol, 2004. **148**(1-2): p. 11-23.

155. Kuerten, S., et al., *Tertiary lymphoid organ development coincides with determinant spreading of the myelin-specific T cell response.* Acta Neuropathol, 2012. **124**(6): p. 861-73.

156. Dang, A.K., et al., *Meningeal Infiltration of the Spinal Cord by Non-Classically Activated B Cells is Associated with Chronic Disease Course in a Spontaneous B Cell-Dependent Model of CNS Autoimmune Disease.* Front Immunol, 2015. **6**: p. 470.

157. Pikor, N.B., et al., *Integration of Th17- and Lymphotoxin-Derived Signals Initiates Meningeal-Resident Stromal Cell Remodeling to Propagate Neuroinflammation.* Immunity, 2015. **43**(6): p. 1160-73.

158. Lehmann-Horn, K., et al., *B cell repertoire expansion occurs in meningeal ectopic lymphoid tissue.* JCI Insight, 2016. **1**(20): p. e87234.

159. Batoulis, H., et al., *Central nervous system infiltrates are characterized by features of ongoing B cell-related immune activity in MP4-induced experimental autoimmune encephalomyelitis.* Clin Immunol, 2015. **158**(1): p. 47-58.

160. Mitsdoerffer, M., et al., *Proinflammatory T helper type 17 cells are effective B-cell helpers.* Proc Natl Acad Sci U S A, 2010. **107**(32): p. 14292-7.

161. Ota, N., et al., *IL-22 bridges the lymphotoxin pathway with the maintenance of colonic lymphoid structures during infection with Citrobacter rodentium.* Nat Immunol, 2011. **12**(10): p. 941-8.

162. Rangel-Moreno, J., et al., *The development of inducible bronchus-associated lymphoid tissue depends on IL-17.* Nat Immunol, 2011. **12**(7): p. 639-46.

163. Lanzavecchia, A., *Receptor-mediated antigen uptake and its effect on antigen presentation to class II-restricted T lymphocytes.* Annu Rev Immunol, 1990. **8**: p. 773-93.

164. Hobeika, E., et al., *Testing gene function early in the B cell lineage in mb1-cre mice.* Proc Natl Acad Sci U S A, 2006. **103**(37): p. 13789-94.

165. Madisen, L., et al., *A robust and high-throughput Cre reporting and characterization system for the whole mouse brain.* Nat Neurosci, 2010. **13**(1): p. 133-40.

166. Barnden, M.J., et al., *Defective TCR expression in transgenic mice constructed using cDNA-based alpha- and beta-chain genes under the control of heterologous regulatory elements.* Immunol Cell Biol, 1998. **76**(1): p. 34-40.

167. Pear, W.S., et al., *Production of high-titer helper-free retroviruses by transient transfection.* Proc Natl Acad Sci U S A, 1993. **90**(18): p. 8392-6.

168. Perera, N.C., et al., *NSP4 is stored in azurophil granules and released by activated neutrophils as active endoprotease with restricted specificity.* J Immunol, 2013. **191**(5): p. 2700-7.

169. Tom, R., L. Bisson, and Y. Durocher, *Culture of HEK293-EBNA1 Cells for Production of Recombinant Proteins.* CSH Protoc, 2008. **2008**: p. pdb.prot4976.

170. Salvador, F., et al., *A Spontaneous Model of Experimental Autoimmune Encephalomyelitis Provides Evidence of MOG-Specific B Cell Recruitment and Clonal Expansion.* Front Immunol, 2022. **13**: p. 755900.

171. Castagna, M., et al., *Direct activation of calcium-activated, phospholipid-dependent protein kinase by tumor-promoting phorbol esters.* J Biol Chem, 1982. **257**(13): p. 7847-51.

172. Chatila, T., et al., *Mechanisms of T cell activation by the calcium ionophore ionomycin.* J Immunol, 1989. **143**(4): p. 1283-9.

173. Griffiths, G., P. Quinn, and G. Warren, *Dissection of the Golgi complex. I. Monensin inhibits the transport of viral membrane proteins from medial to trans Golgi cisternae in baby hamster kidney cells infected with Semliki Forest virus.* J Cell Biol, 1983. **96**(3): p. 835-50.

174. Stoeckius, M., et al., *Cell Hashing with barcoded antibodies enables multiplexing and doublet detection for single cell genomics.* Genome Biol, 2018. **19**(1): p. 224.

175. Stuart, T., et al., *Comprehensive Integration of Single-Cell Data.* Cell, 2019. **177**(7): p. 1888-1902.e21.

176. Butler, A., et al., *Integrating single-cell transcriptomic data across different conditions, technologies, and species.* Nat Biotechnol, 2018. **36**(5): p. 411-420.

177. Bartholomäus, I., et al., *Effector T cell interactions with meningeal vascular structures in nascent autoimmune CNS lesions.* Nature, 2009. **462**(7269): p. 94-8.

178. Quinn, J.L., et al., *Role of TFH Cells in Promoting T Helper 17-Induced Neuroinflammation.* Front Immunol, 2018. **9**: p. 382.

179. Berer, K., et al., *Commensal microbiota and myelin autoantigen cooperate to trigger autoimmune demyelination.* Nature, 2011. **479**(7374): p. 538-41.

180. Stern, J.N., et al., *B cells populating the multiple sclerosis brain mature in the draining cervical lymph nodes.* Sci Transl Med, 2014. **6**(248): p. 248ra107.

181. Ashouri, J.F. and A. Weiss, *Endogenous Nur77 Is a Specific Indicator of Antigen Receptor Signaling in Human T and B Cells.* J Immunol, 2017. **198**(2): p. 657-668.

182. Mittelstadt, P.R. and A.L. DeFranco, *Induction of early response genes by cross-linking membrane Ig on B lymphocytes.* J Immunol, 1993. **150**(11): p. 4822-32.

183. Nus, M., et al., *NR4A1 Deletion in Marginal Zone B Cells Exacerbates Atherosclerosis in Mice-Brief Report.* Arterioscler Thromb Vasc Biol, 2020. **40**(11): p. 2598-2604.

184. Tan, C., et al., *NR4A nuclear receptors restrain B cell responses to antigen when second signals are absent or limiting.* Nat Immunol, 2020. **21**(10): p. 1267-1279.

185. Zikherman, J., R. Parameswaran, and A. Weiss, *Endogenous antigen tunes the responsiveness of naive B cells but not T cells.* Nature, 2012. **489**(7414): p. 160-4.

186. McMahon, S.B. and J.G. Monroe, *The role of early growth response gene 1 (egr-1) in regulation of the immune response.* J Leukoc Biol, 1996. **60**(2): p. 159-66.

187. Ke, J., et al., *The role of MAPKs in B cell receptor-induced down-regulation of Egr-1 in immature B lymphoma cells.* J Biol Chem, 2006. **281**(52): p. 39806-18.

188. Gururajan, M., et al., *Early growth response genes regulate B cell development, proliferation, and immune response.* J Immunol, 2008. **181**(7): p. 4590-602.

189. Jones, S.A., et al., *SOCS3 deletion in B cells alters cytokine responses and germinal center output.* J Immunol, 2011. **187**(12): p. 6318-26.

190. Shiow, L.R., et al., *CD69 acts downstream of interferon-alpha/beta to inhibit S1P1 and lymphocyte egress from lymphoid organs.* Nature, 2006. **440**(7083): p. 540-4.

191. Zimmermann, M., et al., *Antigen Extraction and B Cell Activation Enable Identification of Rare Membrane Antigen Specific Human B Cells.* Front Immunol, 2019. **10**: p. 829.

192. Krzyzak, L., et al., *CD83 Modulates B Cell Activation and Germinal Center Responses.* J Immunol, 2016. **196**(9): p. 3581-94.

193. Cyster, J.G. and C.D.C. Allen, *B Cell Responses: Cell Interaction Dynamics and Decisions.* Cell, 2019. **177**(3): p. 524-540.

194. Franco, A., et al., *CD21 and FCRL5 form a receptor complex with robust B-cell activating capacity.* Int Immunol, 2018. **30**(12): p. 569-578.

195. Won, W.J. and J.F. Kearney, *CD9 is a unique marker for marginal zone B cells, B1 cells, and plasma cells in mice.* J Immunol, 2002. **168**(11): p. 5605-11.

196. Herrero, A.B., et al., *FAM46C controls antibody production by the polyadenylation of immunoglobulin mRNAs and inhibits cell migration in multiple myeloma.* J Cell Mol Med, 2020. **24**(7): p. 4171-4182.

197. Kallies, A., et al., *Initiation of plasma-cell differentiation is independent of the transcription factor Blimp-1.* Immunity, 2007. **26**(5): p. 555-66.

198. Muri, J., et al., *B1 and Marginal Zone B Cells but Not Follicular B2 Cells Require Gpx4 to Prevent Lipid Peroxidation and Ferroptosis.* Cell Rep, 2019. **29**(9): p. 2731-2744.e4.

199. Nojima, T., et al., *In-vitro derived germinal centre B cells differentially generate memory B or plasma cells in vivo.* Nat Commun, 2011. **2**: p. 465.

200. Jacobsen, J.T., et al., *Expression of Foxp3 by T follicular helper cells in end-stage germinal centers.* Science, 2021. **373**(6552).

201. Kyratsous, N.I., et al., *Visualizing context-dependent calcium signaling in encephalitogenic T cells in vivo by two-photon microscopy.* Proc Natl Acad Sci U S A, 2017. **114**(31): p. E6381-e6389.

202. O'Connor, R.A., et al., *Cutting edge: Th1 cells facilitate the entry of Th17 cells to the central nervous system during experimental autoimmune encephalomyelitis.* J Immunol, 2008. **181**(6): p. 3750-4.

203. Lees, J.R., et al., *Regional CNS responses to IFN-gamma determine lesion localization patterns during EAE pathogenesis.* J Exp Med, 2008. **205**(11): p. 2633-42.

204. Stromnes, I.M., et al., *Differential regulation of central nervous system autoimmunity by T(H)1 and T(H)17 cells.* Nat Med, 2008. **14**(3): p. 337-42.

205. Wensky, A.K., et al., *IFN-gamma determines distinct clinical outcomes in autoimmune encephalomyelitis.* J Immunol, 2005. **174**(3): p. 1416-23.

206. Domingues, H.S., et al., *Functional and pathogenic differences of Th1 and Th17 cells in experimental autoimmune encephalomyelitis.* PLoS One, 2010. **5**(11): p. e15531.

207. Hartlehnert, M., et al., *Bcl6 controls meningeal Th17-B cell interaction in murine neuroinflammation.* Proc Natl Acad Sci U S A, 2021. **118**(36).

208. Columba-Cabezas, S., et al., *Suppression of established experimental autoimmune encephalomyelitis and formation of meningeal lymphoid follicles by lymphotoxin beta receptor-Ig fusion protein.* J Neuroimmunol, 2006. **179**(1-2): p. 76-86.

209. Krumbholz, M., et al., *Chemokines in multiple sclerosis: CXCL12 and CXCL13 up-regulation is differentially linked to CNS immune cell recruitment.* Brain, 2006. **129**(Pt 1): p. 200-11.

210. Grogan, J.L. and W. Ouyang, *A role for Th17 cells in the regulation of tertiary lymphoid follicles.* Eur J Immunol, 2012. **42**(9): p. 2255-62.

211. Jones, G.W. and S.A. Jones, *Ectopic lymphoid follicles: inducible centres for generating antigen-specific immune responses within tissues.* Immunology, 2016. **147**(2): p. 141-51.

212. Takatori, H., et al., *Lymphoid tissue inducer-like cells are an innate source of IL-17 and IL-22.* J Exp Med, 2009. **206**(1): p. 35-41.

213. Sawa, S., et al., *Lineage relationship analysis of RORgammat+ innate lymphoid cells.* Science, 2010. **330**(6004): p. 665-9.

214. Louveau, A., et al., *Structural and functional features of central nervous system lymphatic vessels.* Nature, 2015. **523**(7560): p. 337-41.

215. Louveau, A., et al., *CNS lymphatic drainage and neuroinflammation are regulated by meningeal lymphatic vasculature.* Nat Neurosci, 2018. **21**(10): p. 1380-1391.

216. Aspelund, A., et al., *A dural lymphatic vascular system that drains brain interstitial fluid and macromolecules.* J Exp Med, 2015. **212**(7): p. 991-9.

217. Mueller, J., M. Matloubian, and J. Zikherman, *Cutting edge: An in vivo reporter reveals active B cell receptor signaling in the germinal center.* J Immunol, 2015. **194**(7): p. 2993-7.

218. Kennedy, D.E., et al., *Novel specialized cell state and spatial compartments within the germinal center.* Nat Immunol, 2020. **21**(6): p. 660-670.

219. Brooks, J.F., et al., *Negative feedback by NUR77/Nr4a1 restrains B cell clonal dominance during early T-dependent immune responses.* Cell Rep, 2021. **36**(9): p. 109645.

220. Tan, C., et al., *Nur77 Links Chronic Antigen Stimulation to B Cell Tolerance by Restricting the Survival of Self-Reactive B Cells in the Periphery.* J Immunol, 2019. **202**(10): p. 2907-2923.

221. Rauschmeier, R., et al., *Bhlhe40 function in activated B and TFH cells restrains the GC reaction and prevents lymphomagenesis.* J Exp Med, 2022. **219**(2).

222. King, H.W., et al., *Single-cell analysis of human B cell maturation predicts how antibody class switching shapes selection dynamics.* Sci Immunol, 2021. **6**(56).

223. Ersching, J., et al., *Germinal Center Selection and Affinity Maturation Require Dynamic Regulation of mTORC1 Kinase.* Immunity, 2017. **46**(6): p. 1045-1058.e6.

224. O'Neill, S.K., et al., *Expression of CD80/86 on B cells is essential for autoreactive T cell activation and the development of arthritis.* J Immunol, 2007. **179**(8): p. 5109-16.

225. Li, R., et al., *Proinflammatory GM-CSF-producing B cells in multiple sclerosis and B cell depletion therapy.* Sci Transl Med, 2015. **7**(310): p. 310ra166.

226. Reboldi, A., et al., *C-C chemokine receptor 6-regulated entry of TH-17 cells into the CNS through the choroid plexus is required for the initiation of EAE.* Nat Immunol, 2009. **10**(5): p. 514-23.

227. Furlan, R., et al., *Immunological patterns identifying disease course and evolution in multiple sclerosis patients.* J Neuroimmunol, 2005. **165**(1-2): p. 192-200.

228. Ambrosini, E., et al., *Astrocytes produce dendritic cell-attracting chemokines in vitro and in multiple sclerosis lesions.* J Neuropathol Exp Neurol, 2005. **64**(8): p. 706-15.

229. Huang, J., et al., *Inflammation-related plasma and CSF biomarkers for multiple sclerosis.* Proc Natl Acad Sci U S A, 2020. **117**(23): p. 12952-12960.

230. Wojkowska, D.W., et al., *Interactions between neutrophils, Th17 cells, and chemokines during the initiation of experimental model of multiple sclerosis.* Mediators Inflamm, 2014. **2014**: p. 590409.

231. Lee, D.S.W., et al., *CCR6 Expression on B Cells Is Not Required for Clinical or Pathological Presentation of MOG Protein-Induced Experimental Autoimmune Encephalomyelitis despite an Altered Germinal Center Response.* J Immunol, 2021. **207**(6): p. 1513-1521.

232. Reimer, D., et al., *Early CCR6 expression on B cells modulates germinal centre kinetics and efficient antibody responses.* Immunol Cell Biol, 2017. **95**(1): p. 33-41.

233. Suan, D., et al., *CCR6 Defines Memory B Cell Precursors in Mouse and Human Germinal Centers, Revealing Light-Zone Location and Predominant Low Antigen Affinity.* Immunity, 2017. **47**(6): p. 1142-1153.e4.

234. Krumbholz, M., et al., *CCL19 is constitutively expressed in the CNS, up-regulated in neuroinflammation, active and also inactive multiple sclerosis lesions.* J Neuroimmunol, 2007. **190**(1-2): p. 72-9.

235. Bielecki, B., et al., *Central Nervous System and Peripheral Expression of CCL19, CCL21 and Their Receptor CCR7 in Experimental Model of Multiple Sclerosis.* Arch Immunol Ther Exp (Warsz), 2015. **63**(5): p. 367-76.

236. Reif, K., et al., *Balanced responsiveness to chemoattractants from adjacent zones determines B-cell position.* Nature, 2002. **416**(6876): p. 94-9.

237. Okada, T., et al., *Antigen-engaged B cells undergo chemotaxis toward the T zone and form motile conjugates with helper T cells.* PLoS Biol, 2005. **3**(6): p. e150.

238. Palm, A.E. and S. Kleinau, *Marginal zone B cells: From housekeeping function to autoimmunity?* J Autoimmun, 2021. **119**: p. 102627.

239. Segundo, C., et al., *Thyroid-infiltrating B lymphocytes in Graves' disease are related to marginal zone and memory B cell compartments.* Thyroid, 2001. **11**(6): p. 525-30.

240. Mariño, E., et al., *Marginal-zone B-cells of nonobese diabetic mice expand with diabetes onset, invade the pancreatic lymph nodes, and present autoantigen to diabetogenic T-cells.* Diabetes, 2008. **57**(2): p. 395-404.

241. Groom, J., et al., *Association of BAFF/BLyS overexpression and altered B cell differentiation with Sjögren's syndrome.* J Clin Invest, 2002. **109**(1): p. 59-68.

242. Palm, A.K., et al., *Function and regulation of self-reactive marginal zone B cells in autoimmune arthritis.* Cell Mol Immunol, 2015. **12**(4): p. 493-504.

243. Palm, A.K., H.C. Friedrich, and S. Kleinau, *Nodal marginal zone B cells in mice: a novel subset with dormant self-reactivity.* Sci Rep, 2016. **6**: p. 27687.

244. Zhou, Z., et al., *Autoreactive marginal zone B cells enter the follicles and interact with CD4+ T cells in lupus-prone mice.* BMC Immunol, 2011. **12**: p. 7.

245. Singh, N., et al., *Dysregulated Marginal Zone B Cell Compartment in a Mouse Model of Sjögren's Syndrome with Ocular Inflammation.* Int J Mol Sci, 2018. **19**(10).

246. Turpie, B., et al., *Sjögren's syndrome-like ocular surface disease in thrombospondin-1 deficient mice.* Am J Pathol, 2009. **175**(3): p. 1136-47.

247. Zhang, X., *Regulatory functions of innate-like B cells.* Cell Mol Immunol, 2013. **10**(2): p. 113-21.

248. Lenert, P., et al., *TLR-9 activation of marginal zone B cells in lupus mice regulates immunity through increased IL-10 production.* J Clin Immunol, 2005. **25**(1): p. 29-40.

249. Matsushita, T., et al., *BAFF inhibition attenuates fibrosis in scleroderma by modulating the regulatory and effector B cell balance.* Sci Adv, 2018. **4**(7): p. eaas9944.

250. Yang, S.Y., et al., *Characterization of Organ-Specific Regulatory B Cells Using Single-Cell RNA Sequencing.* Front Immunol, 2021. **12**: p. 711980.

251. Carnrot, C., et al., *Marginal zone B cells are naturally reactive to collagen type II and are involved in the initiation of the immune response in collagen-induced arthritis.* Cell Mol Immunol, 2011. **8**(4): p. 296-304.

252. Magliozzi, R., et al., *Cerebrospinal Fluid IgM Levels in Association With Inflammatory Pathways in Multiple Sclerosis Patients.* Front Cell Neurosci, 2020. **14**: p. 569827.

253. Matsushita, T., et al., *Regulatory B cells inhibit EAE initiation in mice while other B cells promote disease progression.* J Clin Invest, 2008. **118**(10): p. 3420-30.

254. Mitsdorffer, M., et al., *Formation and immunomodulatory function of meningeal B-cell aggregates in progressive CNS autoimmunity.* Brain, 2021.

255. Brand, R.M., et al., *Anti-CD20 Depletes Meningeal B Cells but Does Not Halt the Formation of Meningeal Ectopic Lymphoid Tissue.* Neurol Neuroimmunol Neuroinflamm, 2021. **8**(4).

256. Cai, R., et al., *Panoptic imaging of transparent mice reveals whole-body neuronal projections and skull-meninges connections.* Nat Neurosci, 2019. **22**(2): p. 317-327.

257. Schwickert, T.A., et al., *A dynamic T cell-limited checkpoint regulates affinity-dependent B cell entry into the germinal center.* J Exp Med, 2011. **208**(6): p. 1243-52.

258. Benet, Z.L., et al., *CCL3 Promotes Germinal Center B Cells Sampling by Follicular Regulatory T Cells in Murine Lymph Nodes.* Front Immunol, 2018. **9**: p. 2044.

259. Liu, D., et al., *T-B-cell entanglement and ICOSL-driven feed-forward regulation of germinal centre reaction.* Nature, 2015. **517**(7533): p. 214-8.

260. Pesic, M., et al., *2-photon imaging of phagocyte-mediated T cell activation in the CNS.* J Clin Invest, 2013. **123**(3): p. 1192-201.

261. Kivisäkk, P., et al., *Localizing central nervous system immune surveillance: meningeal antigen-presenting cells activate T cells during experimental autoimmune encephalomyelitis.* Ann Neurol, 2009. **65**(4): p. 457-69.

262. Lodygin, D., et al., *A combination of fluorescent NFAT and H2B sensors uncovers dynamics of T cell activation in real time during CNS autoimmunity.* Nat Med, 2013. **19**(6): p. 784-90.

263. Schläger, C., et al., *Effector T-cell trafficking between the leptomeninges and the cerebrospinal fluid.* Nature, 2016. **530**(7590): p. 349-53.

264. Kawakami, N., et al., *Live imaging of effector cell trafficking and autoantigen recognition within the unfolding autoimmune encephalomyelitis lesion.* J Exp Med, 2005. **201**(11): p. 1805-14.

265. Smedler, E. and P. Uhlén, *Frequency decoding of calcium oscillations.* Biochim Biophys Acta, 2014. **1840**(3): p. 964-9.

266. Celli, S., F. Lemaître, and P. Bousso, *Real-time manipulation of T cell-dendritic cell interactions in vivo reveals the importance of prolonged contacts for CD4+ T cell activation.* Immunity, 2007. **27**(4): p. 625-34.

267. Kawakami, N., et al., *The activation status of neuroantigen-specific T cells in the target organ determines the clinical outcome of autoimmune encephalomyelitis.* J Exp Med, 2004. **199**(2): p. 185-97.

268. Odoardi, F., et al., *Blood-borne soluble protein antigen intensifies T cell activation in autoimmune CNS lesions and exacerbates clinical disease.* Proc Natl Acad Sci U S A, 2007. **104**(47): p. 18625-30.

269. Réthi, B., et al., *Flow cytometry used for the analysis of calcium signaling induced by antigen-specific T-cell activation.* Cytometry, 2002. **47**(4): p. 207-16.

270. Thiel, M., et al., *Efficiency of T-cell costimulation by CD80 and CD86 cross-linking correlates with calcium entry.* Immunology, 2010. **129**(1): p. 28-40.

271. Xia, F., et al., *TCR and CD28 Concomitant Stimulation Elicits a Distinctive Calcium Response in Naive T Cells.* Front Immunol, 2018. **9**: p. 2864.

272. Mainero, C., et al., *A gradient in cortical pathology in multiple sclerosis by in vivo quantitative 7 T imaging.* Brain, 2015. **138**(Pt 4): p. 932-45.

273. Mader, S., T. Kümpfel, and E. Meinl, *Novel insights into pathophysiology and therapeutic possibilities reveal further differences between AQP4-IgG- and MOG-IgG-associated diseases.* Curr Opin Neurol, 2020. **33**(3): p. 362-371.

274. Bell, L., et al., *Lymphoid Aggregates in the CNS of Progressive Multiple Sclerosis Patients Lack Regulatory T Cells.* Front Immunol, 2019. **10**: p. 3090.

Supplement

Supplementary Table 1. Top 10 markers in the CNS

Gene	avg_logFC	adjusted p-value
Nr4a1	1.333	0
Ppp1r15a	1.142	0
Junb	1.037	0
Egr1	0.992	0
Gem	0.973	0
Socs3	0.876	0
Cd83	0.831	0
Apoe	0.828	0
Ccnd2	0.796	0
Syngr2	1.333	0

Adjusted p-value is stated as 0 if the value is below 2.3E-300.

Supplementary Table 2. Top 10 markers for each cluster (if applicable)

Cluster	Gene	avg_logFC	adjusted p-value
0	Vpreb3	0.270	1.79E-114
	Emp3	0.301	1.04E-81
	Id3	0.267	3.23E-57
1	Plac8	0.894	0
	Fcrl5	0.786	0
	Cd9	0.527	0
	Dtx1	0.607	2.72E-279
	Pik3r4	0.470	3.57E-267
	Cr2	0.777	2.72E-235
	Rplp1	0.263	6.67E-165
	Cd1d1	0.384	1.08E-161
	Pdia4	0.526	2.66E-146
	Mzb1	0.444	1.18E-128
2	Ncl	1.212	0
	Mif	1.128	0
	Ccnd2	1.105	0
	C1qbp	0.924	0
	Eif4a1	0.898	0
	Pa2g4	0.894	0

2	Ranbp1	0.888	0
	Hspd1	0.888	0
	Eif5a	0.884	0
	Npm1	0.857	0
3	H3f3a	0.564	4.42E-289
	Iglc1	1.004	1.14E-245
	Iglc2	0.657	2.68E-196
	Cd79a	0.316	1.82E-131
	Tmsb10	0.328	6.72E-131
	Iglc3	0.525	6.72E-123
	Vim	0.603	8.60E-100
	Rasgrp2	0.557	6.89E-85
	Cd79b	0.330	1.81E-83
	Serpinb1a	0.475	1.91E-75
4	Gm42418	1.077	1.20E-246
	AY036118	1.571	2.10E-231
	Lars2	1.057	4.58E-153
	Fam107b	0.255	1
	Tsc22d3	0.257	1
	Hist1h1c	0.472	1
5	Irf7	1.131	0
	Rtp4	0.941	0
	Usp18	0.744	0
	Slfn5	0.976	1.82E-281
	Ifi213	0.929	9.24E-246
	Xaf1	0.760	4.60E-222
	Tgtp2	0.738	5.12E-212
	Stat1	0.966	2.15E-209
	Ifi27l2a	1.215	6.63E-199
	Zbp1	0.842	3.07E-193
6	Cfp	0.963	0
	Flt3	0.429	0
	Rplp0	0.481	6.03E-247
	Socs3	0.511	5.89E-244
	Rps12	0.514	1.45E-238
	Rpl41	0.353	3.14E-206
	Lmnb1	0.404	5.73E-206
	Ccr6	0.613	3.26E-200
	Bhlhe40	0.509	6.48E-180
	Rpl3	0.364	5.03E-163

7	Egr3	0.864	0
	Egr1	1.582	2.30E-293
	Egr2	0.547	1.13E-289
	Nr4a1	1.556	5.90E-278
	Cd83	1.002	5.84E-216
	Marcksl1	1.149	4.14E-210
	Nfkbid	1.053	4.25E-209
	Myc	1.077	2.72E-199
	Icam1	0.884	5.59E-135
	Bhlhe40	0.812	1.37E-126
8	Fcrl5	1.058	0
	Emb	0.797	0
	Ccdc28b	0.715	0
	Ctla4	0.582	0
	Lysmd2	0.475	0
	Zbtb20	1.019	5.83E-254
	Cd300lf	0.549	1.50E-253
	Cd9	0.573	4.05E-249
	Apoe	1.739	6.50E-249
	AC133103.1	0.436	8.07E-245
9	Pclaf	2.111	0
	Stmn1	2.054	0
	Top2a	1.568	0
	Mki67	1.422	0
	Birc5	1.349	0
	Rrm2	1.122	0
	Ube2c	1.025	0
	Cks1b	1.003	0
	Cdca3	0.894	0
	Tyms	0.891	0
10	Ccl5	3.501	0
	C1qb	2.961	0
	C1qa	2.764	0
	Hmox1	2.596	0
	C1qc	2.527	0
	Fcer1g	2.519	0
	Cd63	1.900	0
	Tgfbi	1.670	0
	Csf1r	1.549	0
	Mt1	2.213	4.34E-214

	Malat1	2.115	3.33E-62
	Mef2c	1.622	1.66E-26
	Mbnl1	1.550	9.10E-21
	Ptprc	1.461	1.88E-19
11	Gm26917	2.267	2.36E-18
	Macf1	1.770	9.51E-16
	Arhgap15	1.579	5.07E-15
	Pgap1	1.595	3.88E-13
	Fus	1.534	4.91E-13
	Pag1	1.787	8.64E-09

Adjusted p-value is stated as 0 if the value is below 2.3E-300.

Attributions

The stainings of LN and CNS cryosections shown in Figure 10B-D and Figure 15B+C were performed together with Isabel Gök.

The processing of sorted B cells using the 10x Chromium Single Cell 5` Solution described in section 3.13.2 was performed together with Dr. Eduardo Beltran. The construction of the scBCR-seq library was performed by Markus Utzt. scRNA-seq data processing described in section 3.13.3 for Figure 11 - Figure 15 was performed by Dr. Eduardo Beltran and Vladyslav Kavaka.

The BCR clonotype analysis shown in Table 3 was performed by Dr. Anneli Peters.

The anti-MOG IgG1 ELISA shown in Figure 15D was performed by Dr. Anneli Peters and Klaus Hämäläinen.

The intravital two-photon microscopy experiments (Figure 17 - Figure 23) were performed together with Dr. Isabel Bauer under supervision of Dr. Naoto Kawakami. The pMSCV-Δneo-Twitch-2B plasmid was generated in the lab of Dr. Naoto Kawakami.

Acknowledgements

Ich bedanke mich bei Dr. Anneli Peters, die mich als eine von zwei Doktorandinnen für ihre Emmy Noether-Nachwuchsgruppe ausgewählt hat und mir damit eine Promotion im spannenden Feld der Neuroimmunologie ermöglichte. Vielen Dank, Anneli, für Deine unbändige Freude an der Forschung, Deine Unterstützung, Deinen Rat und Deine Begeisterung für mein Projekt. Ich konnte mich immer auf Dich verlassen – egal, ob wir uns gemeinsam über schöne Daten gefreut haben oder ich Aufmunterung brauchte in schwieriger Zeit. Ich habe meine Entscheidung nie bereut, bei Dir zu promovieren!

I would also like to especially thank my TAC members Dr. Naoto Kawakami and Prof. Christina Zielinski for their interest in my project, their support, encouragement and valuable discussions.

Mein Dank gilt auch allen Mitarbeitern der BMC Core Facilities Flow Cytometry, Bioimaging and Animal Models für ihre technische Unterstützung.

A big thank you goes to all members of the Institute of Clinical Neuroimmunology, especially to the Kawakami lab for the enjoyable and fruitful lab meetings, funny lunch and coffee breaks and activities outside of the lab. I am especially thankful to my collaboration partners, who contributed with their time and expertise to the success of my project: Dr. Eduardo Beltran and Vladyslav Kavaka for the scRNA-seq analysis, and Dr. Isabel Bauer and Dr. Naoto Kawakami for the intravital microscopy experiments.

Meine liebe AG Peters - was für eine schöne Zeit wir doch hatten! Anna, ich hätte mir keine bessere Mitstreiterin wünschen können. Wir haben zusammen das Labor aufgebaut, uns gemeinsam über Erfolge gefreut und uns in den schwierigen Zeiten gegenseitig unterstützt. Jetzt haben wir es geschafft!!! Rosa, ich bin so froh, dass Du nun unser Team ergänzt, es ist so, als wärst Du schon immer da gewesen! Mädels, ich freue mich sehr auf mein Postdoc-Jahr mit Euch! Vielen Dank auch an alle Studenten, die einen Teil des Weges mit uns gegangen sind.

Ich möchte mich an dieser Stelle auch bei meinen Freunden bedanken, die mich während meines Studiums und meiner Promotion begleitet haben: Mona, Lisa, Natalie
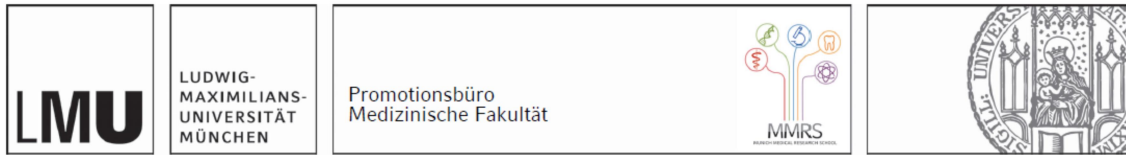
Affidavit

LMU LUDWIG-MAXIMILIANS-UNIVERSITÄT MÜNCHEN	Promotionsbüro Medizinische Fakultät	MMRS	

Eidesstattliche Versicherung

<u>Kolz, Anna</u>

Name, Vorname

Ich erkläre hiermit an Eides statt, dass ich die vorliegende Dissertation mit dem Titel:

T:B cell communication in ectopic lymphoid follicles in CNS autoimmunity

selbständig verfasst, mich außer der angegebenen keiner weiteren Hilfsmittel bedient und alle Erkenntnisse, die aus dem Schrifttum ganz oder annähernd übernommen sind, als solche kenntlich gemacht und nach ihrer Herkunft unter Bezeichnung der Fundstelle einzeln nachgewiesen habe.

Ich erkläre des Weiteren, dass die hier vorgelegte Dissertation nicht in gleicher oder in ähnlicher Form bei einer anderen Stelle zur Erlangung eines akademischen Grades eingereicht wurde.

Martinsried, 02.11.2022   Anna Kolz

Ort, Datum   Unterschrift Doktorandin bzw. Doktorand